David E. Kelsey, Martin Hand **On ultrahigh temperature crustal metamorphism: Phase equilibria, trace element thermometry, bulk composition, heat sources, timescales and tectonic settings**
Geoscience Frontiers, 2015; 6(3):311-356

Geoscience Frontiers 6 (2015) 311–356

HOSTED BY

ELSEVIER

Contents lists available at ScienceDirect

China University of Geosciences (Beijing)

Geoscience Frontiers

journal homepage: www.elsevier.com/locate/gsf

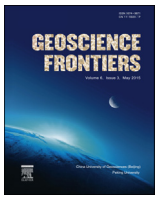

Focus paper

On ultrahigh temperature crustal metamorphism: Phase equilibria, trace element thermometry, bulk composition, heat sources, timescales and tectonic settings

David E. Kelsey*, Martin Hand

Department of Geology and Geophysics, School of Physical Sciences, The University of Adelaide, South Australia 5005, Australia

ARTICLE INFO

Article history:
Received 5 July 2014
Received in revised form
16 September 2014
Accepted 22 September 2014
Available online 11 November 2014

Keywords:
Sapphirine + quartz
P–T pseudosections
Zr-in-rutile
Ti-in-zircon
U–Pb geochronology
Subduction

ABSTRACT

Ultrahigh temperature (UHT) metamorphism is the most thermally extreme form of regional crustal metamorphism, with temperatures exceeding 900 °C. UHT crustal metamorphism is recognised in more than 50 localities globally in the metamorphic rock record and is accepted as 'normal' in the spectrum of regional crustal processes. UHT metamorphism is typically identified on the basis of diagnostic mineral assemblages such as sapphirine + quartz, orthopyroxene + sillimanite ± quartz and osumilite in Mg–Al-rich rock compositions, now usually coupled with pseudosection-based thermobarometry using internally-consistent thermodynamic data sets and/or Al-in-Orthopyroxene and ternary feldspar thermobarometry. Significant progress in the understanding of regional UHT metamorphism in recent years includes: (1) development of a ferric iron activity–composition thermodynamic model for sapphirine, allowing phase diagram calculations for oxidised rock compositions; (2) quantification of UHT conditions via trace element thermometry, with Zr-in-rutile more commonly recording higher temperatures than Ti-in-zircon. Rutile is likely to be stable at peak UHT conditions whereas zircon may only grow as UHT rocks are cooling. In addition, the extent to which Zr diffuses out of rutile is controlled by chemical communication with zircon; (3) more fully recognising and utilising temperature-dependent thermal properties of the crust, and the possible range of heat sources causing metamorphism in geodynamic modelling studies; (4) recognising that crust partially melted either in a previous event or earlier in a long-duration event has greater capacity than fertile, unmelted crust to achieve UHT conditions due to the heat energy consumed by partial melting reactions; (5) more strongly linking U–Pb geochronological data from zircon and monazite to *P–T* points or path segments through using Y + REE partitioning between accessory and major phases, as well as phase diagrams incorporating Zr and REE; and (6) improved insight into the settings and factors responsible for UHT metamorphism via geodynamic forward models. These models suggest that regional UHT metamorphism is, principally, geodynamically related to subduction, coupled with elevated crustal radiogenic heat generation rates.

1. Introduction

Ultrahigh temperature (UHT) metamorphism is the most thermally extreme type of regional crustal metamorphism, defined by Harley (1998b) as non-igneous crustal temperatures above 900 °C. UHT metamorphism of continental crust is now widely accepted as a relatively common—rather than anomalous—characteristic of deep crustal processes, greatly assisted by the large (and growing) number of localities worldwide that contain mineral assemblages whose stability has been constrained experimentally (Schreyer and Seifert, 1969a,b; Hensen and Green, 1970; Hensen, 1971, 1972a,b, 1977; Hensen and Essene, 1971; Hensen and Green, 1971, 1972, 1973; Chatterjee and Schreyer, 1972; Newton 1972; Doroshev and Malinovskiy, 1974; Newton et al., 1974; Seifert, 1974; Ackermand et al., 1975; Kiseleva, 1976; Arima and Onuma, 1977; Annersten and Seifert,

Mineral and phase abbreviations: bi, biotite; cd, cordierite; crn, corundum; cpx, clinopyroxene; g, garnet; ilm, ilmenite; ksp, K-feldspar; ky, kyanite; liq, silicate melt; mt, magnetite; opx, orthopyroxene; osm, osumilite; pl, plagioclase; q, quartz; ru, rutile; sa, sapphirine; sill, sillimanite; sp, spinel.

* Corresponding author. Tel: +61 8 8313 4886.
E-mail address: david.kelsey@adelaide.edu.au (D.E. Kelsey).

Peer-review under responsibility of China University of Geosciences (Beijing).

http://dx.doi.org/10.1016/j.gsf.2014.09.006

1981; Bertrand et al., 1991; Motoyoshi et al., 1993; Audibert et al., 1995; Carrington, 1995; Carrington and Harley, 1995a,b, 1996; Das et al., 2001, 2003; Hollis and Harley, 2003; Brigida et al., 2007; Fockenberg, 2008; Podlesskii et al., 2008; Podlesskii, 2010) and reinforced by calculated phase equilibria (Kelsey et al., 2004; Kelsey et al., 2005; Podlesskii et al., 2008; Podlesskii, 2010; Taylor-Jones and Powell, 2010; Holland and Powell, 2011; Korhonen et al., 2012b; Wheller and Powell, 2014). UHT metamorphism has been documented at relatively local scales (e.g. Sandiford et al., 1987; Harley and Fitzsimons, 1991; Gnos and Kurz, 1994), including adjacent to anorthositic/mafic intrusions (e.g. Berg and Wheeler, 1976; Berg, 1977; Caporuscio and Morse, 1978; Kars et al., 1980; Arima and Gower, 1991; Dasgupta et al., 1997; Westphal et al., 2003; Peng et al., 2010; Kooijman et al., 2011; Guo et al., 2012; Mitchell et al., 2014), as well as on a regional scale (e.g. Ellis et al., 1980; Grew, 1980; Sheraton et al., 1980; Grew, 1982b; Lal et al., 1987; Harley and Hensen, 1990; Dasgupta et al., 1994; Brown and Raith, 1996; Ouzegane and Boumaza, 1996; Raith et al., 1997; Sengupta et al., 1999; Hollis and Harley, 2002; Sarkar et al., 2003a; Schmitz and Bowring, 2003; Sajeev et al., 2004; Santosh and Sajeev, 2006; Bose and Das, 2007; Braun et al., 2007; Harley and Kelly, 2007a; Brandt et al., 2011; Das et al., 2011; Smithies et al., 2011; Adjerid et al., 2013; Korhonen et al., 2013a; Collins et al., 2014; Sarkar and Schenk, 2014; Walsh et al., 2014). Extensive exposures of UHT granulites are an exciting phenomenon as they imply that Earth's crust is mechanically capable of attaining and tolerating extreme thermal conditions on a regional scale (Harley, 2004), perhaps during 'normal' tectonic events (e.g. Vielzeuf et al., 1990; Harley, 2008; Kelsey, 2008). The reality that crustal rocks can be regionally subjected to such extreme temperatures has implications for lithospheric rheology and crust–mantle interactions and coupling (e.g. crustal growth and differentiation) (e.g. Vielzeuf et al., 1990; Collins, 2002; Harley, 2004; Kemp et al., 2007) and the geodynamic setting in which UHT metamorphism can be attained (e.g. Vielzeuf et al., 1990; Harley, 1998b; Harley, 2000; Clark et al., 2011; Sizova et al., 2014). An essential aspect of attempting to constrain the tectonic and/or geodynamic settings in which UHT granulites develop is to accurately constrain the pressure–temperature–time (P–T–t) evolution of UHT granulite terranes, and significant progress has been made in this regard in recent years.

The recent progress has led to numerous advances that have improved our understanding of thermally extreme deep crustal processes. The advances include: (1) expanded thermodynamic models for UHT minerals such as sapphirine; (2) new micro-analytical tools for the chemical analysis of trace elements in minerals, which has proven particularly useful where the concentration of these elements may be calibrated as a thermometer, such as in the slightly pressure-dependent Ti-in-zircon and Zr-in-rutile thermometers; (3) a more realistic consideration of the thermal properties of the crust in geodynamic modelling, and the role these play in the calculated thermal structure/profile of the crust; (4) geodynamic modelling that has specifically targeted the question of how the crust attains temperatures >900 °C and what tectonic settings are most probable for generating UHT conditions; and (5) voluminous geochronological data sets that have provided much-needed information about timescales of UHT (and granulite) metamorphism, particularly where geochronological data has been linked to the growth and/or breakdown of rock-forming minerals (usually garnet), and thus to P–T points or segments, via constraints from trace element partitioning. In addition, there is an increased global interest in UHT metamorphism, as shown by the greater-than-threefold (>300%) increase in the number of scientific papers published on or around the topic of UHT metamorphism since 2007 compared with the interval 2000–2006. In view of these considerations, it is useful to provide an update of the advances and progress from the past five years or so.

First we will provide an overview of what is currently known about UHT metamorphism (see Kelsey (2008) and Harley (2008) for additional details), including UHT localities identified since 2007. The second part of this review will discuss new advances outlined above that have improved our understanding of UHT metamorphism. This contribution is provided primarily as a comprehensive update of Kelsey (2008) and Harley (2008). Nevertheless, much of the information provided in Kelsey (2008) and Harley (2008) remains relevant.

2. What is UHT crustal metamorphism?

Ultrahigh temperature crustal metamorphism was defined by Harley (1998b) as a subdivision of granulite facies metamorphism, with temperatures in excess of 900 °C at pressures of 7–13 kbar (Fig. 1; *metamorphic petrologists subdivision* in Stüwe, 2007). The UHT subdivision was proposed partly in response to the (then) new concept of ultrahigh pressure metamorphism, reasoning that accepting that the crust can sustain thermally extreme conditions provides a new challenge to understand the tectonic and geodynamic drivers. The low-temperature bound of 900 °C for UHT metamorphism was defined on the basis of the experimentally-constrained location of the spinel-absent invariant point, which marks the low P–T stability limit of the comparatively rare orthopyroxene + sillimanite + quartz + silicate melt assemblage (see later) in the K_2O–FeO–MgO–Al_2O_3–SiO_2–H_2O, or KFMASH, model (experimental) chemical system (Carrington and Harley, 1995a; Harley, 1998b). As anticipated by Harley's (1998b) original definition of UHT, Pattison et al. (2003) demonstrated that there is no thermal gap between UHT and high-temperature (HT; ~750–900 °C) granulite facies metamorphism. Rather, there is a continuum in the distribution of temperature conditions retrieved from granulite facies rocks, from approximately 750 °C up to approximately 1100 °C (see also Brown, 2014).

Brown (2006, 2007a,b) and Stüwe (2007) also defined UHT metamorphic conditions in terms of the apparent thermal gradient of the crust (Fig. 1; *tectonicists subdivision* in Stüwe, 2007). UHT (and granulite) conditions are defined as those where the thermal gradient exceeds 75 °C kbar^{-1}, or approximately 20 °C km^{-1} (Brown, 2007a; Stüwe, 2007; Brown, 2010b, 2014). The logic behind characterising the crust in terms of thermal gradient (dT/dz, or dT/dP, where z is depth), or thermal structure, is that different tectonic settings are characterised by different thermal regimes. Characterising Earth's crust in terms of apparent thermal gradients is useful for appreciating that UHT metamorphism is probably occurring at depth in numerous parts of the modern/contemporary world (e.g. Sandiford and Powell, 1986a; Harley, 1989; Hayob et al., 1989; Hayob and Essene, 1990; Hacker et al., 2000; Blackburn et al., 2011; Ortega-Gutiérrez et al., 2012), and that many regional lower grade, high-geothermal gradient terranes are likely to be underlain by UHT rocks. Therefore, our view of UHT metamorphism should not be restricted only to exhumed terranes. Indeed, the notion of recognising, via xenoliths for example, or hypothesising (probable) UHT metamorphism at depth in the crust on the basis of contemporary heat flow is powerful as it allows for tectonic/geodynamic settings of the modern Earth to be interrogated as potential sites of modern as well as ancient UHT metamorphism (Sandiford and Powell, 1986a; Hyndman et al., 2005; Currie and Hyndman, 2006; Brown, 2007a,b; Hyndman and Currie, 2011).

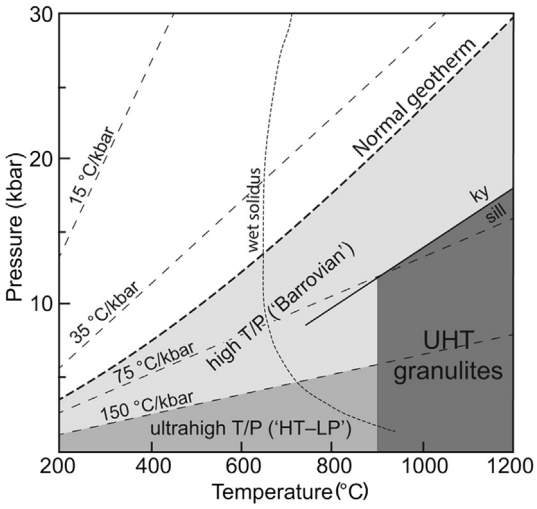

Figure 1. Pressure–temperature (P–T) diagram showing the classification of ultrahigh temperature (UHT) conditions above 900 °C (the '*petrologists view*' in terms of facies). Although UHT granulite metamorphism was originally defined as spanning the pressure range 7–13 kbar, it is now defined to cover the range from zero kbar up to the kyanite–sillimanite reaction. Thermal gradients (the '*tectonicists view*') indicate that UHT granulites require steep thermal gradients, and encompass the high-temperature–low-pressure (HT–LP) as well as part of the Barrovian range. Adapted from Brown (2006, 2007a,b, 2014) and Stüwe (2007).

3. Newly identified UHT localities

Figure 2 and Table 1 show an updated graphic and list of the world wide localities of UHT metamorphism. Recently recognised localities (Fig. 2; Table 1) include the Acadian Orogen in northeast USA (Ague and Eckert, 2012; Ague et al., 2013), the Garzón Massif in Colombia (Altenberger et al., 2012), the Schirmacher Hills in Dronning Maud Land, Antarctica (Baba et al., 2006; Baba et al., 2010), the Central Indian Tectonic Zone (Bhandari et al., 2011; Bhowmick et al., 2014), the Anosyen domain of SE Madagascar (Jöns and Schenk, 2008; Rakotonandrasana et al., 2010; Jöns and Schenk, 2011; Boger et al., 2012), the South Altay Belt in NW China (Chen et al., 2006; Li et al., 2010), the Lapland Granulite Belt on the Kola Peninsula, Russia (Bushmin et al., 2007; Lebedeva et al., 2010), the Musgrave Province, central Australia (Smithies et al., 2011; Walsh et al., 2014; Gorczyk et al., 2015) and the young 16 Ma UHT granulites of Seram, eastern Indonesia (Pownall et al., 2014). In addition, UHT rocks or terranes at depth—within the 7–13 kbar range—have been recognised from xenoliths in volcanic rocks from Tibet (Hacker et al., 2000), southern Mexico (Ortega-Gutiérrez et al., 2012) and central Mexico (Hayob et al., 1989; Hayob and Essene, 1990). Whereas the number of newly identified localities/terranes is modest, most of the many studies concerning UHT metamorphism since 2007 have involved more comprehensively documenting and understanding already known UHT metamorphic terranes (Table 1), in particular, for UHT terranes in India (Southern Granulite Terrane, Palghat Cauvery Tectonic Zone and Eastern Ghats; Sajeev et al., 2001; Tateishi et al., 2004; Bose et al., 2006; Tsunogae and Santosh, 2006; Bose and Das, 2007; Braun et al., 2007; Prakash et al., 2007; Sato and Santosh, 2007; Tadokoro et al., 2007; Tsunogae et al., 2008; Clark et al., 2009; Kanazawa et al., 2009; Kondou et al., 2009; Santosh et al., 2009c; Sato et al., 2009; Shimizu et al., 2009; Nishimiya et al., 2010; Tsunogae and Santosh, 2010; Brandt et al., 2011; Das et al., 2011; Dharma Rao and Chmielowski, 2011; Korhonen et al., 2011; Tsunogae and Santosh, 2011; Dharma Rao et al., 2012; Shazia et al., 2012; Korhonen et al., 2013a,b; Sarkar and Schenk, 2014; Sarkar et al., 2014) and China (Inner Mongolia Suture Zone, or Khondalite Belt, of North China Craton; Santosh et al., 2006, 2007a,b, 2008, 2009b,d, 2012, 2013; Liu et al., 2010; Peng et al., 2010; Jiao and Guo, 2011; Jiao et al., 2011; Liu et al., 2011; Tsunogae et al., 2011; Guo et al., 2012; Liu et al., 2012; Jiao et al., 2013a,b; Wan et al., 2013; Yang et al., 2014).

4. Identifying UHT metamorphism

4.1. Diagnostic mineral assemblages

UHT metamorphism is primarily recognised and documented on the basis of mineral assemblages found in Mg–Al-rich 'pelitic' rocks or in Mg–Al-rich layers in more siliceous rocks (the Mg–Al-rich part of rock can be either quartz-bearing or quartz-absent).

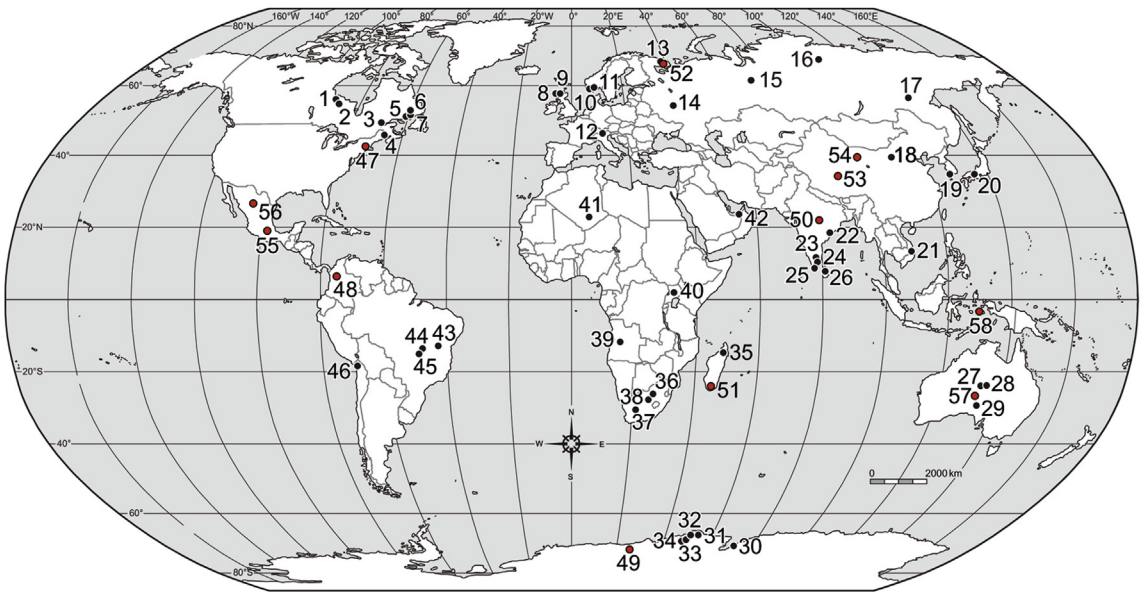

Figure 2. World map of exposed ultrahigh temperature metamorphic rocks (including xenoliths in some cases). The red filled circles denote newly found localities and localities not included in Kelsey (2008). The black filled circles represent localities reported in Kelsey (2008). See Table 1 herein and table 1 in Kelsey (2008) for the studies conducted for each locality.

Table 1
Geographic and/or geologic locations of UHT occurrences either documented since (and including) 2007 or not included in Kelsey (2008). The numbering system in the left-hand column follows that of table 1 in Kelsey (2008). Newly discovered UHT terranes/localities, and ones not reported in Kelsey (2008), are denoted in bold.

No.	Location	Studies
2	Pikwitonei granulite terrane/Sipiwesk Lake, Canada	Kooijman et al. (2012)
9	Lewisian Complex, Mainland Scotland	Johnson and White (2011); Johnson et al. (2012); Zirkler et al. (2012)
10	Rogaland Anorthosite Complex, Norway	Drüppel et al. (2013)
11	Bamble Sector, Norway	Kihle et al. (2010)
12	Gruf Complex, Italy	Galli et al. (2011, 2012)
13	Central Kola Granulite-Gneiss area (Kola Peninsula, Russia)	Dolivo-Dobrovol'skii et al. (2013)
14	Kursk–Besedino block, Voronezh Crystalline Massif, Russia	Pilugin et al. (2009)
18	North China Craton, China	Santosh et al. (2007a, 2009b, 2012, 2013); Liu et al. (2010, 2011, 2012); Peng et al. (2010); Jiao and Guo (2011); Jiao et al. (2011, 2013a,b); Tsunogae et al. (2011); Guo et al. (2012); Wan et al. (2013); Yang et al. (2014)
19	Odesan area (Gyeonggi Massif), South Korea	Oh and Kusky (2007)
20	Higo metamorphic terrane, Japan	Osanai et al. (1998, 2006); Oh and Kusky (2007)
21	Kontum Massif, central Vietnam	Nakano et al. (2007a,b, 2013)
22	Eastern Ghats Province, India	Bose et al. (2006); Bose and Das (2007); Das et al. (2011); Dharma Rao and Chmielowski (2011); Korhonen et al. (2011, 2013a,b, 2014); Dharma Rao et al. (2012)
22	Eastern Ghats belt (Ongole Domain of Krishna Province)	Sarkar and Schenk (2014); Sarkar et al. (2014)
23	Palghat Cauvery Tectonic Zone, India	Tsunogae et al. (2008); Clark et al. (2009); Kanazawa et al. (2009); Sato et al. (2009); Nishimiya et al. (2010); Tsunogae and Santosh (2011)
24	Southern Granulite Terrane, India	Sajeev et al. (2001); Tateishi et al. (2004); Tsunogae and Santosh (2006, 2010, 2011); Braun et al. (2007); Prakash et al. (2007); Sato and Santosh (2007); Tadokoro et al. (2007); Kondou et al. (2009); Santosh et al. (2009c); Shimizu et al. (2009); Brandt et al. (2011); Shazia et al. (2012)
26	Highland Complex, Sri Lanka	Sajeev et al. (2007, 2009, 2010)
29	Ooldea, Gawler Craton, Australia	Cutts et al. (2013)
29	Coober Pedy Ridge, Gawler Craton, Australia	Cutts et al. (2011a)
32	Napier Complex, Antarctica	Osanai et al. (2001); Yoshimura et al. (2001); Hokada (2007); Hokada et al. (2008); Shimizu et al. (2013)
34	Lützow-Holm Bay/Complex, Antarctica	Yoshimura et al. (2008); Kawasaki et al. (2011); Iwamura et al. (2013)
37	Southern Marginal Zone, Limpopo Belt, southern Africa	Tsunogae and van Reenen (2007); Belyanin et al. (2010, 2012a,b); Rajesh et al. (2014)
39	Epupa Complex, Namibia	Brandt et al. (2007); Meyer et al. (2011)
41	In Ouzzal, western Hoggar, Algeria	Aït-Djafer et al. (2009); Adjerid et al. (2013)
43	Salvador–Curaçá Belt (São Francisco Craton), Bahia, Brazil	Leite et al. (2009)
45	Anápolis-Itauçu Complex, Southern Brasília Belt, central Brazil	Baldwin et al. (2007a); Baldwin and Brown (2008); Giustina et al. (2011)
47	**Merrimack synclinorium, Connecticut, USA**	**Ague and Eckert (2012); Ague et al. (2013)**
48	**Garzón Massif, Colombia**	**Altenberger et al. (2012)**
49	**Schirmacher Hills, Dronning Maud Land, East Antarctica**	**Baba et al. (2006); Baba et al. (2010)**
50	**Central Indian Tectonic Zone, India**	**Bhandari et al. (2011); Bhowmick et al. (2014)**
51	**Anosyen domain, SE Madagascar**	**Jöns and Schenk (2008, 2011); Raith et al. (2008); Rakotonandrasana et al. (2010); Boger et al. (2012)**
52	**Lapland Granulite Belt (Por'ya Guba Block), Kola Peninsula, Russia**	**Bushmin et al. (2007); Lebedeva et al. (2010)**
53	**Tibetan Plateau, China**	**Hacker et al. (2000)**
54	**South Altay Belt, NW China**	**Chen et al. (2006); Li et al. (2010)**
55	**Chalcatzingo subvolcanic field, southern Mexico**	**Ortega-Gutiérrez et al. (2012)**
56	**El Toro, La Joya Honda and Los Palau, central Mexican plateau**	**Hayob et al. (1989); Hayob and Essene (1990)**
57	**Musgrave Province, central Australia**	**Smithies et al. (2011); Walsh et al. (2014); Gorczyk et al. (2015)**
58	Seram, eastern Indonesia	Pownall et al. (2014)

Typically, Mg–Al-rich rocks are volumetrically rare in nature (Chinner and Sweatman, 1968) and thus also in granulite facies terranes. Numerous origins have been proposed for Mg–Al-rich rocks, including metamorphism of hydrothermally altered mafic to ultramafic rocks or high-Mg clays/sediments (e.g. Vallance, 1967; Chinner and Sweatman, 1968; Chinner and Fox, 1974; Sheraton, 1980; Moine et al., 1981; Grew, 1982b; Reinhardt, 1987; Harley et al., 1990; Harley, 1993; Baba et al., 2008), syn-metamorphic metasomatism (e.g. Tilley, 1935; Herd et al., 1969; Sheraton et al., 1982; Warren and Hensen, 1987; Vry and Cartwright, 1994; Dunkley et al., 1999), metasomatic alteration of S-type granites (e.g. Möller et al., 2003) or formation of residual Mg–Al-rich domains in metasedimentary rocks via partial melting (e.g. Lal et al., 1978; Clifford et al., 1981; Droop and Bucher-Nurminen, 1984; Raith et al., 1997; Baba, 2003; Brandt et al., 2007). Kelsey et al. (2003a) argued that production of Mg–Al-rich rock compositions through melt loss is improbable, as although Fe does have a greater affinity for melt than Mg, very little Fe and Mg partition into melt (much less than 1%). Hence the cumulative effect on the bulk $X_{Mg,residue}$ (=MgO/(MgO + FeO)) would be minor, resulting in only a slight Mg-enrichment. This implies that in most cases, except perhaps for syn-metamorphic metasomatism, Mg–Al-rich rock compositions must source from protoliths enriched in Mg and Al (e.g. Grew, 1982b). The assertion that Mg–Al-rich rocks are commonly of sedimentary origin is based on the presence of detrital zircons (e.g. Drüppel et al., 2013), as well as on field associations with other, more obviously metasedimentary rock types (e.g. Ellis et al., 1980; Sheraton et al., 1980; Reinhardt, 1987; Sheraton et al., 1987).

A more comprehensive overview of the mineral assemblages that occur at and/or are diagnostic of UHT conditions is provided in Kelsey (2008) and Harley (2008). However, it is pertinent to restate here that the diagnostic mineral assemblages are sapphirine + quartz (Fig. 3a), high-Al orthopyroxene + sillimanite ± quartz (Fig. 3b, c) and osumilite-bearing (Fig. 3d) mineral assemblages, all of which occur in Mg–Al-rich rock compositions. Other sapphirine-bearing mineral assemblages such as sapphirine + cordierite (usually quartz-absent; Fig. 3c),

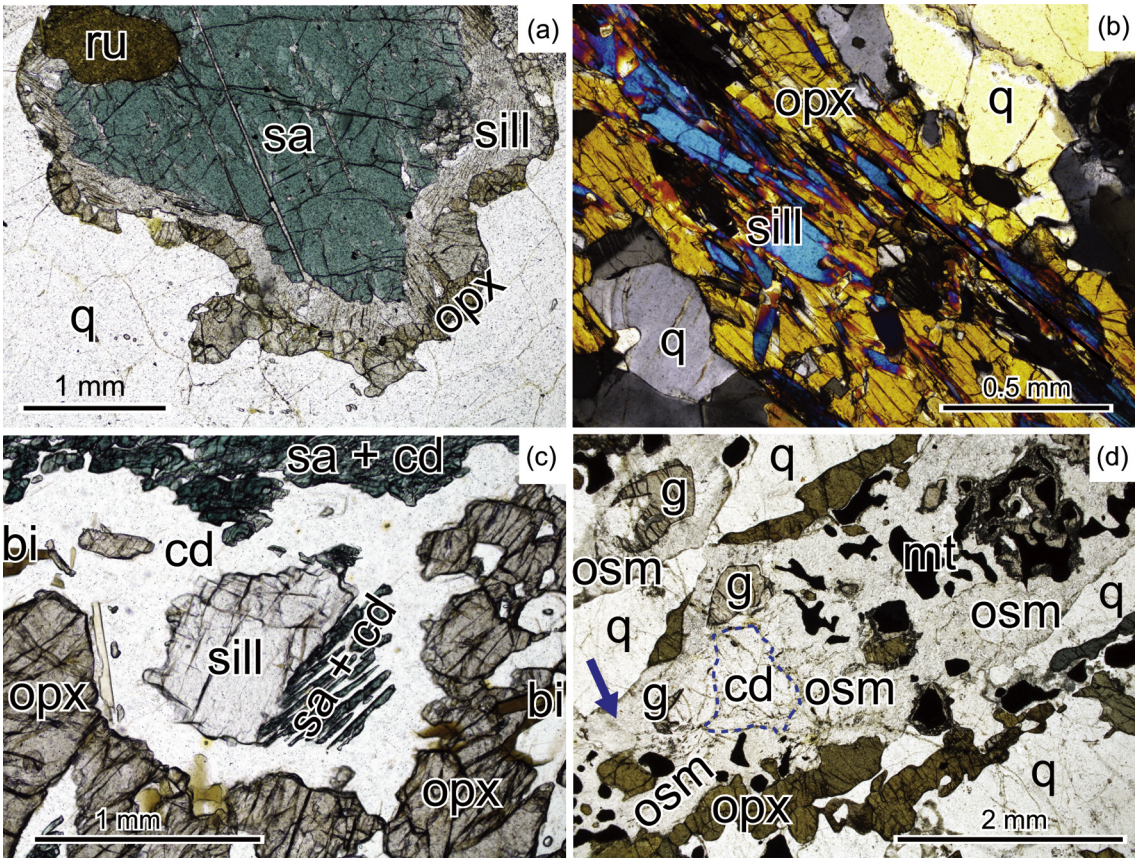

Figure 3. Minerals and mineral assemblages diagnostic of ultrahigh temperature metamorphic conditions. (a) Sapphirine + quartz. Photo depicts the frozen reaction sapphirine + quartz = orthopyroxene + sillimanite. Thus, the former stability of sapphirine + quartz in this example is inferred. Note presence of rutile, indicating relatively reduced rock composition. From Napier Complex, East Antarctica; (b) high-Al orthopyroxene + sillimanite + quartz. From Rauer Group, east Antarctica; (c) high-Al orthopyroxene + sillimanite with no quartz. The former stability of orthopyroxene with sillimanite is inferred on the basis of inferred reaction products (cordierite corona and symplectic sapphirine + cordierite corona) systematically separating orthopyroxene and sillimanite. From Rauer Group, East Antarctica; (d) osumilite as a corona between garnet, quartz, cordierite, coarse-grained orthopyroxene and magnetite. Osumilite has then reacted with magnetite to produce narrow coronae of garnet (on magnetite) and with coarse garnet to produce cordierite ± K-feldspar (narrow corona between garnet and osumilite). The blue arrow points to a region where some osumilite has commenced breakdown to the cordierite + K-feldspar + quartz ± orthopyroxene intergrowth that is more common (globally) in nature than fresh osumilite. Presence of magnetite indicates relatively oxidised rock composition. From Rogaland, Norway.

sapphirine + orthopyroxene ± biotite ± cordierite (quartz-absent), sapphirine + garnet and sapphirine ± spinel ± corundum are generally indicative of UHT conditions (Kelsey et al., 2005; Harley, 2008; Kelsey, 2008), particularly if silicate melt can be demonstrated to have been part of the assemblage and the amount of ferric iron in the minerals is low (approaching negligible). Sapphirine-absent mineral assemblages such as spinel + quartz, corundum + quartz and orthopyroxene + corundum (Halpin et al., 2007b) are suggestive rather than diagnostic of UHT conditions since there are usually additional elements such as Zn, Cr and Fe^{3+} that influence the *P*–*T* stability of minerals in these assemblages (e.g. Krogh, 1977; Stoddard, 1979; Annersten and Seifert, 1981; Vielzeuf, 1983; Harley, 1986; Hensen, 1986; Sandiford et al., 1987; Powell and Sandiford, 1988; Clarke et al., 1989; Schulters and Bohlen, 1989; Motoyoshi et al., 1990; Sengupta et al., 1991; Waters, 1991; Nichols et al., 1992; Harlov and Newton, 1993; Dasgupta et al., 1995; Guiraud et al., 1996a,b; Shaw and Arima, 1998; White et al., 2002; Ouzegane et al., 2003a; Kelly and Harley, 2004; Mouri et al., 2004; Kelsey et al., 2005; Tajčmanová et al., 2009; Diener and Powell, 2010; Belyanin et al., 2012b).

Sapphirine is typically indicative of high to extreme crustal temperatures (e.g. Hensen, 1971, 1972b, 1986, 1987; Hensen and Green, 1971, 1973; Chatterjee and Schreyer, 1972; Newton 1972; Newton et al., 1974; Ellis et al., 1980; Grew, 1980; Harley, 1985, 1986; Sandiford, 1985a; Sandiford et al., 1987; Powell and Sandiford, 1988; Bertrand et al., 1991; Motoyoshi et al., 1993; Audibert et al., 1995; Das et al., 2001, 2003; Hollis and Harley, 2003; Podlesskii et al., 2008; Podlesskii, 2010), with sapphirine stability in silica-undersaturated rock compositions expanded to lower temperatures than for sapphirine + quartz bearing assemblages (e.g. Schreyer and Seifert, 1969a; Seifert, 1974; Ackermand et al., 1975; Hensen, 1987; Kelsey et al., 2005). However, the presence of sapphirine in a rock does *not* immediately indicate that the rock—and terrane—necessarily records temperatures in excess of 900 °C. For example, Kruckenberg and Whitney (2011) and Goergen and Whitney (2012b) reported symplectic sapphirine in quartz-absent Mg–Al-rich rocks that attained temperatures of approximately 750 °C. In addition, there are a number of occurrences of sapphirine–spinel–biotite-bearing rocks (± corundum ± orthopyroxene ± plagioclase ± sillimanite ± garnet ± chlorite, and all quartz-absent) that appear to record temperatures less than 900 °C (e.g. Oliver and Jones, 1965; Kelsey et al., 2005; Prakash and Sharma, 2008; Raith et al., 2008; Sharma and Prakash, 2008; Nasipuri et al., 2009; Tsunogae et al., 2011; Prakash et al., 2013; Sarbajna et al., 2013). Ferric iron is known to expand the stability of sapphirine to lower temperatures (e.g. Caporuscio and Morse, 1978; Ellis et al., 1980; Steffen et al., 1984; Hensen, 1986; Sandiford et al., 1987; Powell and Sandiford, 1988; Das et al., 2001, 2003; Taylor-Jones and Powell, 2010; Wheller and Powell,

2014), and as such, ferric iron should be taken into account for all future thermobarometry on sapphirine-bearing rocks.

In addition to Mg–Al-rich rocks, sapphirine can occur with (or as) a variety of even more exotic minerals such as orthoamphibole, kornerupine, grandidierite, dumortierite, prismatine, surinamite and khmaralite (e.g. Wilson and Hudson, 1967; Balasubrahmanyan, 1976; Schreyer and Abraham, 1976; Lal et al., 1978; Grew, 1982b, 1983a,b; Herd et al., 1984; Lal et al., 1984; Nixon et al., 1984; Waters and Moore, 1985; Schumacher and Robinson, 1987; Droop, 1989; Grew et al., 1989; Goscombe, 1992; Grew et al., 1992; Vry, 1994; Vry and Cartwright, 1994; Baba et al., 2000; Sajeev et al., 2001; Sriramguru et al., 2002; Jöns and Schenk, 2004; Kelly and Harley, 2004; Sajeev and Osanai, 2004; Sajeev et al., 2004; Aleksandrov and Troneva, 2006; Tsunogae et al., 2007; Clark et al., 2009; Kanazawa et al., 2009; Kondou et al., 2009). However, *P–T* conditions are difficult to ascertain directly from the majority of such rocks and mineral assemblages as the thermodynamic properties of the borosilicates is not well known. Such mineral assemblages will not be considered further here, suffice it to say that if these mineral assemblages occur in the same terranes as diagnostic UHT mineral assemblages then robust *P–T* conditions can probably be estimated by inference.

Sapphirine can also be found in aluminous, commonly kyanite-bearing mafic rocks, including eclogites (e.g. Baldwin et al., 2007b; Groppo et al., 2007; Dawson and Harley, 2009; Morishita et al., 2009; Berger et al., 2010; Engvik and Austrheim, 2010; Engvik et al., 2011; Janák et al., 2012). Sapphirine is commonly part of a symplectic breakdown product of kyanite, developing during exhumation of high-pressure mafic rocks (e.g. Spear and Selverstone, 1983; Spear, 1988b; Godard and Mabit, 1998; Möller, 1999; Elvevold and Gilotti, 2000; Săbău et al., 2002; Moulas et al., 2013). These occurrences of sapphirine occur in calcic and quartz-absent rock compositions, where temperatures are not necessarily in the UHT realm.

Post-peak, or retrograde, cordierite is (almost) ubiquitous in UHT rocks, occurring as a corona (commonly symplectic) separating interpreted peak metamorphic minerals. This is typically related to many UHT rocks recording 'clockwise' *P–T* paths. However, the occurrence of retrograde cordierite is also documented from UHT rocks recording 'anticlockwise' *P–T* paths (e.g. Ellis, 1980; Ellis et al., 1980; Grew, 1980; Lal et al., 1987; Currie and Gittins, 1988; Sengupta et al., 1990; Dasgupta and Sengupta, 1995; Dasgupta et al., 1995; Bose et al., 2000). The most common occurrences of cordierite are as: (1) single mineral coronae mantling garnet or orthopyroxene or biotite or sapphirine or sillimanite; (2) sapphirine + cordierite symplectic coronae mantling sillimanite; (3) orthopyroxene + cordierite symplectic coronae mantling garnet; (4) spinel + cordierite symplectic coronae mantling sillimanite (Kelsey et al., 2005; Kelsey, 2008). The development of cordierite is commonly extensive enough to give fresh UHT rocks a characteristic bluish-purple colour in outcrop. At UHT conditions, Fe-rich metapelitic rocks will not be characterised by diagnostic mineral assemblages but will typically contain the mineral assemblage garnet + sillimanite + spinel + quartz ± magnetite ± rutile ± K-feldspar (Ellis et al., 1980; Sandiford, 1985a; Sarkar and Schenk, 2014; Walsh et al., 2014) with little or no biotite. For a more comprehensive account of mineral assemblages in UHT rocks and the use of mineral assemblages to identify UHT metamorphism refer to Kelsey (2008) and Harley (2008).

4.2. Mineral chemistry

UHT metamorphism is traditionally identified on the basis of mineral *assemblages* such as those outlined above. Mineral *chemistry* has not traditionally been (solely) used to identify UHT metamorphism because most ferro-magnesian minerals do not preserve compositions that are reflective of the extreme peak or near-peak thermal conditions because of the efficiency of Fe–Mg diffusion, which means that many Fe–Mg compositions record temperatures in the range 600–750 °C (e.g. Ellis and Green, 1985; Frost and Chacko, 1989; Harley, 1989; Spear, 1991; Fitzsimons and Harley, 1994; Pattison and Bégin, 1994; Pattison et al., 2003). Consequently, conventional Fe–Mg exchange-based thermobarometric techniques are generally not applicable for quantifying UHT conditions (e.g. Ellis and Green, 1985; Sandiford and Powell, 1986b). However, it is well documented that Al diffusivity is significantly slower than Fe and Mg (O'Hara, 1977; Frost and Chacko, 1989; Ashworth and Birdi, 1990; Ashworth et al., 1992; Ashworth, 1993; Fitzsimons and Harley, 1994; Pattison and Bégin, 1994) since Al diffusion in minerals is usually coupled via Tschermaks (or similar) exchange and/or Al is commonly bound to oxygen atoms as part of the framework of mineral lattices. The Al content of orthopyroxene is strongly temperature dependent and is controlled by the Tschermaks exchange vector (Fe,Mg)Si ↔ AlAl. As such, the Al content of orthopyroxene has been recognised as a case where mineral chemistry can be a reliable indicator of granulite facies temperatures in metasedimentary UHT rocks (Harley and Green, 1982; Harley, 1984, 2004; Aranovich and Podlesskii, 1989; Anovitz, 1991; Fitzsimons and Harley, 1994; Pattison and Bégin, 1994; Aranovich and Berman, 1997; Harley, 1998a; Kelsey et al., 2003a,b; Pattison et al., 2003; Halpin et al., 2007b; Kelsey, 2008). In the absence of any of the diagnostic mineral assemblages of Mg–Al-rich rock compositions, the Al-content of orthopyroxene in other metasedimentary mineral assemblages such as garnet + orthopyroxene has been used to identify UHT metamorphism (e.g. Harley, 1998a; Hacker et al., 2000; Nandakumar and Harley, 2000; Brandt et al., 2003; Pattison et al., 2003; Ishii et al., 2006; Tadokoro et al., 2007; Santosh et al., 2009c; Shimizu et al., 2009; Bhandari et al., 2011; Ague et al., 2013).

The combined or integrated Ca content of ternary feldspar (mesoperthite) has also been widely used to either independently identify or circumstantially support extreme thermal conditions in metasedimentary granulites (Sandiford, 1985a; Pilugin et al., 2009; Santosh et al., 2009c; Das et al., 2011; Jiao and Guo, 2011; Jöns and Schenk, 2011; Belyanin et al., 2012b; Guo et al., 2012; Liu et al., 2012; Ague et al., 2013; Sarkar and Schenk, 2014). More recently, the trace element concentration of Zr in rutile and Ti in zircon and quartz have been proposed as thermometers (Zack et al., 2004; Watson and Harrison, 2005; Wark and Watson, 2006; Watson et al., 2006; Ferry and Watson, 2007; Tomkins et al., 2007; Fu et al., 2008; Kawasaki and Osanai, 2008; Thomas et al., 2010; Huang and Audétat, 2012; Hofmann et al., 2013), and these have been applied to UHT granulites with mixed success (Baldwin et al., 2007a; Baldwin and Brown, 2008; Clark et al., 2009; Liu et al., 2010; Jiao et al., 2011; Kawasaki et al., 2011; Ague and Eckert, 2012; Altenberger et al., 2012; Kooijman et al., 2012; Liu et al., 2012; Ague et al., 2013; Korhonen et al., 2014). Titanium content in garnet and orthopyroxene (Kawasaki and Motoyoshi, 2007) has also seen limited application as a thermometer and barometer (Kawasaki et al., 2011; Ague and Eckert, 2012; Ague et al., 2013). Trace element thermometry is discussed in greater detail in section 6.

Of the studies tabulated in Table 1, approximately 40% document UHT metamorphic conditions in the absence of diagnostic Mg–Al-rich mineral assemblages. These studies report UHT metamorphism on the basis of: (1) spinel + quartz assemblages where the spinel has low Zn and Cr concentrations (Boger et al., 2012; Sarkar and Schenk, 2014; Walsh et al., 2014); (2) mafic granulites, some of which are garnet-bearing (Johnson et al., 2012) and/or

feature orthopyroxene + plagioclase symplectites (Sajeev et al., 2009) mantling garnet (Sajeev et al., 2007); (3) garnet + high-Al orthopyroxene assemblages (Bhandari et al., 2011; Altenberger et al., 2012); (4) reintegrated ternary feldspar compositions (see references in previous paragraph); (5) trace element thermometry (see references in previous paragraph); and (6) exsolved Ti ± Fe oxides in garnet, quartz, orthopyroxene, plagioclase and K-feldspar from quartzofeldspathic and garnet–sillimanite gneisses (Ague and Eckert, 2012; Ague et al., 2013). That UHT metamorphism has been reported on the basis of such numerous lines of evidence indicates that: (1) the petrologic/geologic community is eager to reinforce the acceptance of UHT as a 'normal' (i.e. not anomalous) type of metamorphism; and (2) UHT metamorphism is probably far more common and widespread than the rare occurrence of diagnostic mineral assemblages in Mg–Al-rich rocks indicates.

4.3. Volumetrically minor mineral assemblages and other proposed UHT localities

In a number of studies, UHT conditions have been inferred on the basis of rare composite sapphirine + quartz and/or spinel + quartz inclusions in porphyroblastic garnet (Sajeev et al., 2003; Tateishi et al., 2004; Tsunogae and Santosh, 2006, 2010, 2011; Tadokoro et al., 2007; Tsunogae et al., 2008; Yoshimura et al., 2008; Sato et al., 2009; Shimizu et al., 2009; Nishimiya et al., 2010; Sajeev et al., 2010). In some cases sapphirine and/or spinel is not in direct contact with quartz (e.g. Sato et al., 2009) and possibly formed in a silica-undersaturated micro-chemical domain. Harley (2008) argued that such examples of sapphirine (or spinel) + quartz should not be taken as *diagnostic* of UHT when the sapphirine and quartz are not observed as major minerals in a rock in demonstrably stable coexistence. Harley (2008) further stated that the use of (e.g.) sapphirine + quartz as a diagnostic assemblage should be restricted to cases such as the Napier Complex where both minerals are modally abundant. That the above occurrences of sapphirine and/or spinel and quartz occur inside garnet is intriguing, as the garnet porphyroblast is commonly many hundreds (or thousands) of times larger than the composite inclusion(s). An important implication must be that a significant portion of the growth of the garnet host post-dates the development of sapphirine + quartz (in particular) inclusions. The presence of these composite inclusions probably indicates either: (1) a polymetamorphic history for the rocks, whereby the inclusions are relics of an older history (Vernon, 1996); and/or (2) earlier prograde growth of Fe^{3+}-rich sapphirine or spinel (± Zn, Cr) with quartz (see next section for stability of such assemblages in ferric system), followed by growth of garnet later on the prograde path; and/or (3) that the composite inclusions (as opposed to a single included mineral) may represent the former presence of another mineral(s) that has been consumed. In summary, whereas these examples do preserve evidence for UHT mineral assemblages "sensu stricto", their interpretation is not necessarily straightforward.

Granulites of the Bohemian Massif (Saxon/Moldanubian zones) in eastern Europe have not been included in Table 1 as there is some dispute over whether the rocks—which are predominantly quartzofeldspathic gneisses—preserve UHT metamorphism, or whether the evidence is a relic from igneous crystallisation (e.g. Werner, 1987; Rötzler and Romer, 2001; Štípská and Powell, 2005; Hagen et al., 2008; O'Brien, 2008; Racek et al., 2008; Rötzler et al., 2008; Kotková and Harley, 2010). In addition, the pressures reported for these rocks (>15 kbar) are in excess of the normal range for UHT granulite metamorphism (see Fig. 1; Štípská and Powell, 2005; Tajčmanová et al., 2006; O'Brien, 2008). These granulites provide an example of how care is required in the interpretation of UHT conditions if diagnostic rock compositions (Mg–Al-rich) and mineral assemblages are not present.

5. *P–T* stability of UHT mineral assemblages

Constraining the *P–T* stability of UHT mineral assemblages has a long history dating back to the 1960s and 1970s (Schreyer and Seifert, 1969a,b; Hensen and Green, 1970, 1971, 1972, 1973; Hensen and Essene, 1971; Hensen, 1972a,b; Newton, 1972; Newton et al., 1974). The experimental studies of Hensen and Green were particularly significant as they resulted in the development of a univariant reaction grid (i.e. '*P–T* grid')—notionally in the chemical system FeO–MgO–Al_2O_3–SiO_2 (FMAS)—that was widely used until the mid-2000s to interpret the *P–T* evolution of UHT mineral assemblages, and they also introduced pseudosections (e.g. Hensen, 1971), which are slices, depicted graphically, through a multivariate phase diagram where the phases are not all in the plane of the section (Powell et al., 2005). Uncertainty regarding the locations of the invariant points and univariant reactions in the (notionally) FMAS system *P–T* grid (Hensen and Green, 1971, 1973; Harley, 1989, 1998b; Hensen and Harley, 1990; Bertrand et al., 1991; Hollis and Harley, 2002) was reconciled by quantifying the effect H_2O has on controlling the location of phase equilibria (Kelsey et al., 2004; Baldwin et al., 2005). Calculated phase equilibria (e.g. Berman et al., 1987; de Capitani and Brown, 1987; Spear, 1988a,b; Spear and Cheney, 1989; Spear and Menard, 1989; Frey et al., 1991; Spear et al., 1991, 1999; Connolly, 1995; Spear and Markussen, 1997; Simpson et al., 2000), especially in the form of calculated pseudosections (e.g. Spear and Selverstone, 1983; Connolly, 1990; Powell and Holland, 1990; Will et al., 1990; Xu et al., 1994; Stüwe and Powell, 1995; Mahar et al., 1997; Meyre et al., 1997; White et al., 2000, 2001, 2002; Guiraud et al., 2001; Kerrick and Connolly, 2001; Connolly and Petrini, 2002; White and Powell, 2002; Kelsey et al., 2004, 2005, 2008; Connolly, 2005; Powell et al., 2005; Gaidies et al., 2006, 2008, 2011; Caddick and Thompson, 2008; Diener et al., 2008a; Caddick et al., 2010; de Capitani and Petrakakis, 2010; Spear, 2010; Spear and Pyle, 2010; Taylor-Jones and Powell, 2010; Diener and Powell, 2012; Green et al., 2012; Moynihan and Pattison, 2013; White et al., 2014a,b), have revolutionised the way in which metamorphic analysis of terranes is undertaken (see Kelsey (2008) for more extensive detail on the positive attributes of calculated pseudosections and history of experimental work on UHT mineral assemblages). It is now entrenched that calculated phase diagrams are part of routine analysis of metamorphic rocks, usually along with geochronology (see section 9). Internally consistent thermodynamic data sets for phase end-members provide the crucial link between experimental and natural mineral assemblage data and calculated phase diagrams (Berman et al., 1985; Holland and Powell, 1985, 1998, 2011; Berman, 1988; Sack and Ghiorso, 1989; Fei and Saxena, 1990; Holland and Powell, 1990; Gottschalk, 1997; Stixrude and Lithgow-Bertelloni, 2005).

5.1. Thermodynamic model for ferric sapphirine

One of the most significant advances to occur in recent years has been the development—already with numerous iterations—of a thermodynamic mixing ('*a–x*') model for sapphirine that incorporates ferric iron (Taylor-Jones and Powell, 2010; Wheller and Powell, 2014). It has been recognised for many years that natural sapphirine commonly contains appreciable ferric iron (e.g. McKie, 1963; Leong and Moore, 1972; Caporuscio and Morse, 1978; Steffen et al., 1984; Hensen, 1986; Ackermand et al., 1987; Herd et al., 1987; Sandiford et al., 1987; Currie and Gittins, 1988; Powell and Sandiford, 1988; Christy, 1989; Gnos and Kurz, 1994;

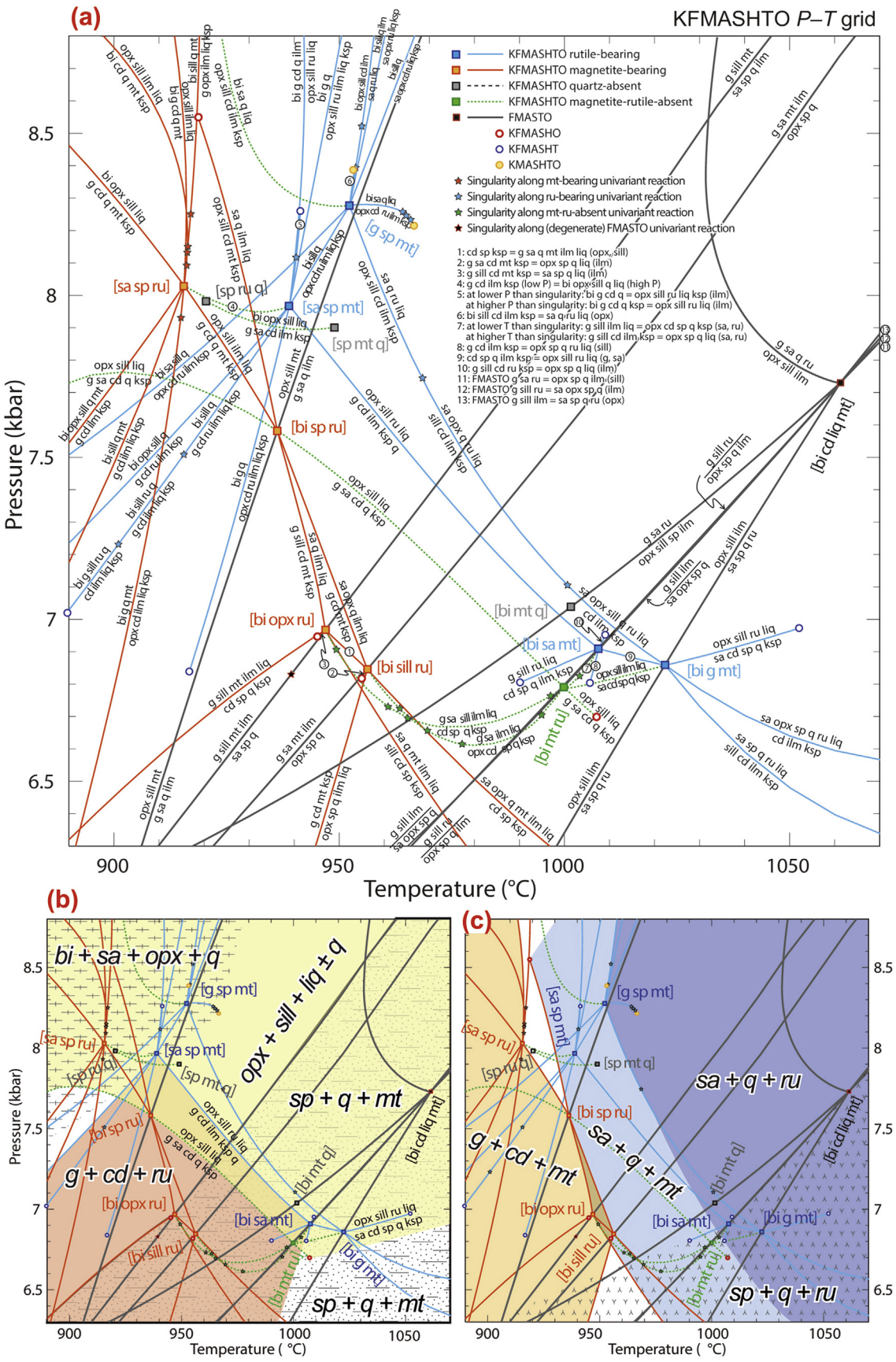

Figure 4. (a) Pressure–temperature (*P*–*T*) grid (petrogenetic grid) showing univariant reaction lines and invariant reaction points for the KFMASHTO model chemical system, calculated using THERMOCALC 3.41 and the new ds62 thermodynamic data set of Holland and Powell (2011). The grid is analogous to that of Wheller and Powell (2014) but here

Korhonen et al., 2012b), and that the *P–T* stability range of sapphirine (as well as spinel and to a lesser degree orthopyroxene), is likely to be strongly influenced by the oxidation state of the rock (e.g. Caporuscio and Morse, 1978; Grew, 1980; Hensen, 1986; Powell and Sandiford, 1988; Sengupta et al., 1991; White et al., 2002; Taylor-Jones and Powell, 2010). The inability to account for the stabilising effect of Fe^{3+} on sapphirine has long been viewed as a significant impediment to rigorously evaluating the evolution of sapphirine-bearing UHT rocks, particular for mineral assemblages containing magnetite and/or ilmenite-haematite solid-solution (e.g. Hensen, 1986; Hensen and Harley, 1990; Harley, 2004; Harley, 2008). Expansion of the FMAS (Hensen, 1971, 1987), FMASH (Bertrand et al., 1991) and KFMASH (Audibert et al., 1995; Carrington and Harley, 1995a,b; Kelsey et al., 2004, 2005) chemical systems historically used to interrogate the metamorphic evolution of UHT granulites to include Fe^{3+} (as 'O' or Fe_2O_3) and Ti (as TiO_2) allows for Fe-Ti oxides magnetite, ilmenite-haematite and rutile to be included as an integral part of the phase assemblage analysis (Hensen, 1986; Sandiford et al., 1987; Powell and Sandiford, 1988; Taylor-Jones and Powell, 2010; Korhonen et al., 2012b; Wheller and Powell, 2014), as well as the incorporation of Fe^{3+} and Ti into the *a–x* models of major silicate phases (White et al., 2000; White et al., 2002; White et al., 2007; White et al., 2014a).

Expansion to FMASO, FMASTO and KFMAS(H)TO involves an 'inversion' of the underlying FMAS univariant phase reaction (*P–T*) grid, in that a different set of FMAS-based invariant points become stable (Vielzeuf, 1983; Hensen, 1986; Powell and Sandiford, 1988; Sengupta et al., 1991; Das et al., 2001, 2003; Taylor-Jones and Powell, 2010), allowing for 'alternative' mineral assemblages such as orthopyroxene + sillimanite + spinel + quartz to become stable (Annersten and Seifert, 1981; Das et al., 2003). With the ferric sapphirine model, it is now possible to rigorously explore the *P–T* conditions and constrain the *P–T* evolution of rocks across the entire spectrum of oxidation state, from highly oxidised, magnetite- and/or haematite-bearing sapphirine granulites (e.g. Morse and Talley, 1971; Caporuscio and Morse, 1978; Grew, 1982b; Sandiford et al., 1987; Currie and Gittins, 1988; Kamineni and Rao, 1988a,b; Arima and Gower, 1991; Bose et al., 2000; Das et al., 2003; Korhonen and Stout, 2004) to reduced, rutile-bearing sapphirine granulites (e.g. Ellis, 1980; Grew, 1980, 1982a; Sandiford, 1985a; Schmitz and Bowring, 2003).

5.2. *P–T grid for Mg–Al-rich rocks in KFMASHTO (KFMASH + TiO_2 + Fe_2O_3) model chemical system*

In this and the next subsection, the model chemical system KFMASHTO is used to present and discuss calculated phase equilibria. The KFMASHTO system, rather than the larger (Mn)NCKFMASHTO system, is used here as KFMASHTO is the largest model chemical system in which all the 'backbone' univariant and invariant reactions—i.e. those depicted on a *P–T* grid—that underpin higher-variance phase equilibria (of pseudosections) can be graphically depicted and best understood. In addition, presenting calculations in KFMASHTO allow for direct correlation with calculations presented in the study of Korhonen et al. (2012b) as well as for easier comparison with the smaller KFMASH system. In applying phase equilibria to an actual, specific rock, the largest model chemical system possible should be used (see subsection 7.2). As such, the phase equilibria presented here are for instructive purposes, as explained below.

The most widely used internally consistent thermodynamic data set used for calculating the stability of mineral assemblages observed in rocks is that generated and regularly updated by Tim Holland and Roger Powell (Holland and Powell, 1985, 1990, 1998, 2011). This data set can be utilised for petrological forward modelling using several codes (THERMOCALC, Perple_X, Theriac Domino) that are widely used by the petrological community (Powell and Holland, 1988; Powell et al., 1998; Connolly and Petrini, 2002; de Capitani and Petrakakis, 2010). The thermodynamic data set released in 2011 ('ds6', Holland and Powell, 2011) is for use with revised activity–composition (*a–x*) models (Powell et al., 2014; White et al., 2014a), the first of which became available for public use late in 2013. However, *a–x* models for numerous phases are still being finalised and are not yet available. Principally, in the context of UHT metamorphism, osumilite is among these phases. Nevertheless, KFMASHTO (± CaO) *a–x* models for all other phases of interest to the study of 'pelitic' UHT rocks are now available for use with ds6 (Wheller and Powell, 2014; White et al., 2014a). Of import to investigating UHT rocks, the redevelopment of the Holland and Powell thermodynamic data set involves two features: (1) placing sapphirine in the same thermodynamic data set (i.e. ds6) as all other phases, negating the previous need to use a separate data set (ds55s) for calculations involving sapphirine (Holland and Powell, 2011; Wheller and Powell, 2014); and (2) updating and/or expanding the *a–x* models for phases for use with ds6, thus superceding the *a–x* models used for calculating the sapphirine-bearing phase diagrams in Ouzegane et al. (2003a), Kelsey et al. (2004, 2005), Taylor-Jones and Powell (2010) and Korhonen et al. (2012b). A very recent comparison of pseudosections calculated using the Holland and Powell ds55s versus ds6 thermodynamic datasets is presented in a study on UHT metamorphism in the Eastern Ghats Province (Korhonen et al., 2014). Their Figs. 1 and 2 show that for the particular bulk composition used, sapphirine, orthopyroxene and orthopyroxene + sillimanite stability is more restricted in calculations with the ds6 data set. Overall, the ferromagnesian minerals are slightly more Mg-rich in the pseudosection calculated with ds6 and that pseudosection allows for greater compatibility with the sequence of mineral assemblage evolution in their studied rock sample (Korhonen et al., 2014).

As outlined in Kelsey (2008) and in Wheller and Powell (2014), the thermodynamics of sapphirine are ultimately still limited by a lack of detailed petrological experiments that monitor its composition as a function of pressure, temperature and composition. Nevertheless, the current ferric sapphirine model is an important step, particularly as the thermodynamic properties of phase end-members in internally-consistent data sets are correlated to each other. Therefore, in principal and in practice, the thermodynamics of sapphirine can be tied to thermodynamic information from end-members of other phases that are better thermodynamically

shows all quartz-bearing phase equilibria, i.e. no phases are 'in excess'. The thermodynamic model for sapphirine was calibrated on the basis of stable sapphirine + quartz + biotite bearing mineral assemblages Rutile-bearing equilibria shown in blue are offset to higher temperature than magnetite-bearing equilibria shown in red. Dashed green equilibria are magnetite- and rutile-absent and provide the link from smaller chemical systems to KFMASHTO as well as the link between rutile-bearing and magnetite-bearing equilibria. The position of quartz-absent invariant points are shown in grey, but the univariant reaction lines emanating from each of these invariant points are not shown for the sake of clarity. Thick grey reaction lines are FMASTO univariant equilibria that are degenerate in KFMASHTO. Fluorine in biotite will stabilise biotite-bearing equilibria to higher temperatures than calculated here. Osumilite is not included in the calculations. Insets (b) and (c) are shaded to highlight the potential stability range of numerous UHT mineral assemblages found in Mg–Al-rich rocks. Since *P–T* grids show the potential stability of mineral assemblages and not the actual stability for a specific rock composition, *P–T* grids should not be used to constrain the *P–T* history of specific rocks. In (b) the yellow shading of opx + sill + liq ± q stability overlaps with the light-red shading of g + cd + ru stability, producing an orange colour. In (c) the light blue shading of sa + q + mt stability continues underneath the dark blue shading of sa + q + ru stability; and the orange shading for g + cd + mt stability overlaps slightly with sa + q + mt stability, producing a narrow region of brown-orange shading.

constrained (Holland and Powell, 2011; Powell et al., 2014; White et al., 2014a). The phase diagrams presented in Figs. 4, 5 and 6 were calculated using THERMOCALC v3.41 and the thermodynamic data set ds62 (filename tc-ds62.txt).

Wheller and Powell (2014) present a KFMASHTO *P*–*T* grid for sapphirine ± biotite-bearing UHT phase assemblages that were calculated using the new ds6 thermodynamic data set as well as the new *a*–*x* model formulations. A recalculated version of that grid, calculated using the publically released data set 'ds62', and showing all the quartz-bearing invariant and univariant reactions (i.e. no phases in excess) is presented in Fig. 4a. One of the most notable aspects of the *P*–*T* grid is the temperature location of sapphirine + quartz bearing phase equilibria, which are shifted down-temperature, as expected, in KFMASHTO (Fig. 4a; Korhonen et al., 2012b; Wheller and Powell, 2014) by comparison with the smaller FMAS and KFMASH systems (e.g. Kelsey et al., 2004; Taylor-

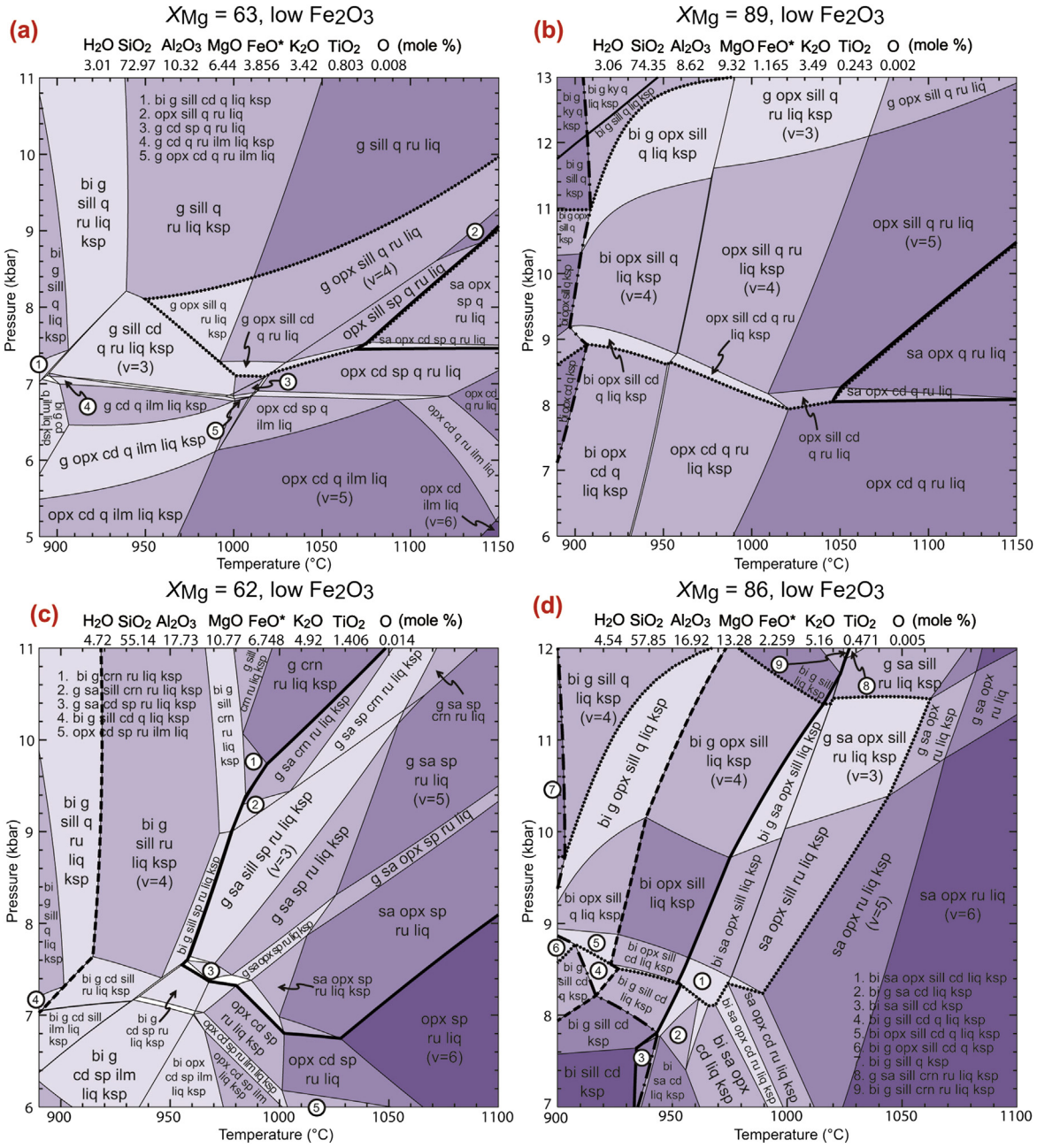

Figure 5. Pressure–temperature (*P*–*T*) pseudosections for low Fe_2O_3 (i.e. reduced) bulk compositions calculated for the KFMASHTO model chemical system, using THERMOCALC 3.41 and the ds62 thermodynamic data set of Holland and Powell (2011). The KFMASH part of the bulk composition for each of (a) to (d) is the same as the corresponding (a) to (d) pseudosections in Kelsey (2008) to facilitate comparison between KFMASH and KFMASHTO. Bold dotted line outlines limit of orthopyroxene + sillimanite ± quartz bearing assemblages, bold line outlines limit of sapphirine bearing assemblages and dash–dot line denotes the solidus. In reduced compositions sapphirine + quartz stability is restricted to extreme temperatures, for example >1050 °C in (a) and (b). Sapphirine + quartz stability does not necessarily require very high X_{Mg} (see (a)). The absence of quartz allows sapphirine stability to expand down temperature, for example to approximately 950 °C in (c) and (d). Stability of orthopyroxene + sillimanite bearing assemblages shrinks in *P*–*T* extent as X_{Mg} decreases. Orthopyroxene + sillimanite + spinel assemblages are stable in the iron-rich composition of (a). The addition of TiO_2 and Fe_2O_3 to KFMASH serves to greatly enhance the stability of spinel-bearing assemblages – compare (a) and (c) with (a) and (c) in Fig. 10 of Kelsey (2008) and restrict the stability of sapphirine to higher temperatures than in KFMASH. Rather than the KFMASHTO system used for calculations presented here, the larger NCKFMASHTO model chemical system should be used for constraining the *P*–*T* evolution of specific rocks.

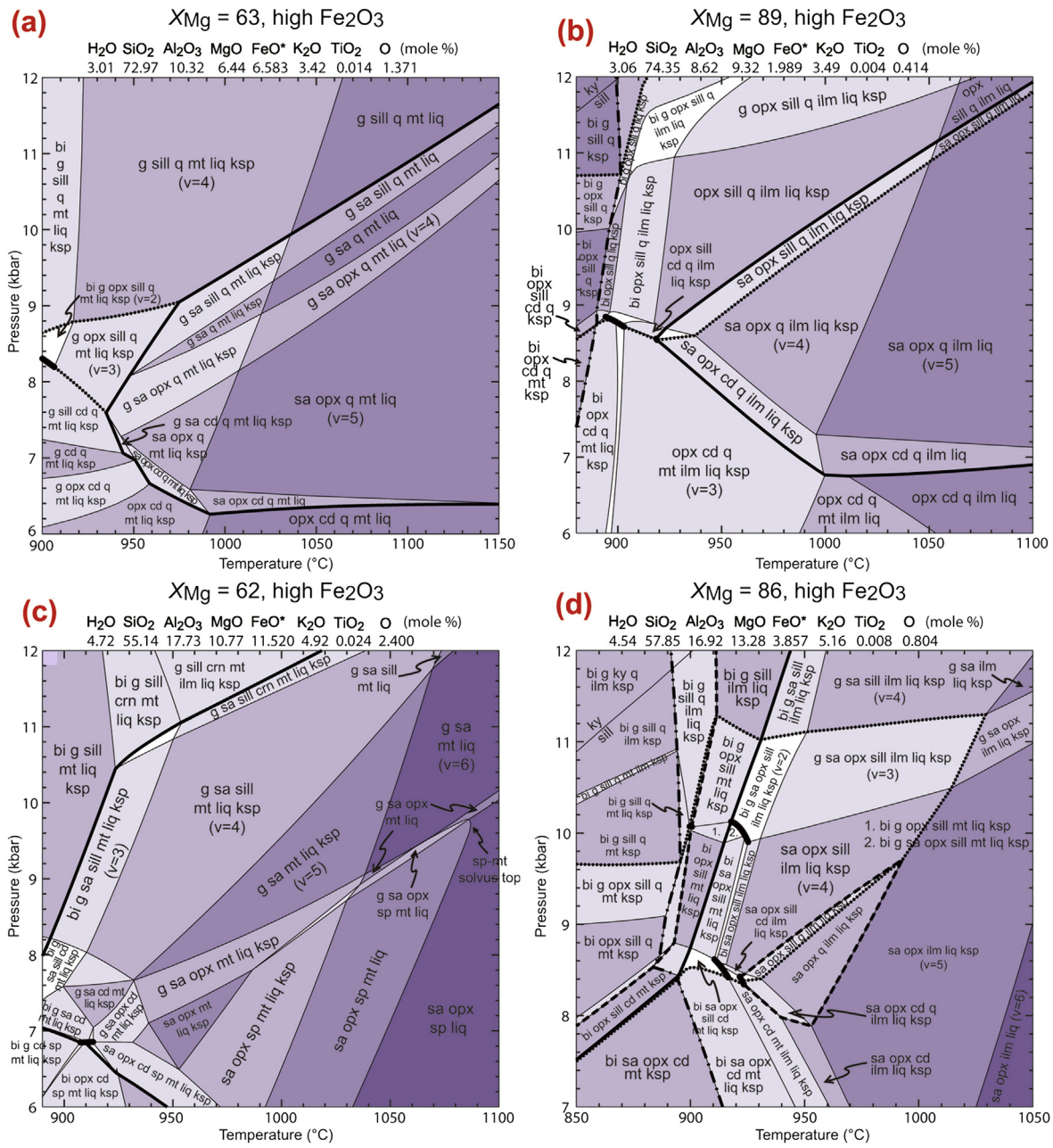

Figure 6. Pressure–temperature (P–T) pseudosections for high Fe_2O_3 (i.e. oxidised) bulk compositions calculated for the KFMASHTO model chemical system, using THERMOCALC 3.41 and the ds62 thermodynamic data set of Holland and Powell (2011). The KFMASH part of the bulk composition for each of (a) to (d) is the same as the corresponding (a) to (d) pseudosections in Kelsey (2008) to facilitate comparison between KFMASH and KFMASHTO. Bold dotted line outlines limit of orthopyroxene + sillimanite ± quartz bearing assemblages, bold line outlines limit of sapphirine bearing assemblages, dashed line outlines limit of quartz stability and dash–dot line denotes the solidus. Sapphirine + quartz stability is expanded down-temperature (compared to KFMASH and Fig. 5) to between 900 and 950 °C in oxidised compositions in (a) and (b). Sapphirine + quartz stability does not necessarily require very high X_{Mg} (see (a)), but sapphirine + quartz + magnetite stability occurs over a wider range of P–T space in lower X_{Mg} compositions (compare (a) with (b) and (d)). The absence of quartz allows sapphirine stability to expand to temperatures less than 900 °C, (c) and (d), even in the presence of silicate melt (c). Stability of orthopyroxene + sillimanite ± quartz bearing assemblages shrinks as a function of decreasing X_{Mg} (compare (b) to (d) to (a) to (c)), and overall has a more restricted stability in oxidised compositions compared to reduced compositions (compare with Fig. 5). This is due to the enhanced stability of sapphirine in oxidised (this Figure) compared to reduced (Fig. 5) compositions. Contrary to intuition, spinel stability is not greatly enhanced in oxidised compositions compared to reduced compositions (compare with Fig. 5). Rather, oxidised compositions preferentially expand the stability of sapphirine ± orthopyroxene bearing assemblages instead of spinel bearing assemblages (e.g. compare Fig. 5a and 5c with (a) and (c) here). Rather than the KFMASHTO system used for calculations presented here, the larger NCKFMASHTO model chemical system should be used for constraining the P–T evolution of specific rocks.

Jones and Powell, 2010). As predicted theoretically (Hensen, 1986; Powell and Sandiford, 1988), magnetite-bearing phase equilibria (in red) occur at lower temperatures than rutile-bearing phase equilibria (in blue) (Fig. 4a). The magnitude of the down-temperature shift of the magnetite + sapphirine + quartz bearing equilibria (Fig. 4a; Korhonen et al., 2012b; Wheller and Powell, 2014) in comparison to Fe^{3+}-absent sapphirine + quartz equilibria in FMAS (Kelsey et al., 2004; Taylor-Jones and Powell, 2010) and KFMASH (Kelsey et al., 2004) is approximately 50 and 70 °C, respectively, using the analogous [sp] invariant point in each model system as a reference.

One of the reasons why the KFMASHTO sapphirine + quartz bearing equilibria occur towards the lower temperature end of the

UHT spectrum (Fig. 4a; Korhonen et al., 2012b; Wheller and Powell, 2014) is that the enthalpy of formation of the Fe–Mg-ordered sapphirine end-member 'ospr' was set (by adjusting the DQF parameter in the *a–x* description of ferric sapphirine) such that stable biotite + sapphirine + quartz bearing assemblages are allowed in the *P–T* grid (Korhonen et al., 2012b; Wheller and Powell, 2014), on the basis that such assemblages occur naturally at Wilson Lake, Labrador, Canada (Korhonen et al., 2012b). Such 'low' temperatures for sapphirine + quartz-bearing equilibria would appear to conflict with the natural rock record in which sapphirine + quartz assemblages are very rare. However, it must be remembered that *P–T* grids project all possible rock compositions in a given system, here KFMASHTO, and therefore define the *absolute* stability of a phase assemblage such as sapphirine + quartz. By contrast, in application to a specific rock (i.e. with a single composition), a calculated *P–T* pseudosection will display the *actual* stability of a phase assemblage as stable phase assemblage fields. The *actual* stability of a particular assemblage in *P–T* space could be quite different to the *absolute* stability, as highlighted by the following example. Consider the K-feldspar absent KFMASHTO univariant reaction bi + opx + sill + cd + ilm (low-temperature side) = sa + q + ru + liq (high-temperature side) that extends up-pressure from the blue [g sp mt] invariant point in Fig. 4a. This univariant reaction defines that sapphirine, quartz, rutile and silicate melt together can stably coexist to temperatures *no lower* than approximately 950 °C, and therefore defines the *absolute* stability limit of this assemblage for all possible KFMASHTO compositions. However, by contrast, the single KFMASHTO composition used to calculate the *P–T* pseudosection in Fig. 5b shows that for this bulk composition sapphirine, quartz, rutile and silicate melt together will only stably coexist at temperatures in excess of approximately 1045 °C. Therefore, this example illustrates that the *actual* stability of a phase assemblage defined for a single (rock) composition can be very different to that governed by the *P–T* grid, and reinforces the crucial and fundamental point that *P–T* grids should not be used to interpret the *P–T* evolution of specific rocks. Nevertheless, the calculated phase equilibria in Fig. 4a do place sapphirine + quartz bearing assemblages in close (thermal) proximity to the 'orthopyroxene + sillimanite + quartz in' invariant point [sa sp ru] (equivalent to point (b) in Fig. 3 in White et al. (2014a) and [sa osm sp] and [os] in KFMASH in Kelsey et al. (2004) and Carrington and Harley (1995a,b), respectively), which means there is substantially more overlap of orthopyroxene + sillimanite ± quartz bearing assemblages with sapphirine + quartz bearing assemblages in KFMASHTO (Fig. 4b, c) compared to Fe^{3+}-Ti-absent systems. In nature orthopyroxene + sillimanite ± quartz bearing assemblages are far more common than sapphirine + quartz bearing assemblages (Kelsey et al., 2003a, 2004), and sapphirine + quartz assemblages appear to be restricted to terranes that record near-isobaric cooling *P–T* paths (Kelsey et al., 2003a). Other key features of the *P–T* grid, Fig. 4a, are:

(1) The triangular geometry of spinel-, orthopyroxene- and sillimanite-absent invariant points, as [bi sp ru], [bi opx ru] and [bi sill ru], respectively, are retained from the familiar triangular invariant geometry of the FMAS system (Hensen, 1971, 1986; Harley, 1989, 1998b; Hensen and Green, 1973; Kelsey et al., 2004; Kelsey, 2008; Taylor-Jones and Powell, 2010);
(2) High-temperature rutile-bearing invariant points [bi sa mt] and [bi g mt] reflect the stability of 'alternate' invariant points (e.g. Vielzeuf, 1983) relating to a topological inversion (Hensen, 1986; Powell and Sandiford, 1988) that occurs in the smaller FMASO system (Taylor-Jones and Powell, 2010). The third invariant point resulting from topological inversion, [cd] (Hensen, 1986; Powell and Sandiford, 1988), occurs as a degenerate FMASTO invariant point [bi cd liq mt] in KFMASHTO;
(3) Rutile–magnetite-absent univariant reactions (green lines) link rutile-bearing and magnetite-bearing phase equilibria;
(4) Biotite + spinel bearing equilibria are not predicted for quartz-bearing or quartz-absent equilibria;
(5) Orthopyroxene + sillimanite + spinel + quartz bearing assemblages (Annersten and Seifert, 1981; Vielzeuf, 1983; Das et al., 2001, 2003) are calculated to only occur in rutile-bearing assemblages emanating from the [bi g mt] and [bi sa mt] invariant points in the lower right-hand corner at high *T*/*P*. Many of the orthopyroxene + sillimanite + spinel + quartz bearing assemblages occur as FMASTO (degenerate KFMASHTO) univariant reactions. This assemblage cannot occur in the smaller FMAS and KFMASH systems;
(6) Univariant reactions that are analogous, differing only by rutile versus magnetite, mostly occur emanating from [sa sp ru] and [sa sp mt]. The rutile-bearing equivalent to the garnet-absent univariant reaction extending up-pressure from [bi sp ru] (i.e. opx + sill + cd + mt + ksp = sa + q + ilm + liq) links [g sp mt] and [bi g mt];
(7) Quartz-absent, sapphirine-bearing invariant points occur slightly down temperature from the 'equivalent' quartz-sapphirine-bearing invariant points, analogous to the topological pattern calculated by Kelsey et al. (2005).

The *absolute* stability of some key phase assemblages in UHT rocks are highlighted using different coloured shading in Fig. 4b, c (see also Wheller and Powell, 2014). The significant overlap of orthopyroxene + sillimanite + silicate melt ± quartz with sapphirine + quartz can be seen (compare yellow shading in Fig. 4b with blue shading in Fig. 4c). Fig. 4c shows that sapphirine + quartz + magnetite assemblages (lighter blue shading) have an absolute stability that is expanded to lower temperatures than for sapphirine + quartz + rutile assemblages (darker blue shading). The stability of biotite + sapphirine + quartz (with orthopyroxene) assemblages (natural Wilson Lake assemblages; Korhonen et al., 2012b) are shown in Fig. 4b by cross-hatched shading.

Informative orthogonal compatibility diagrams are presented by Korhonen et al. (2012b) (their Fig. 3) and Wheller and Powell (2014) (their Figs. 3, 4, 7). Each compatibility diagram is calculated for a fixed *P–T* condition and allows phase assemblages to be monitored as a function of variations to (rock) composition. The compatibility diagrams all convey that sapphirine + quartz can occur in ferrous-rich (approximately X_{Mg} = MgO/(MgO + FeO) = 0.2–0.6) rock compositions if the composition is also moderately to highly oxidised. Sapphirine + quartz is restricted to more magnesian (approximately $X_{Mg} > 0.5$–0.6) rock compositions if the composition is also more reduced. In relation to *P–T* space, what this means is that reduced sapphirine + quartz (± rutile) assemblages will tend to occur at higher temperatures and pressures than more oxidised sapphirine + quartz assemblages. Indeed, this is what calculated pseudosections show (Figs. 5 and 6 and see next subsection).

5.3. Calculated pseudosections

Natural mineral assemblages in rocks typically evolve via multivariant (variance ≥2) or *continuous* reactions rather than via *discontinuous* in-/uni-variant reactions that characterise *P–T* grids (e.g. Hensen, 1971; Stüwe and Powell, 1995; Kelsey et al., 2003a,b, 2005; Kelsey, 2008). Continuous reaction progress for a given (rock) composition is depicted in *P–T–composition* space by a map of phase assemblage stability *fields*, i.e. a pseudosection. Therefore, pseudosections, rather than *P–T* grids, are a far better way to investigate/

constrain the *P–T* history of rocks. However, there are differences in the approach used to model prograde versus retrograde parts of the metamorphic evolution of rocks—especially granulite facies rocks—by means of pseudosections, as outlined in section 7.

A series of calculated KFMASHTO *P–T* pseudosections are presented in Figs. 5 and 6 to convey the influence of oxidation on the stability of key UHT phase assemblages. The KFMASH part of the composition for each pseudosection was taken directly from the KFMASH pseudosections in Fig. 10 in Kelsey (2008) to allow for direct comparison of results. Fig. 5 shows pseudosections calculated for reduced (low O) and high TiO_2 compositions whereas Fig. 6 shows pseudosections calculated for highly oxidised (high O) and low TiO_2 compositions. The TiO_2 and O content used for each pseudosection is such that the ratio of TiO_2 : O ratio is identical in all four of the reduced compositions (Fig. 5), and is similarly identical, but a different value to the ratio of Fig. 5, in all four of the oxidised compositions (Fig. 6). This approach was used for each figure in order to negate differences in oxidation impacting upon comparisons between pseudosections in a given figure. The amount of FeO* (= FeO + 2×O) in all eight compositions in Figs. 5 and 6 is calculated such that the same X_{Mg} ratio is retained from the corresponding KFMASH composition in Fig. 10 in Kelsey (2008), again for ease of comparison. Enough O was chosen to enable stability of sapphirine + quartz + magnetite assemblages in at least some part of *P–T* space in Fig. 6. Nearly 36% of total iron is Fe_2O_3 for Fig. 6, which represents extremely oxidised metapelitic compositions.

P–T pseudosections for reduced compositions, Fig. 5, do not differ greatly from those in Kelsey (2008). This is an unsurprising result given that the KFMASH system (Kelsey, 2008) is a totally reduced system. The biggest changes in KFMASHTO include stability of orthopyroxene + sillimanite + spinel + quartz bearing assemblages (not present in any purely KFMASH compositions) in the $X_{Mg} = 63$ composition (Fig. 5a) and enhanced stability of garnet to lower pressures (Fig. 5a, b, d), biotite to higher temperatures (Fig. 5d) and spinel to higher pressures and lower temperatures (Fig. 5a, c). In these compositions sapphirine + quartz bearing assemblages are calculated to stabilise at approximately the same temperature in the $X_{Mg} = 63$ (Fig. 5a) and $X_{Mg} = 89$ (Fig. 5b) compositions, supporting the results from orthogonal compatibility diagrams summarised above. Sapphirine + quartz bearing assemblages do not develop in the $X_{Mg} = 62$ and 86 compositions (Fig. 5c, d) as the SiO_2 contents are too low. More magnesian and/or SiO_2-rich compositions (Fig. 5a, b, d) are characterised by widespread orthopyroxene + sillimanite ± quartz stability, whereas garnet is much more prevalent in lower X_{Mg} compositions (Fig. 5a, c).

P–T pseudosections for oxidised compositions, Fig. 6, differ markedly from those in Fig. 5 and therefore also those in Kelsey (2008). Possibly the most notable change is that sapphirine + quartz bearing assemblages are stabilised to considerably lower temperatures in the oxidised compositions (compare 920–935 °C in Fig. 6a, b with 1045–1070 °C in Fig. 5a, b). This is due to the (purposely done) extremely oxidised nature of the compositions used for Fig. 6. Sapphirine + quartz bearing assemblages are additionally stabilised in the oxidised $X_{Mg} = 86$ composition (Fig. 6d) compared to being absent in the equivalent reduced composition (Fig. 5d). As a result of the significant down-temperature expansion of sapphirine + quartz bearing assemblages in oxidised $X_{Mg} = 63$ and 89 compositions (Fig. 6a, b) the stability of orthopyroxene + sillimanite + quartz assemblages is correspondingly restricted. Garnet + sapphirine + quartz bearing assemblages are calculated in oxidised, high silica compositions (Fig. 6a, b) but not in reduced, high silica compositions (Fig. 5a, b). Sapphirine + quartz + magnetite bearing assemblages are calculated to be very restricted for the compositions used here, despite the extremely oxidised nature of the compositions. A possible reason for such limited stability of this assemblage could relate to the very low TiO_2 contents of these Fig. 6 compositions, in that magnetite (and ilmenite) require higher Ti to stabilise over larger parts of *P–T* space at these conditions; or possibly it could be that too much Fe^{3+} is being partitioned into sapphirine and other ferric phases (orthopyroxene, ilmenite) to allow for more extensive magnetite stability.

The purpose of presenting these pseudosections is to convey, using 'extreme' compositions, the influence that oxidation plays for a number of different KFMASH-based compositions. These diagrams should serve as a guide for the mineral assemblages that can form in oxidised, reduced, high and low SiO_2 compositions and so on, but should not be applied to explain the specific *P–T* evolution of a rock because melt loss (White and Powell, 2002), for example, has not been considered in these calculations. In addition, forward modelling in application to specific, actual rocks should be done using the largest model chemical system possible (see White et al., 2014a,b and subsection 7.3).

5.4. Relating predictions from pseudosections to the evolution of natural mineral assemblages interpreted from petrography

In deducing the *P–T* evolution of a specific rock from a *P–T* pseudosection (see also Kelsey, 2008), the principal task is to identify a successive sequence of phase assemblage stability fields that explain the mineral assemblage evolution interpreted from petrographic observation. Contouring of fields for phase abundance and/or chemistry can also assist in deducing the locus of the *P–T* paths trajectory (e.g. Stüwe and Powell, 1995; Vance and Mahar, 1998; Will et al., 1998; Martinez et al., 2001; Zeh, 2001; White et al., 2002; Kelsey et al., 2003a,b; Kelsey, 2008). A common feature of many pseudosections for UHT rocks, particularly for silica-undersaturated compositions (Figs. 5c, d, 6c, d; Kelsey et al., 2005), is the presence of a large number of phase assemblage stability fields with limited *P–T* extent. Therefore, a potential issue that could arise is that the peak (phase) assemblage field is small (approximately <0.5 kbar and <50 °C) and a number of relevant phase assemblage fields describing the retrograde evolution are small. In itself this is not necessarily problematic as the most rapid changes to phase mode and composition typically occur across *some* narrow phase assemblage stability fields (e.g. White et al., 2001). However, the reason that small fields deemed relevant to a particular rock raise concern is two-fold. First, one must consider how sensitive the petrological response of a rock will be to a number of small fields in succession in relation to reaction kinetics (e.g. Droop, 1989; Rubie, 1998; Carlson, 2002; Pattison and Tinkham, 2009; Pattison et al., 2011; White and Powell, 2011; Dharma Rao et al., 2012; Kelly et al., 2013). Since reaction overstepping could be an issue where melt fractions are low, even at UHT metamorphic conditions (cf. Austrheim, 1987; e.g. Manning et al., 1993; Dharma Rao et al., 2012), the relationship of the petrological and microstructural (spatial) development of a rock to the fields portrayed on a pseudosection should still be considered (White and Powell, 2011). Second, within the uncertainty of the thermodynamic calculations and the bulk composition, questions are raised as to the significance of fields with limited pressure and temperature extent. For example, does a particular field exist within error of the thermodynamic uncertainties? How sensitive is the existence of a particular phase assemblage field(s) to the bulk composition? As sensitivity analysis (see subsection 7.1) is rarely done (cf. Walsh et al., 2014) for entire rock compositions, i.e. not just for H_2O and/or Fe^{3+}, the significance of small fields is usually difficult to assess, other than to recognise that the fields correspond to interpretations from petrographic observations. A case example is used here to raise an important third point.

Korhonen et al. (2013a) presented a pseudosection analysis of a former osumilite-bearing UHT granulite (amongst other rocks) from the Eastern Ghats Province in India to propose that the *P*–*T* evolution, at least in this part of the belt, is characterised by a tight 'anticlockwise' path that features retrograde near-isobaric cooling. The mineralogical evolution of the rock(s) is conveyed on *P*–*T* pseudosections by a series (around 6–8) of very small (<<0.5 kbar, <<50 °C) phase assemblage fields (see their Fig. 9a, b). Normally such an interpretation would bring a degree of suspicion. However, crucially, the Eastern Ghats Province is characterised by a very prolonged (>100 Myr) high-temperature evolution (Korhonen et al., 2013b; see subsection 9.1 and Table 2). Therefore, the third important point is that the *rate* at which a rock travels through *P*–*T* space, defined by geochronological data collected from the same rock used for *P*–*T* analysis, is vitally important. In the current example, the extremely slow passage of the osumilite-bearing UHT granulite through the crust potentially allows the tiny fields of the *P*–*T* pseudosection to carry more significance—petrologically and for *P*–*T* path definition—than if the passage of the rock through the crust was more rapid.

An additional aspect of linking *P*–*T* pseudosections to mineral assemblages is the interpretation of reaction microstructures. Classically microstructures such as coronas, including symplectites, have been interpreted to reflect the destabilisation of the reactants and the stabilisation of the products in *P*–*T* space (see White and Powell, 2011). While this seems self-evident, in practice the interpretation of reaction microstructures even in *P*–*T* space may not be so straight forward, notwithstanding the complexities of chemical potential gradients (e.g. Hensen, 1988). In many instances, mineral assemblages contain well developed reaction microstructures, but also volumetrically significant remnants of the reactants, which in places may also still be in limited contact. The question is whether the reaction microstructures reflect the terminal stability of the reactants with kinetic effects preserving reaction remnants, resulting in a disequilibrium mineral association in the rock, or whether the rock records an equilibrium assemblage, where the microstructures record the downward adjustment in mineral modes of the reactants, and a modal increase in the products. The difference between these two interpretations has important implications for the way in which a *P*–*T* pseudosection is related to the mineral reaction

Table 2
Summary of the timescales and/or cooling rates that are proposed for UHT metamorphism from numerous terranes and/or localities. The amount of data listed here represents a vast increase in such information since the earlier UHT reviews of Kelsey (2008) and Harley (2008). For many UHT terranes/localities tabulated below the timescale of UHT metamorphism is cryptically contained in the publications – very rarely do the authors explicitly state the timescale. The numbering system in the left-hand column follows that of table 1 in Kelsey (2008) and Table 1 (this contribution). Newly discovered UHT terranes/localities, and ones not reported in Kelsey (2008), are denoted in bold.

No.	Location	Study	Timescale for UHT and/or cooling rate	Accessory mineral used
10	Rogaland Anorthosite Complex, Norway	Drüppel et al. (2013)	Possibly approx. 60 Myr	Zircon
12	Gruf Complex, Italy	Galli et al. (2011)	<<20 Myr	Zircon
18	North China Craton, China	Guo et al. (2012)	Approx. 10 Myr	Compilation of published zircon data
21	Kontum Massif, central Vietnam	Nakano et al. (2013)	Possibly <<40 Myr (Triassic age group)	Monazite
22	Eastern Ghats Province, India	Korhonen et al. (2011, 2013b)	>>50 Myr, possibly as long as 200 Myr; retrograde cooling rate of ~1 °C Ma^{-1}	Zircon and monazite
22	Eastern Ghats Province, India	Das et al. (2011)	Approx. 40–50 Myr	Monazite and zircon
22	Eastern Ghats belt (Ongole Domain of Krishna Province)	Sarkar et al. (2014)	Approx. 25 Myr	Zircon
24	Palni Hills, Southern Granulite Terrane, India	Brandt et al. (2011)	"Short-lived" because of strongly decompressive *P*–*T* path	Zircon and monazite
24	Southern Granulite Terrane, India	Clark et al. (2009)	Approx. 10 Myr	Zircon, monazite
29	Coober Pedy Ridge, Gawler Craton, Australia	Cutts et al. (2011a)	Approx. 10–30 Myr	Monazite
32	Napier Complex, Antarctica	Kelly and Harley (2005)	Tentatively >20 Myr	Zircon
32	Napier Complex, Antarctica	Carson et al. (2002); Horie et al. (2012)	Approx. 30 Myr	Zircon
32	Napier Complex, Antarctica	Harley and Black (1997); Crowe et al. (2002)	Approx 40 Myr	Zircon
32	Napier Complex, Antarctica	Hokada et al. (2003); Hokada and Harley (2004); Suzuki et al. (2006)	Approx. 50 Myr	Zircon
36	Central Kaapvaal Craton, South Africa	Schmitz and Bowring (2003)	5–10 Myr	Zircon and monazite
36	Kaapvaal Craton, South Africa	Baldwin et al. (2007a)	Approx. 7 °C Ma^{-1}	Zircon
43	Salvador–Curaçá Belt (São Francisco Craton), Bahia, Brazil	Leite et al. (2009)	Possibly approx. >35 Myr	Monazite
45	Anápolis-Itauçu Complex, Southern Brasília Belt, central Brazil	Baldwin and Brown (2008)	Approx. 15 Myr	Zircon
45	Anápolis-Itauçu Complex, Southern Brasília Belt, central Brazil	Giustina et al. (2011)	Possibly up to ~30–40 Myr	Zircon
49	**Schirmacher Hills, Dronning Maud Land, Antarctica**	**Baba et al. (2010)**	**Approx. 45 Myr**	**Zircon**
50	**Central Indian Tectonic Zone**	**Bhowmick et al. (2014)**	**Approx. <20 Myr**	**Monazite and zircon**
51	**Southern Madagascar**	**Jöns and Schenk (2011)**	**Approx. 5 Myr**	**Monazite ± zircon**
53	**Tibetan Plateau, China**	**Hacker et al. (2000)**	**Possibly up to 45 Myr**	**Monazite and detrital zircon**
57	**Musgrave Province, central Australia**	**Smithies et al. (2011); Walsh et al. (2014); Gorczyk et al. (2015)**	**Approx. 100 Myr; possibly up to 150 Myr**	**Zircon and monazite**

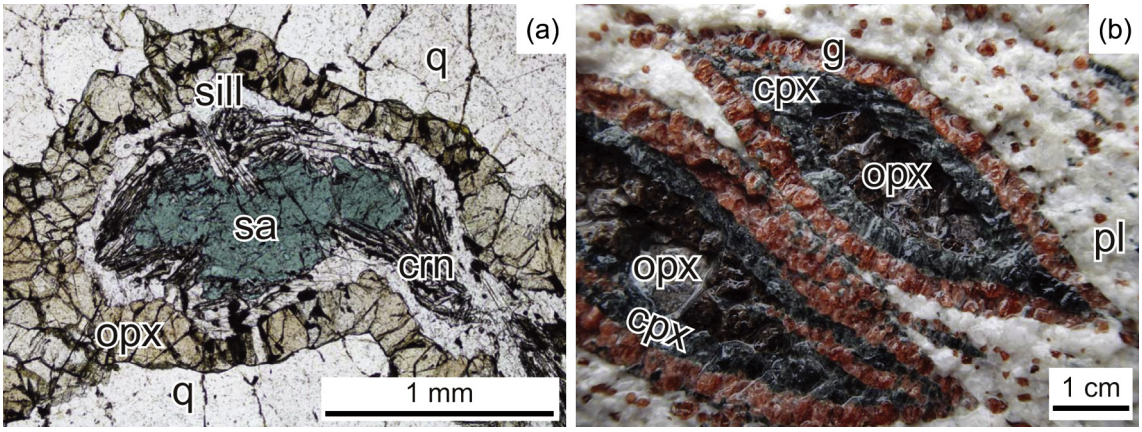

Figure 7. Photos of layered corona microstructures developed as a result of reaction. Whereas reaction progress is driven by changes to *P–T*, the spatial organisation of reaction products, the coronae, is driven by chemical potential gradients. (a) Layered corundum–sillimanite, sillimanite and orthopyroxene coronae occurring between the reactant minerals sapphirine and quartz. (b) Layered clinopyroxene and garnet coronae occurring between the reactant minerals orthopyroxene and plagioclase.

microstructures. In the former case, the rock records gross disequilibrium, and by definition the equilibrium thermodynamic basis for *P–T* pseudosection construction is no longer valid for the interpretation of the reaction microstructures. In this case, the best approach is to attempt to model the reaction microstructures using a much more local domain composition (see Section 7). In the latter case, the rock may still record an equilibrium mineral assemblage associated with a decrease in variance reflecting the growth of new minerals and the decrease in abundance of pre-existing minerals. *P–T* diagrams that depict phase modes (e.g. Stüwe and Powell, 1995) highlight that as rocks transect *P–T* space the proportions of phases change across phase assemblage fields that also record different variances. Therefore some care is required in considering if a reaction microstructure reflects a kinetically controlled—essentially disequilibrium—situation or an equilibrium system in which mineral modes had adjusted from one *P–T* condition to another.

A feature of many reaction microstructures is the systematic spatial arrangement of the reaction products (Fig. 7). Whereas such reaction microstructures are ultimately driven by changes in *P–T*, and therefore can be modelled using *P–T* pseudosections, the spatial arrangement of the minerals is controlled by diffusion effects, as opposed to infiltration (e.g. Ashworth, 1993; White et al., 2008; White and Powell, 2011), and in detail cannot be rationalised in *P–T–X* space. In such reaction microstructures, the driving force for diffusion is the chemical potential gradients that are established between the minerals or groups of minerals (White et al., 2008; White and Powell, 2011). Change in mineral assemblages, mineral modes and mineral compositions is driven spatially by these chemical potential gradients and accommodated via the diffusion that occurs as a consequence of them[1].

Fig. 7a shows a layered reaction microstructure in an anhydrous UHT granulite from the Fyfe Hills, Enderby Land (Napier Complex), whose development has been modelled in detail by White et al. (2008). The microstructure involves sequential layers of corundum, sillimanite and orthopyroxene, or sillimanite and orthopyroxene, that separate sapphirine from quartz. Corundum or sillimanite are always adjacent to sapphirine, and orthopyroxene is always adjacent to quartz. From the macroscopic microstructure, it is apparent that the reaction can be interpreted in FMAS as sapphirine + quartz = orthopyroxene + sillimanite. However, in detail, the reaction products also include corundum and were probably organised in response to comparatively inefficient diffusion of Si and Al that established a series of reaction product subassociations that progressively track outwards from the core of the microstructure to more siliceous and less aluminous compositions. Such reaction microstructures can be modelled using chemical potential diagrams (e.g. White et al., 2008). A further example of layered reaction microstructures is shown in Fig. 7b. This large-scale example, from anhydrous anorthositic granulite in western Norway, shows the overall reaction plagioclase + orthopyroxene = clinopyroxene + garnet. The spatial organisation of garnet adjacent to plagioclase and clinopyroxene adjacent to orthopyroxene is probably due to relatively inefficient diffusion of Al and Si, with the overall microstructure becoming progressively more aluminous outwards from orthopyroxene.

6. Trace element thermometry

A number of trace element thermometers have been proposed over the past decade or so and applied with some success to granulite facies rocks, including UHT rocks. The development and increased application of trace element thermometry provides a useful and independent mechanism by which to (ideally) substantiate metamorphic temperatures constrained from phase diagram thermobarometry. Trace element thermometry has developed as a result of the increasingly high spatial and analytical resolution, and also time- and cost-effectiveness, facilitated by equipment such as SIMS and LA–ICP–MS. Trace element thermometry is based on two main premises: first, that the incorporation of tetravalent cations into a mineral lattice is mostly temperature dependent, with little influence from pressure; and second, that these same tetravalent cations diffuse at sluggish rates once they have entered a mineral lattice, meaning that the concentration of a trace element measured in a host mineral should closely reflect the concentration at the thermal maximum to which the mineral/rock was subjected. Indeed, conceivably diffusion is sufficiently sluggish that minerals like rutile that grow on the prograde path could, in principal, preserve domains with pre-peak compositions. In the context of UHT metamorphism the apparently slow diffusion of temperature-sensitive trace elements is important because the resetting of major element chemistry (particularly Fe–Mg) as rocks cool from extreme temperatures renders many conventional thermometers ineffective. If trace element

[1] As an alternative to corona formation being driven by chemical potential gradients, pressure gradients arising from strength contrasts between minerals at chemical equilibrium have been argued to be the driver for the formation and preservation of simple coronae in high-pressure granulite (Tajčmanová et al., 2014). The high-pressure granulite records decompression occurring over a timescale argued to be significantly greater than that required for chemical equilibration.

concentrations do not reset with cooling from extreme temperatures, trace element thermometry provides an alternative to conventional thermometric techniques, and indeed, where diagnostic Mg–Al-rich mineral assemblages are absent, provides an alternative even to calculated phase equilibria (e.g. Ague and Eckert, 2012; Ague et al., 2013). The main trace element thermometers are Ti-in-zircon (Watson and Harrison, 2005; Watson et al., 2006; Ferry and Watson, 2007; Hofmann et al., 2013), Zr-in-rutile (Zack et al., 2004; Watson et al., 2006; Ferry and Watson, 2007; Tomkins et al., 2007; Hofmann et al., 2013) and Ti-in-quartz (Wark and Watson, 2006; Kawasaki and Osanai, 2008), which has also been recalibrated as a thermobarometer (Thomas et al., 2010; Huang and Audétat, 2012). Application of the thermometers and thermobarometers ideally requires the trace element of interest (Ti or Zr) to be present in the whole rock in concentrations high enough to saturate the rock in that element, resulting in the presence of the saturating phase rutile (for Ti-in-zircon and Ti-in-quartz thermometry) or zircon (for Zr-in-rutile thermometry). If the trace element is not present in high enough concentration to saturate the rock, then the application of the thermometers requires an estimation of the activity of that trace element (as an oxide), which opens the thermometry to a higher degree of uncertainty. Additional trace element thermometers include Ti-in-garnet and Ti-in-orthopyroxene (Kawasaki and Motoyoshi, 2007) but these have been little utilised.

The main limitation of these thermometers in application to UHT rocks is usually taken to be the diffusivity of Zr or Ti in rutile and zircon or quartz, based on the experimental diffusion studies of Cherniak et al. (2007a,b) and Cherniak and Watson (2007). These experimental diffusion studies indicated that Ti diffusion in zircon is approximately ten orders of magnitude slower than Zr in rutile at 900 °C, and approximately 12 orders of magnitude slower than Ti diffusion in quartz (Fig. 8). However, Ewing et al. (2013) reported that Zr-in-rutile is probably the most robust of the three thermometers for granulite facies rocks owing to the exsolution of zircon or baddelyite from rutile with cooling (see also Bingen et al., 2001; Kooijman et al., 2012), rather than diffusive loss of Zr. Similarly, Kooijman et al. (2012) stated that Zr is highly immobile in rutile based on a detailed compositional mapping study of rutile in rocks that reached approximately 900 °C. By contrast, Taylor-Jones and Powell (2015) argue that the robustness of the Zr content of rutile to record high temperatures (i.e. granulite facies, including UHT) is not because Zr diffusion in and out of rutile is sluggish—they argue it is efficient—but rather due to rutile being or becoming chemically isolated from an external Zr reservoir, namely zircon, during cooling. Very large inter-grain ranges of Zr contents in rutile at the thin section scale (Racek et al., 2008; Luvizotto and Zack, 2009; Jiao et al., 2011; Meyer et al., 2011; Kooijman et al., 2012; Korhonen et al., 2014) can be correlated with proximity to zircon (Luvizotto and Zack, 2009; Jiao et al., 2011; Kooijman et al., 2012; Ewing et al., 2013), including zircon that grew from expulsion of Zr from rutile, with rutile in immediate proximity to zircon recording lower Zr-in-rutile temperatures than rutile grains (chemically) isolated from zircon (Taylor-Jones and Powell, 2015). Placing the Zr content of rutile in the context of chemical communication with the external Zr (and Si) reservoir zircon—i.e. rutile's ability or inability to exchange Zr and Si with zircon—implies that the Zr diffusion data of Cherniak et al. (2007a) is reliable; that is, if rutile is in chemical communication with zircon during cooling, Zr diffusion within and out of rutile will continue to occur down to the (lower than UHT) closure temperature of Zr implied by the experimental data of Cherniak et al. (2007a; see Fig. 4 in Taylor-Jones and Powell, 2015). Using the chemical communication logic of Taylor-Jones and Powell (2015), Blackburn et al. (2012) are incorrect with their statement

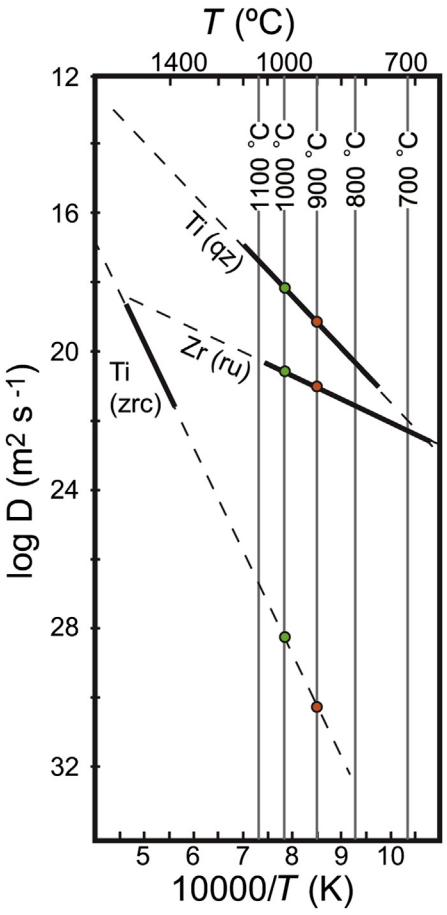

Figure 8. Summary of experimentally-derived diffusivity data for Zr in rutile, Ti in zircon and Ti in quartz from the studies of Cherniak et al. (2007a,b) and Cherniak and Watson (2007). The temperature range of the experiments performed is denoted on the plot by a bold black line, whereas extrapolation of the diffusivity data to other temperatures is denoted by a dashed line. Coloured dots are shown at UHT conditions of 900 and 1000 °C to highlight that experimentally derived diffusivity data indicates that Ti in zircon diffuses considerably slower (largest log D) than Zr in rutile, with Ti in quartz being the fastest diffuser (lowest log D value). However, contrary to this experimental data set, Zr in rutile is the most robust trace element thermometer for UHT rocks. Adapted from Fig. 8 in Cherniak and Watson (2007).

that rocks must be exhumed extremely rapidly (>10^4 °C/Ma) if rutile is to preserve a record of high-temperature (and UHT) conditions.

That rutile can preserve its Zr content from peak or near-peak granulite facies temperatures is shown by a number of studies where Zr-in-rutile thermometry provides a robust record of the high (approximately 750 to 900 °C) or ultrahigh temperatures of metamorphism (Fig. 9a) that are also recorded by other (independent) means such as silicate mineral assemblages, ternary feldspar thermometry and/or Al-in-orthopyroxene thermometry (e.g. Baldwin and Brown, 2008; Racek et al., 2008; Luvizotto and Zack, 2009; Kotková and Harley, 2010; Jiao et al., 2011; Meyer et al., 2011; Ague and Eckert, 2012; Blackburn et al., 2012; Kooijman et al., 2012; Ague et al., 2013; Ewing et al., 2013; Korhonen et al., 2014). Additional benefits of Zr-in-rutile thermometry include: (1) rutile located in different microstructural settings and/or of differing morphology within high-grade rocks has, in some cases, been correlated with differences in Zr-in-rutile temperatures (e.g. Ague et al., 2013; Baldwin and Brown, 2008; Luvizotti and Zack, 2009; contrast with Meyer et al., 2011), thus making Zr-in-rutile thermometry useful over an appreciable portion of the *P*–*T* evolution of rocks; (2) by contrast to zircon (see below), rutile may be

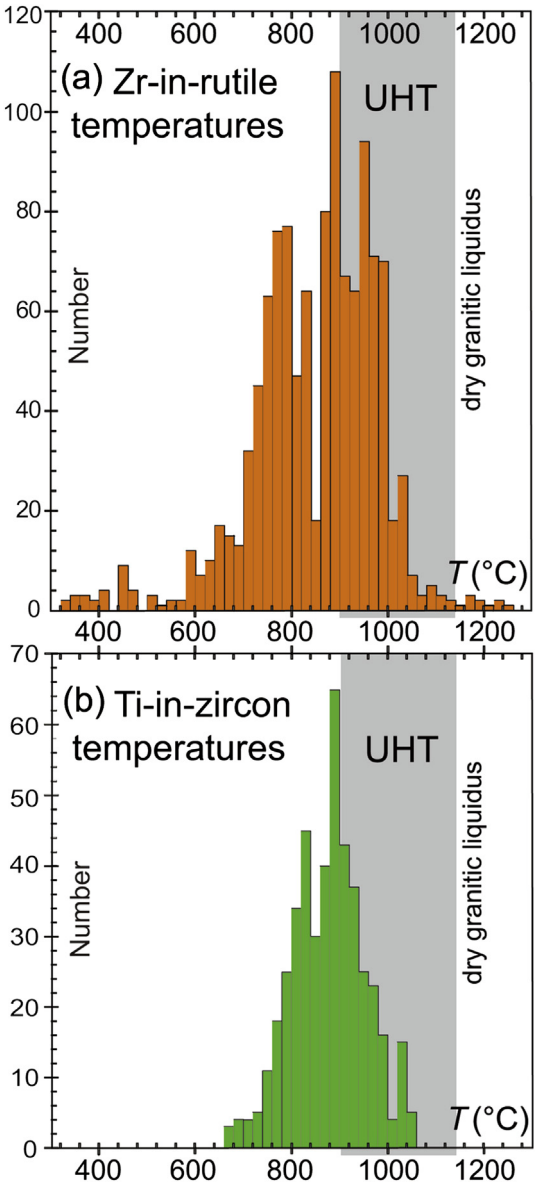

Figure 9. Summary of Zr-in-rutile (a) and Ti-in-zircon (b) thermometry data from studies that report or argue for UHT temperatures on either a regional or local scale. Data was sourced from Baldwin et al. (2007a), Baldwin and Brown (2008), Clark et al. (2009), Liu et al. (2010, 2012), Jiao et al. (2011), Meyer et al. (2011), Kooijman et al. (2012), Ague et al. (2013), Drüppel et al. (2013), Ewing et al. (2013), Walsh et al. (2014) and Korhonen et al. (2014). (a) Zr-in-rutile temperatures were calculated using the pressure-dependent Tomkins et al. (2007) formulation for alpha quartz at 8 kbar and assuming (for the sake of simplicity) $a_{SiO_2} = 1$ for all data; (b) Ti-in-zircon temperatures were calculated using the Ferry and Watson (2007) formulation assuming (for the sake of simplicity) $a_{SiO_2} = a_{TiO_2} = 1$ for all data. Zr-in-rutile thermometry data define three separate peaks/distributions at approximately 940 °C, 765 °C and (poorly defined at) 480 °C whereas the Ti-in-zircon thermometry data define two broad distributions with peaks at approximately 925 and 810 °C. Ultrahigh temperatures are shown by the range of temperatures shaded grey and labelled 'UHT'. The upper temperature limit is limited by the dry (granitic) liquidus, shown here for 8 kbar at approximately 1140 °C (Holland and Powell, 2001).

stable up to and at the peak of (UHT) metamorphism (Kooijman et al., 2012); (3) considerable retrogression does not appear to significantly modify the Zr content of rutile established at granulite facies conditions (e.g. Ewing et al., 2013); (4) the ability to forward model Zr-bearing rutile in calculated phase diagrams (Kelsey and Powell, 2011), thus providing a link between the stability and evolution of major silicate minerals and accessory minerals such as rutile and zircon (e.g. Kelsey and Powell, 2011; Skrzypek et al., 2012); (5) in granulite facies rocks the Zr content of rutile is high enough to allow analysis with an electron probe micro-analyser (EPMA); and (6) rutile grains are usually large enough (>>50 μm) to allow many analyses on a single grain, e.g. detailed compositional traverses.

Whereas it is apparent that Zr-in-rutile can preserve high temperature compositions in UHT rocks, it also apparent from Fig. 9a that a significant number of rutile compositions show temperatures well below UHT conditions. Furthermore, there is a suggestion of a bimodal distribution of derived temperatures. It is beyond the remit of this review to interrogate this data set in detail, examining the relationships between rutile composition, grain size, exsolution history, microstructural setting and paragenesis. However, the apparent bimodality of the Zr-in-rutile temperature data set suggests that the temperatures well below UHT conditions are not directly a function of retrograde diffusional modification. If this were the case, we should expect to see a continuous distribution of temperatures that span the UHT-to-normal granulite temperature interval. Conceivably, the well-defined temperature mode around 750–800 °C reflects exsolution of micro grains of zircon or baddelyite that reduced the Zr content of the analysed rutile grains.

Similar to Zr-in-rutile thermometry, a significant number (62%) of derived Ti-in-zircon temperatures fall below UHT conditions (Fig. 9b; Baldwin et al., 2007a; Baldwin and Brown, 2008; Clark et al., 2009; Liu et al., 2010, 2012; Drüppel et al., 2013; Ewing et al., 2013). Reasons why Ti-in-zircon thermometry commonly does not record UHT temperatures (cf. Baldwin et al., 2007a; Baldwin and Brown, 2008), or perhaps even peak metamorphic temperatures in lower-temperature granulite facies rocks (e.g. Bowman et al., 2011), are numerous, including: (1) zircon growth not commencing until after the peak of metamorphism (e.g. Baldwin et al., 2007a; Baldwin and Brown, 2008; Kelsey et al., 2008; Kelsey and Powell, 2011; Ewing et al., 2013; Yakymchuk and Brown, 2014a). In this scenario, Ti-in-zircon temperatures will probably record close-to-solidus temperatures along the retrograde part of the *P*–*T* path (Brown and Korhonen, 2009; Korhonen et al., 2013b); (2) under-saturation of the sampled rock in TiO_2 (i.e. non-rutile-bearing) (e.g. Hiess et al., 2008; Drüppel et al., 2013); (3) under-saturation of the rock in SiO_2 (i.e. quartz-absent) (Drüppel et al., 2013, contrast with Ferry and Watson, 2007; Page et al., 2007; Tailby et al., 2011); (4) recrystallisation of zircon (e.g. Ewing et al., 2013); (5) uncalibrated *a*–*x* effects (Ferriss et al., 2008; Fu et al., 2008; Bowman et al., 2011; Tailby et al., 2011) such as which site(s) in zircon Ti substitutes into (Tailby et al., 2011), and the energetic efficiency of this substitution, and the potential effect of other heavy elements affecting Ti partitioning into zircon (e.g. Hofmann et al., 2013); (6) disequilibrium amongst zircon and quartz and/or rutile in natural and/or experimental samples and/or disequilibrium partitioning of Ti in zircon (Fu et al., 2008; Hofmann et al., 2009; Bowman et al., 2011; Tailby et al., 2011) between zircon and quartz and/or rutile or ilmenite; (7) zircon lattice distortions (e.g. Timms et al., 2011; MacDonald et al., 2013); and (8) complex intra-crystalline variability in Ti concentration—at scales similar to typical SIMS analytical volumes—for which the controls are poorly known (Fu et al., 2008; Kusiak et al., 2013b; Hofmann et al., 2014). Ti-in-zircon thermometry applied to magmatic rocks is similarly problematic, as magmatic crystallisation temperatures appear to be rarely recorded (e.g. Hiess et al., 2008; Fu et al., 2008). This is most marked for high-temperature magmatic rocks such as anorthosite–gabbro suites where Ti-in-zircon thermometry can underestimate initial crystallisation temperatures by approximately >250 °C (e.g. Fu et al., 2008).

Ti-in-quartz thermobarometry (Thomas et al., 2010; Huang and Audétat, 2012) has not found much application in granulite facies rocks (cf. Altenberger et al., 2012) most probably because the experimental diffusion data of Cherniak et al. (2007b) indicates Ti diffusion in quartz is quite efficient. However, analogously to Zr distribution in rutile (Ewing et al., 2013), Ti is able to exsolve from quartz, as rutile, with cooling. This could imply, by analogy to Zr-in-rutile, that Ti-in-quartz thermometry may be similarly robust at recording high temperatures if the primary mechanism by which Ti 'leaves' quartz is driven by proximity to, and thus chemical communication with, a Ti reservoir, namely rutile. Thomas et al. (2010) suggested that Ti-in-quartz thermobarometry could be applicable to rocks at UHT conditions, but this is, as yet, largely untested. Thomas et al. (2010) further stated that a better methodology for trace element thermo(baro)metry is to simultaneously use Zr-in-rutile and/or Zr-in-titanite (Hayden et al., 2008) with Ti-in-quartz (e.g. Ewing et al., 2013), and/or to use Ti-in-quartz with fluid inclusion thermometry. Ti-in-quartz thermo(baro)metry has been applied to granulites (including UHT) in a small number of studies (Storm and Spear, 2005; Sato and Santosh, 2007; Altenberger et al., 2012; Ewing et al., 2013). The results in these studies are, variously, extremely high Ti-in-quartz temperatures (many >1100 °C; Sato and Santosh, 2007), temperatures that somewhat correlate with either microstructural setting of quartz or mineral parageneses (Storm and Spear, 2005), highly variable temperatures (Altenberger et al., 2012) and temperatures that correlate well with independent constraints on temperature (Ewing et al., 2013). In addition, quartz lattice distortions and differences in quartz recrystallisation mechanisms seem to affect Ti-in-quartz thermometry (Grujic et al., 2011; Altenberger et al., 2012; Ewing et al., 2013). Three of the four studies were conducted prior to recalibration of the Ti-in-quartz thermometer to include the significant effect of pressure (Thomas et al., 2010; Huang and Audétat, 2012), and as such, it is difficult to assess how the newly calibrated Ti-in-quartz thermobarometer might affect the results of those three case studies.

In summary, trace element thermometry on UHT rocks should preferentially focus on Zr-in-rutile, as numerous studies have indicated that peak temperatures are recoverable using this method, whereas Ti-in-zircon is less likely to record UHT conditions. In addition, since rutile is an integral part of a mineral assemblage, is usually much coarser-grained than zircon (allowing many analyses), can be analysed for Zr using an electron microprobe and is easily included in petrologic forward modelling (pseudosections), Zr-in-rutile thermometry is preferred over Ti-in-zircon thermometry for UHT rocks. Ti-in-quartz remains a largely unproven methodology in application to granulite facies—including UHT—rocks, but appears to have potential based on the limited case studies that have been conducted so far, as well as the realisation that pressure plays a significant role in Ti-in-quartz temperatures.

7. Compositions for pseudosection calculations

The topic of deriving an appropriate/representative rock or domain composition for use to calculate *P*–*T* pseudosections for granulite facies rocks is in some ways like the 'elephant in the room'. The topic is non-trivial, subjective and as yet there is no paper published that establishes a universally best practice for implementation. The main reason for the complexity of choosing a relevant composition is because of open system behaviour, particularly drainage of melt from suprasolidus crust, which is a major process of granulite facies metamorphism (e.g. von Platen, 1965; Mehnert, 1968; Brown and Fyfe, 1970; Fyfe, 1973a,b; McCarthy, 1976; White and Chappell, 1977; O'Hara et al., 1978; Thompson, 1982; Powell, 1983; Ellis and Thompson, 1986; Clemens and Vielzeuf, 1987; Le Breton and Thompson, 1988; Vielzeuf and Holloway, 1988; Waters, 1988; Peterson and Newton, 1989; Clemens, 1990; Powell and Downes, 1990; Patiño Douce and Johnston, 1991; Peterson et al., 1991; Stevens and Clemens, 1993; Brown, 1994, 2004, 2008a; Sawyer, 1994, 2001, 2014; Vielzeuf and Montel, 1994; Gardien et al., 1995; Patiño Douce and Beard, 1995, 1996; Stevens et al., 1997; Tareen et al., 1998; Gardien et al., 2000; Tareen and Ganesha, 2001; Nair and Chacko, 2002; White and Powell, 2002, 2010; Guernina and Sawyer, 2003; Johnson and Brown, 2005; Johnson et al., 2010, 2011; Sawyer et al., 2011; Yakymchuk et al., 2013). Indeed, partial melting of deeper crustal rocks is the major process of crustal differentiation and, eventually through erosion, cratonisation (e.g. Lambert and Heier, 1968; Fyfe, 1973b; Sighinolfi and Gorgoni, 1978; Vielzeuf et al., 1990; Sandiford et al., 2001, 2002; Solar and Brown, 2001; Sandiford and McLaren, 2002; Brown and Rushmer, 2006; Brown, 2010a; Sandiford, 2010; Sawyer et al., 2011; Jamieson and Beaumont, 2013). The process of melt loss is critical to the preservation of granulite facies mineral assemblages (Brown and Fyfe, 1970; Fyfe, 1973b; McCarthy, 1976; O'Hara et al., 1978; Powell, 1983; Powell and Downes, 1990; Sawyer, 1994; Brown, 2002; White and Powell, 2002; Guernina and Sawyer, 2003) as melt loss dehydrates the rock mass and inhibits retrogression during cooling. Granulite facies metamorphism is essentially a one-way process in that progressive dehydration through partial melting leads a progressively decreased capacity to continue to generate appreciable volumes of melt (White and Powell, 2002). That is, the rock becomes less fertile and more residual/'mature' (e.g. Vielzeuf et al., 1990).

The open system process of melt loss implies that the equilibrium composition of a rock changes for as long as melting occurs along the prograde path and melt drains from the system. This is the major reason why an analysed (residual) rock composition is inappropriate for forward modelling the prograde evolution of granulite facies rocks. Obtaining well-constrained, quantitative information about the prograde history of partially-melted, granulite facies rocks is fraught with difficulty and uncertainty. However, inverse—rather than forward—modelling involving melt reintegration can be done to gain potential insight into the prograde history, covered in subsection 7.2. Conversely, the analysed composition of a residual granulite facies rock may be suitable for constraining the peak and possibly retrograde *P*–*T* evolution, subject to caveats outlined below, by means of forward modelling (i.e. where the rock composition is assumed as known), and this is the focus of the following and subsection 7.1.

In terms of considering the appropriateness of a composition for forward modelling the peak and particularly retrograde *P*–*T* evolution, there is additional complexity introduced by different length scales of diffusion for different elements in different minerals (e.g. Fitzsimons and Harley, 1994; Pattison and Bégin, 1994). The ability of a cation of a given element to diffuse within and between minerals is a function of the interplay between the lattice siting of that cation (i.e. the strength of the bond by which that element is held within the mineral structure), the size of the cation, the presence and abundance of a physical transport mechanism (fluid/melt), temperature, strength differences between contacting minerals (leading to pressure gradients) and deformation induced lattice dislocations (e.g. Passchier and Trouw, 2005). Consequently, each element diffuses at different rates in and between different minerals, resulting in decoupled diffusion. Comparatively slow rates of diffusion for elements such as Si and Al manifest as the development of spatially organised coronae in granulite facies rocks (e.g. Fisher, 1973; Joesten, 1977; Nishiyama, 1983; Ashworth and Birdi, 1990; Ashworth et al., 1992, 1998; Ashworth, 1993;

Ashworth and Sheplev, 1997; Carlson, 2002; Tajčmanová et al., 2007; Reverdatto, 2010; Štípská et al., 2010; Tajčmanová et al., 2011; White and Powell, 2011; Goergen and Whitney, 2012a,b). Indeed, it is the very presence of coronae in UHT and HT rocks that allows for such detailed analysis of *P*–*T* histories (e.g. White and Powell, 2011). The impact of melt loss and decreasing temperature on impeding physical and chemical movement of elements is that many Mg–Al-rich UHT rocks cooling from peak UHT conditions develop (micro-)domains of different composition, that develop different mineral assemblages (e.g. Kriegsman and Schumacher, 1999; Rickers et al., 2001; Kelsey et al., 2005 and references therein; White and Powell, 2011). Further, the temperature dependency of diffusion implies that the equilibration volume (or the 'effective bulk composition') also changes with changing temperature (e.g. Stüwe, 1997). In the context of the retrograde evolution of rocks, the equilibration volume shrinks with decreasing temperature (Spear, 1993; Stüwe, 1997; Brown, 2002; Carlson, 2002; White and Powell, 2011) but shrinks at different rates for different elements in different minerals (White and Powell, 2011). Large mineral grains (e.g. garnet) additionally cause fractionation of the rock composition, implying that grain size further impacts the effective equilibration volume and thus composition (e.g. Spear and Selverstone, 1983; Spear et al., 1990; Florence and Spear, 1991; Stüwe, 1997; Marmo et al., 2002; Evans, 2004; Tinkham and Ghent, 2005; Cutts et al., 2009; Caddick et al., 2010; Cutts et al., 2010, 2014). Thus, the effective bulk composition of a rock—in *P*–*T* space and in terms of mineral assemblages—is not fixed and primarily changes as a complex function of melt loss, temperature and grain size.

The consequence of melt loss and temperature-dependent diffusion is that many Mg–Al-rich UHT rocks cooling from peak UHT conditions become mineralogically and microstructurally complex. If the interpretations of petrographic relationships are incorrect, calculated phase diagrams will also be interpreted incorrectly which can, for example, lead to erroneous propositions about *P*–*T* path trajectories and thus tectonic setting.

7.1. Methods for deriving a relevant composition for forward modelling of the peak and/or retrograde *P*–*T* evolution

In the following, 'bulk composition' will be used when referring to a whole-rock composition; and 'domain composition' when referring to the composition of a region of a rock smaller than thin-section scale (i.e. on the order of mm^2). There is no single 'correct' composition for a rock for the purposes of calculating *P*–*T* pseudosections due to the reasons outlined above. This means that for every rock or local mineral reaction microstructure there are a variety of compositions that can be used to constrain the *P*–*T* evolution, or more precisely parts of the *P*–*T* evolution. Whether that variety of compositions spans a large or tiny range of composition (e.g. as for *T*–*X* or *P*–*X* sections; see Fig. 5 in Johnson et al., 2004) is commonly not tested via 'sensitivity analysis' of calculated *P*–*T* pseudosections or interpreted *P*–*T* path. The main constraints that must be considered when determining an appropriate bulk or domain composition are: (1) that the correct, full phase assemblages are present in the calculated *P*–*T* pseudosection, including phases such as K-feldspar, plagioclase, magnetite, ilmenite and/or rutile; (2) that the paragenetic sequence of mineral assemblage development interpreted from petrography is predicted by the appropriate sequence of phase assemblage stability fields in *P*–*T* space; (3) that the chemistry of minerals, especially in regard to slow diffusing elements (e.g. Al), are accurately predicted inside the appropriate phase assemblage stability fields; and (4) that open system behaviour has been adequately and justifiably accounted for.

If a rock is homogeneous[2], the whole-rock composition should be appropriate for use to calculate a geologically meaningful *P*–*T* pseudosection (e.g. Kelsey et al., 2005; Hollis et al., 2006). Whole-rock chemistry may be appropriate for constraining the peak metamorphic conditions if the assumptions that extremely efficient element diffusion occurs up to and at peak conditions, and that the preserved (measured) composition of the rock was frozen in at the peak of metamorphism (i.e. system effectively remains isochemical on the retrograde path), are valid. This approach for constraining peak metamorphic conditions is applicable even if (retrograde) coronae are developed in the rock(s) being studied, since coronae typically develop at very local scales and probably under quasi-closed system conditions (White and Powell, 2011). Therefore, in homogeneous rocks the bulk composition may also be appropriate for characterising the retrograde part of the *P*–*T* evolution with the caveat that the interiors of large grains with comparatively slow diffusing components (e.g. Ca in garnet) will become increasingly isolated from the reactive rock during the retrograde evolution. However, if there are different coronae or symplectic assemblages present, greater care and consideration must be taken to derive an appropriate composition for each in order to constrain the development of each microstructure during the retrograde part of the *P*–*T* path. That is, each different micro-assemblage needs to be treated separately with a separate domain composition and calculated pseudosection (e.g. Anderson et al., 2013), since each has developed independently of each other and possibly at different times. If the different coronae developed at different times, they should record different parts of the retrograde *P*–*T* path (e.g. *P*–μ and *P*–*X* diagrams; Hensen, 1971, 1988; Mohan et al., 1986; Lal et al., 1987; Hensen and Harley, 1990; Harley, 1998c). Mapping (or point counting) local domains in a thin section and combining the abundance of minerals in that mapped area with analysed mineral compositions to derive a domain composition is a method by which the *P*–*T* information of individual mineral reaction microstructures can be investigated (e.g. Friedman, 1960; White et al., 2003; Corvino et al., 2007; Chatterjee and Ghose, 2010; Cutts et al., 2011a, 2013; Forbes et al., 2011; Droop and Brodie, 2012; Anderson et al., 2013; Walsh et al., 2014). Alternatively, quantitative mapping of local domains in a thin section can be undertaken, negating the need to combine maps with separately measured mineral compositions (e.g. Clarke et al., 2001, 2006; Marmo et al., 2002; Fitzherbert et al., 2005; Kelsey et al., 2005; Tinkham and Ghent, 2005; Halpin et al., 2007b; Brovarone and Agard, 2013).

A useful question to pose when considering mapping a local domain of a thin section for the purpose of deriving a domain composition is how large an area should be mapped? There is no unique answer to this question, but an important point to consider, as outlined earlier, is whether the reaction microstructure of the local domain reflects terminal stability of the reactant minerals or a continuous decrease of modes of the reactant minerals to accommodate the appearance of product minerals. If the former case applies, then a suitable map area would encompass just the reaction products as the reactant minerals are not involved in the equilibrium. If the latter case applies, more consideration is required regarding the scale/size of the mineral reaction microstructure with respect to the reactant minerals. More specifically, the map area should include reactants (peak minerals) as well as products (coronae) (Fig. 10), but if the peak minerals are

[2] Homogeneous is used here in the sense that: (1) porphyroblasts, if present, are evenly distributed through the rock and there are not significant grain size differences among them; (2) other minerals are evenly distributed such that the rock is not strongly layered at the scale at which the bulk composition is measured; and (3) if coronae are developed they are mineralogically identical throughout the sample.

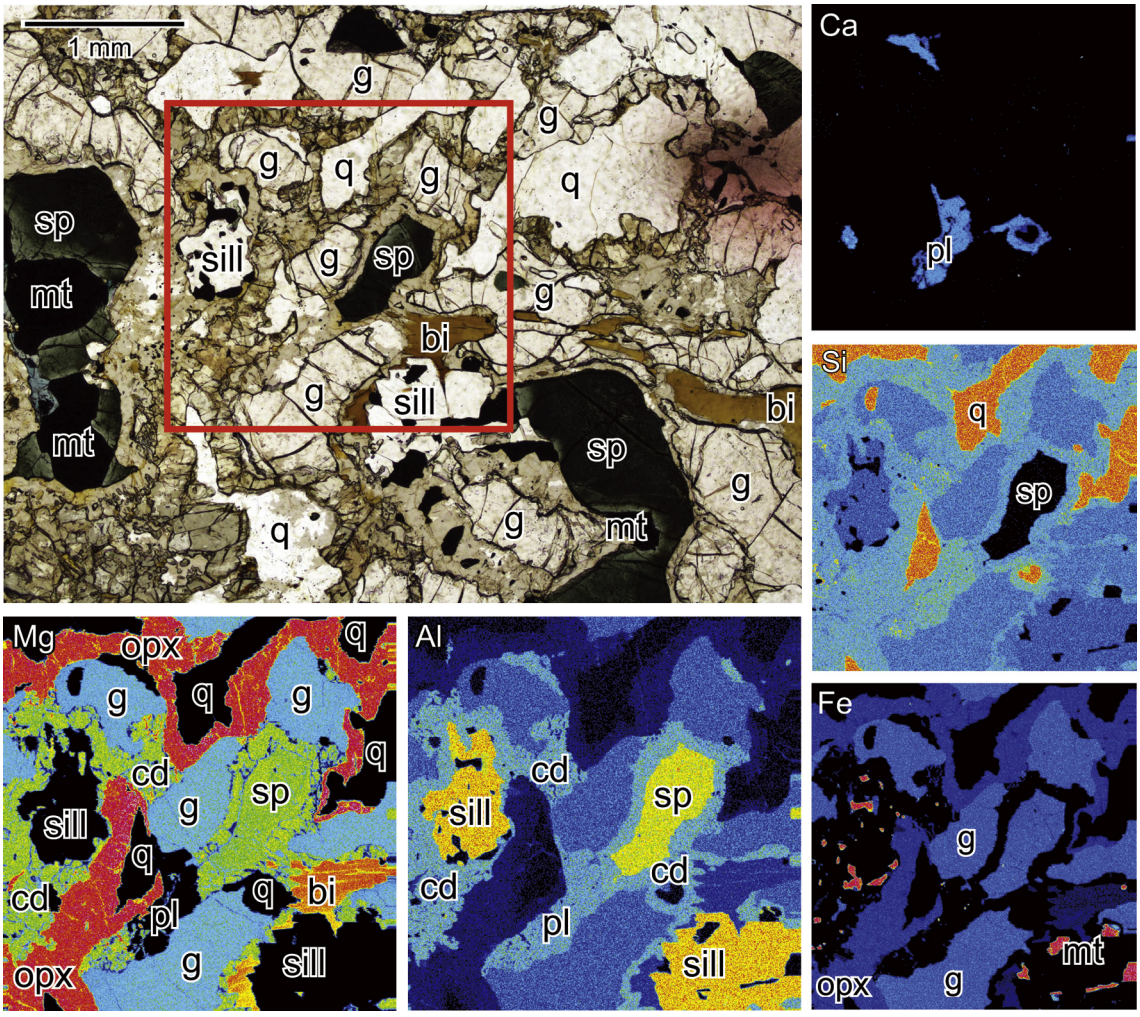

Figure 10. Example of the scale at which to choose an area suitable for obtaining a domain composition to forward model, with a *P–T* pseudosection, the retrograde evolution of a granulite/UHT rock with many and varied compositional and mineralogical domains. The upper left shows a photograph of a thin section in plane polarised light. The red square indicates the area chosen for element mapping using the electron microprobe. The overall continuous reaction recorded inside the boxed area is biotite + garnet + spinel + sillimanite + quartz = orthopyroxene + cordierite ± plagioclase. Magnetite is interpreted to have either co-existed with spinel as part of the peak mineral assemblage, or exsolved from spinel during cooling. The reactant minerals are preserved as moderately coarse-grained. The product minerals are developed on a scale of similar size/coarseness to the reactant minerals. The coloured images around the photograph are element maps of Mg, Al, Ca, Si and Fe for the red boxed area. The ratio of reactant to product minerals in the mapped area is approximately 55:45. Rock is from the North China Craton.

appreciably coarser-grained than the combined size (2D area) of the coronal mineral(s), it will not be necessary to include entire grains of the peak assemblage (e.g. Anderson et al., 2013) since: (1) the cores/inner parts of coarse minerals are probably not participating in the reaction to produce the coronae – this can be confirmed by clarifying whether the peak minerals are compositionally zoned; and (2) if the peak minerals are compositionally zoned, inclusion of too much of the (zoned) peak minerals in the map area will dilute the abundance of the coronal mineral(s) and skew the composition of the mapped area towards that of the (zoned) non-participating parts of the peak minerals. To reduce the potential influence of the (zoned) interiors of coarse peak minerals diluting the influence of the coronal minerals in a domain composition, the map area should be chosen such that the abundance of coronal minerals in the map area is roughly greater than or equal to the abundance of the coarse-grained, peak minerals (Fig. 10). Once these issues have been accounted for, one approach to use is to modify the map area size—simulated using *T–X* (or *P–X*) sections where the compositional span involves varying the proportions of minerals in the effective equilibration volume—until the sequence of phase assemblage fields and the phase abundances on the calculated *P–T* pseudosection match the mineral assemblage evolution interpreted from petrography and the mineral abundances (e.g. see Fig. 5 in Johnson et al., 2004)

These methodologies do not constrain the Fe_2O_3 and H_2O content of the composition. The best practice for constraining the amounts of these two variables is a matter of some debate, and consequently there are a number of different methods for their estimation. These methods are discussed in the next two sub-subsections.

7.1.1. Measuring or estimating Fe_2O_3 content of the bulk or domain composition

Addressing Fe_2O_3 first, quantification of the valence state of Fe in minerals has typically involved methods such as wet chemical analyses, ^{57}Fe Mössbauer spectroscopy, electron energy loss spectroscopy, X-ray photoelectron spectroscopy, and X-ray absorption spectroscopy. However, some of these methods require mineral separation and analysis of bulk samples. Whereas the amount of sample required may be small for some techniques, in situ analyses

are often not possible and therefore of limited application to detect intra-granular zoning of Fe^{3+}/Fe^{T}. Where in situ analyses are possible (e.g. micro-XANES, Borfecchia et al., 2012) specialized facilities are required. However, there are some electron microprobe-based methods that show promise for determining in situ Fe^{3+}/Fe^{T}. One of these uses the Fe $L\alpha$ to $L\beta$ peak intensity and has been used to determine Fe^{3+}/Fe^{T} in different minerals including garnet (e.g. Creighton et al., 2009; Creighton et al., 2010). A second method is based on the energy of the Fe $L\alpha$ peak (Fialin et al., 2001; Fialin et al., 2004; Lamb et al., 2012). Although not widely adopted, these methods offer promise particularly because they can give information about intra-granular Fe^{3+}/Fe^{T} zoning, which could have important consequences for the way forward modelling of mineral assemblages is undertaken.

Whole rock geochemical analyses report total iron, which may be either $FeO^{\dagger}$ or (usually) $Fe_2O_3^{\ddagger}$, where '†' means no distinction has been made between the oxidation state of the Fe cations. Titration on solutions of dissolved rocks powders is used to measure how much of the total iron is ferrous (Fe^{2+}). From that information it is possible to calculate the amount of FeO vs. Fe_2O_3 from the total iron reported in a whole rock geochemical analysis. The results of the titration method can therefore be directly used for the purposes of constraining the *P–T* evolution of the peak metamorphic conditions in homogeneous and heterogeneous rocks via pseudosection calculations (e.g. Johnson and White, 2011), assuming that little or no externally-driven retrogression has occurred post-peak. The amounts of FeO and Fe_2O_3 determined from the results of whole rock titration data are not directly useful for compositions used to constrain the retrograde evolution of rocks containing local domains of mineral reaction microstructures, but can potentially be useful for bulk compositions for rocks where local domains of retrograde mineral reaction microstructures are not developed. Weathering and crushing (e.g. Schafer, 1966; Fitton and Gill, 1970) can lead to erroneous analysis of FeO (versus Fe_2O_3). Therefore, wherever possible, the freshest samples (e.g. freshly quarried, or drill core stored in a dry environment) should be used for whole-rock geochemical analysis and titration to measure FeO. However, commonly it has been found that the titration value of FeO is a good approximation of an acceptable value (Korhonen et al., 2013a; Korhonen et al., 2014). In summary, the Fe^{3+} and Fe_2O_3 amount calculated on the basis of titration and whole rock geochemical data should be treated as a maximum.

If titration data is not available and only total iron oxide is available from whole rock geochemical analysis, or if mapping an area of a thin section is the methodology being used to derive a domain composition, then constraining the amount of Fe_2O_3 versus FeO requires more of an informed estimate. There are three methods outlined below that have been used to estimate Fe_2O_3:

1. Fe^{3+} calculated on the basis of stoichiometric mineral composition analyses (e.g. Droop, 1987) and then using those mineral compositions, expressed with Fe_2O_3 wt.% and FeO wt.%, in combination with mineral abundances in the mapped area of a thin section to derive a domain composition. In this way, the amount of ferric iron in the domain composition is tied to the analysed solid solution composition of minerals such as magnetite, ilmenite, spinel, sapphirine, orthopyroxene, sillimanite and biotite (± garnet) used as part of the domain composition calculation procedure (e.g. Walsh et al., 2014).
2. If whole rock geochemical data is available, but neither Fe^{2+} data from titration nor mineral compositional data has been collected, and the rock is relatively homogeneous, the method above can be similarly applied. That is, using estimations of the abundance of minerals in a thin section of the sample and realistic estimations of the ferric iron content of requisite minerals, the two can be combined to provide an estimate of Fe_2O_3 for the bulk composition. This approach is somewhat similar to the approach used by some authors who set the ferric iron content at, say, 5 or 10% of total iron based on a consideration of the oxide + silicate mineralogy of the rock (e.g. Diener et al., 2008b; Cutts et al., 2010, 2011a,b; Dziggel et al., 2012; Korhonen et al., 2012a; Cutts et al., 2013).
3. Fe^{3+} (or 'O' in THERMOCALC) estimated on the basis of calculated *P–X* or *T–X* (or *P–M* or *T–M*) section analysis (e.g. Korhonen et al., 2012b). Using this methodology, the impact of changing Fe_2O_3 across a range of compositions on the phase relationships is graphically displayed. An appropriate Fe_2O_3 content for the bulk or domain composition of *P–T* pseudosection calculations is selected based upon where in compositional space the peak mineral assemblage interpreted from petrographic analysis occurs in the calculated section. This forward modelling approach may show there to be a large range of Fe_2O_3 contents that can be deemed appropriate.

The merit of method 1 is that the solid solution compositions of minerals are directly used to estimate the Fe_2O_3 content. Resetting of mineral compositions during cooling, an inherent feature of granulite facies metamorphism, can influence the oxide amount of Fe_2O_3 since minerals tend to become more FeO-rich and less MgO-rich with cooling. That is, increasing FeO could lead to an overestimation of Fe_2O_3 by stoichiometry. However, in light of all the other uncertainties associated with deriving a domain composition, mineral compositional (Fe–Mg) resetting of the major Fe_2O_3 reservoirs will probably not greatly affect the estimation of Fe_2O_3. The merit of method 2 is that is that is provides a rapid assessment of the Fe_2O_3 content of a bulk composition, but does contain unquantified uncertainties. The merit of method 3 is that a sensitivity analysis of the composition to changing Fe_2O_3 is performed for a single pressure (or temperature). However, there is a degree of ambiguity in that a *P–T* pseudosection will not yet have been calculated, so it will not necessarily be clear which pressure (or temperature) the sensitivity analysis should be conducted at. Regardless, all methods have their own merits and if the adopted composition used for forward modelling models the observed mineral assemblages in their interpreted paragenetic sequence, then the most important outcome from deriving a composition has been successful.

7.1.2. Estimating the H_2O content of composition

Estimation of the H_2O content of the composition is probably more uncertain, and therefore more challenging, than estimation of Fe_2O_3. Moreover, the H_2O content of a composition has greater consequences for phase diagram topologies than Fe_2O_3 because the H_2O content largely controls the location in *P–T* space of the solidus (in concert with K_2O and Na_2O) (e.g. White et al., 2001). Perhaps as a reflection of the uncertainty in estimating H_2O in bulk and domain compositions, there are a variety of published methods in the metamorphic phase diagram literature for its estimation. The main methods are:

1. Loss on ignition (LOI) content from whole rock geochemical analysis: the LOI value in whole rock analyses is a measure of the amount of weight loss or gain in the sample during analysis. Essentially it is a measure of the volatile content in the sample as it is heated and oxidised prior to dissolution for ICP–MS whole rock analysis. However, LOI is sensitive to the oxidation state of the sample (see above for factors influencing oxidation state of sample) and in rocks there are likely to be other volatiles besides H_2O, such as CO_2, Cl and F. Regarding oxidation state, the greater the amount of FeO, the greater will

be LOI (Lechler and Desilets, 1987). Thus, to get the best estimation of LOI, titration of whole rock powders should be done to determine how much of the total iron is FeO (see above). Due to all the variables that influence and 'contaminate' LOI, LOI should be taken as a maximum estimate of the H_2O content if it is to be used for H_2O in phase diagram calculations (e.g. Halpin et al., 2007a,b; Johnson and White, 2011).

2. Estimation based on the H_2O content of H_2O-bearing minerals in the rock (or mapped region of a thin section): this estimation is used in concert with the abundance of those H_2O-bearing minerals to establish a conservative H_2O content for the bulk or domain composition. Uncertainties in this method include the (in) accuracy of the abundance of the H_2O-bearing phases and uncertainty about the actual H_2O content of biotite and cordierite relative to total volatiles. However, given the uncertainty relating to LOI above, it is not clear that LOI is necessarily a better approach.
3. $T - M_{H_2O}$ (commonly incorrectly called $T-X_{H_2O}$) sections: this method has gained popularity (e.g. De Paoli et al., 2012; Korhonen et al., 2012b; Cutts et al., 2013) as a means to constrain H_2O for a composition, primarily because it allows for two features to be explored: (1) the influence of H_2O on the (temperature) location of the solidus; and (2) what range of H_2O contents are required in order to develop the mineral assemblage (e.g. peak) observed in the rock. Whereas there are merits in this approach, there are some assumptions that need to be made clear. This method assumes that there is crystallised melt in the sample, and that the H_2O content chosen from the $T-M_{H_2O}$ section will contribute to that melt as well as biotite and cordierite (if present) in the sample. The reason why this method assumes there is crystallised melt in the sample is because when thermodynamic calculations are performed, a portion of the total composition will be 'partitioned' into making silicate melt as one of the phases. For most granulite facies rocks (or thin sections of) it is quite a difficult process to unequivocally determine whether there is crystallised melt present (cf. Vernon and Collins, 1988; Sawyer, 1999; White et al., 2003; Holness et al., 2011). Nevertheless, there are multiple lines of evidence to support some melt presence on grain boundaries post-peak conditions, but perhaps the most persuasive is the requirement for some melt to balance retrograde reactions that have not gone to completion. In situations—even if hypothetical—where there is no crystallised melt in a sampled rock (or thin section), then H_2O on the axis of a $T-M_{H_2O}$ section applied to the rock in effect becomes the proxy for melt composition and abundance. In these situations, a portion of the non-H_2O part of the composition, none of which is actually crystallised melt, will be partitioned into making silicate melt in the thermodynamic calculations for the P–T pseudosection, thereby changing the composition of phases that are calculated from the remainder of the bulk or domain composition. In essence, if it is unclear whether there is crystallised melt in a sample, then H_2O may be a poor proxy for melt because melt is not composed of just H_2O.
4. T–M_{melt} melt re-integration sections: one of the tacit assumptions employed in the calculation of most P–T pseudosections for establishing peak and retrograde conditions for granulite facies rocks is that melt production *and* melt loss is complete by the time the rock has reached peak (thermal) conditions. In other words, the amount of H_2O (and other components in melt) remains fixed for the calculation(s) of peak and retrograde conditions in a closed model chemical system, implying that any melt in the calculated assemblages crystallises within the equilibration volume during cooling (e.g. Carson et al., 1999; Carswell et al., 1999; Guiraud et al., 2001; Brown, 2002; White and Powell, 2002; Štípská and Powell, 2005; Brown and Korhonen, 2009). Indeed, pseudosection calculations show that the thermal maximum corresponds to the least hydrated state of a (rock) composition (e.g. Guiraud et al., 2001). It is probably valid that melt production ceases once the rock begins to pass along its retrograde P–T path (contrast with Carson et al., 1997), especially for extremely residual UHT granulites, but it is not necessarily true that melt loss is complete by the peak of metamorphism, largely depending on whether the peak of metamorphism outlasts pervasive strain. Using the assumption that melt loss is complete by the metamorphic peak allows for the metamorphic peak to be considered as the minimum hydration state of the rock, allowing for a simpler justification of a choice of H_2O for the bulk or domain composition. However, if the rock has not lost all its melt by the metamorphic peak, but loses some or all of the remaining melt after the metamorphic peak, then the rock reaches its minimum hydration state after the thermal peak. Indeed, there is evidence in numerous granulite terranes for late melt in the form of, for example, meso-scale leucosomes with diffuse margins that cross-cut the main gneissic fabric (Anderson et al., 2013). Such leucosomes could indicate that melt was locally sourced or was infiltrated from below. However, in either case, the diffuse nature strongly suggests the rock containing the leucosomes was suprasolidus at the time the leucosomes were generated, and the field relationships suggest melt was present during the suprasolidus retrograde P–T evolution (e.g. Anderson et al., 2013; Morrissey et al., 2014; Yakymchuk and Brown, 2014b). Additionally, the existence of melt in granulite and UHT rocks during at least part of the retrograde history is provided by its requirement for balancing retrograde reactions that have not gone to completion (e.g. Sawyer, 1999; Johnson and Brown, 2005; White and Powell, 2011; Korhonen et al., 2013a). In order to take the existence of melt remaining in the rock after the thermal peak into account, a method has been devised whereby a small amount of leucogranitic melt—granitic rocks derived from the melting of aluminous metasedimentary rocks (Inger and Harris, 1993; Ayres and Harris, 1997; Patiño Douce and Harris, 1998)—is added to a residual bulk or domain composition via a calculated T–M_{melt} section (Anderson et al., 2013; Morrissey et al., 2013). The amount of melt chosen to be integrated should be guided by the critical threshold deemed to apply for melt loss in rocks (i.e. approximately 7 mol% melt; Rosenberg and Handy, 2005; Brown and Korhonen, 2009; Brown, 2010a; Yakymchuk et al., 2013; Yakymchuk and Brown, 2014b) as well as by how abundant evidence for 'late' melt is in the terrane (Greenfield et al., 1996; Anderson et al., 2013; Morfin et al., 2013; Morrissey et al., 2014). The T–M_{melt} section method provides an estimation of H_2O in the context of the full NCKFMASH composition of silicate melt and also allows for quantitative appraisal of the effect of the abundance of melt on the temperature location of the solidus (Anderson et al., 2013; Morrissey et al., 2013). The approximately 4 wt.% H_2O content of the leucogranitic melt used for calculation of these T–M_{melt} sections is based on a comprehensive compilation of over 4600 analysed melt inclusions in granitic rocks (Thomas and Davidson, 2012).
5. Wet solidus: Enforcing a wet solidus is convenient in terms of 'estimating' H_2O as the H_2O content can be set such that there is a very minor amount of silicate melt (approximately <0.005 mol%) at the water-out field boundary (i.e. the high-temperature boundary of the narrow wet-melting field) at pressures of approximately 4–6 kbar. Indeed, there are many published phase diagrams for granulite facies conditions that

feature a wet solidus (e.g. White et al., 2001, 2007, 2014a; Boger and White, 2003; Kelsey et al., 2003a, 2004, 2005, 2008). However, it is not known whether all rocks will be water-saturated at the onset of partial melting (Guiraud et al., 2001). Phase diagrams with a water-saturated wet solidus are in many ways illustrative only as they convey closed system behaviour, i.e. no melt loss, and therefore should not be taken as blueprints for investigating the *P–T* evolution of a specific rock in which open system behaviour has occurred. Such diagrams are most commonly calculated with generalised or experimental bulk compositions when presenting a new or revised *a–x* model(s) in increasingly larger model chemical systems (e.g. White et al., 2001, 2007, 2014a,b; Kelsey et al., 2004, 2005) and to illustrate the topology of phase assemblage fields and show phase assemblages that can develop as a function of *P–T* above the solidus. Because granulite facies metamorphism is in most cases an open system process, phase diagrams with a wet solidus are rarely used to investigate in detail the *P–T* evolution of specific rocks—especially at high temperatures where melt modal abundance is calculated to be >>7 mol%—and if they have been used for rocks preserving a record of open system behaviour their application is erroneous.

7.2. Insight into the prograde evolution of granulite facies rocks through inverse modelling

Another type of melt re-integration has been applied in numerous studies, not for the estimation of H_2O, but for trying to 'back-track' or unwind (the reverse of White and Powell, 2002) the process of open-system behaviour in granulite facies rocks (e.g. Johnson and Brown, 2004; White et al., 2004; Diener et al., 2008b, 2013; Indares et al., 2008; Korhonen et al., 2010, 2013a; Boger et al., 2012; Groppo et al., 2012; Redler et al., 2012). This approach has been used mostly to try to understand more about the possible prograde history of, and/or protolith to, granulite facies rocks (e.g. Diener et al., 2008b; Korhonen et al., 2013a). There is a degree of uncertainty in this procedure as the accurate composition of melt, as well as the abundance of melt, the number of melt re-integration steps to implement and the *P–T* condition(s) at which to add melt into the existing bulk composition to track back towards wet solidus-type conditions (or even to sub-solidus conditions) is not clear from preserved granulite facies rocks. However, as a general procedure overall, this approach may provide some insight into the prograde history of granulite/UHT rocks.

7.3. Choice of model chemical system for phase diagram calculations

In terms of thermodynamic (phase diagram) calculations involving a bulk or domain rock composition for an applied study of P–T evolution, the largest possible model chemical system should be used. There are two main reasons for this: (1) the larger the model chemical system, the more closely it approaches an appropriate approximation of the natural major element composition of the rock being investigated. To date, the most reliable large model chemical system with which to perform phase diagram calculations is NCKFMASHTO (Na_2O–CaO–K_2O–FeO–MgO–Al_2O_3–SiO_2–H_2O–TiO_2–O, where 'O' represents ferric iron) for pelitic rocks (e.g. Korhonen et al., 2010, 2011, 2012b, 2013a; Liu et al., 2012; Shimizu et al., 2013; White et al., 2014a) and NCFMASHTO for mafic rocks (e.g. Johnson and White, 2011). Other major elements that can be included in phase diagram calculations include MnO (Mahar et al., 1997; White et al., 2014b) and Cr_2O_3 (Holland and Powell, 2011). Activity-compositions models for phases containing Mn have recently been updated for the first time since 1997, allowing for reliable calculations with bulk or domain compositions with MnO <0.3 wt.%. The reliability of the *a–x* models for Mn-bearing phases has not yet been tested for UHT conditions where, in addition, MnO in sapphirine and osumilite (not a feature of current *a–x* models) may have an important control on their stability (White et al., 2014b). Chromium-bearing *a–x* models have been formulated for the first time for the new ds6 thermodynamic data set (Holland and Powell, 2011). These *a–x* models are primarily for calculations on mantle rocks, and as such, Cr-bearing *a–x* models for common crustal phases other than spinel (e.g. garnet, mica) have not been formulated; (2) complications arise in reducing whole rock geochemical data in order to use a smaller model chemical system for phase diagram calculations. For example, if one chose to use KFMASHTO for calculations but the rock being modelled contains appreciable amounts of plagioclase, the whole rock composition to extract from the entirety of the whole rock geochemical data is not one that simply ignores CaO wt.% and Na_2O wt.%. The reason is that plagioclase is not only composed of Na_2O and CaO, but also significant amounts of SiO_2 and Al_2O_3. Therefore, one would need to know the abundance of plagioclase in the rock and then subtract the correspondingly appropriate amount of Al_2O_3 wt.% and SiO_2 wt.% (as well as Na_2O and CaO) from the whole rock data in order to extract the bulk composition to use for KFMASHTO calculations. Due to the unnecessary effort involved, it is better to simply use the larger (Mn) NCKFMASHTO system wherever possible for calculating phase diagrams for specific rocks. However, for the purposes of illustrating and understanding the phase equilibria that provide the underlying 'backbone' of classic UHT mineral assemblage development (e.g. the classic FMAS system), smaller systems such as KFMASH and KFMASHTO still remain useful, as discussed and shown in section 5.

8. Thermal properties of rocks

Now that UHT metamorphism has been accepted as a common mode of crustal metamorphism, and geodynamic models have historically been largely unable to predict UHT conditions at appropriate depths within continental crust (e.g. Jamieson et al., 1998; Jamieson et al., 2002), questions have been increasingly posed as to what tectonic/geodynamic scenarios are required to generate regional UHT crustal metamorphism. Consequently, more geodynamic modelling studies have been conducted with a greater focus on generating UHT conditions in Earth's crust. Two important characteristics of the crust that were not considered in the UHT reviews of Kelsey (2008) or Harley (2008) pertain to the thermal properties of rocks (e.g. Clauser, 2006, 2009) and the impact of pre-conditioning (fertility) of the crust (e.g. Vielzeuf et al. 1990; Brown and Korhonen 2009; Clark et al 2011).

8.1. Thermal properties of the crust

It has been recognised for many years that the thermal diffusivity, κ, of rocks and minerals is temperature dependent (e.g. Birch and Clark, 1940a,b; Horai and Simmons, 1969; Hasan, 1978). However, this does not appear to have featured in most geodynamic modelling studies (cf. Clark et al., 2011), where, instead, a fixed thermal diffusivity was commonly allocated to the crust. Motivated partly by the common occurrence of UHT metamorphism as well as the inability of geodynamic models to predict UHT conditions in the deep crust, there has been a resurgence in appreciating and quantifying the impact that temperature-dependent thermal diffusivity has on the thermal structure of the crust, and hence temperatures in the deep crust (e.g. McKenzie et al., 2005; Mottaghy et al., 2008; Whittington et al., 2009; Clark et al., 2011; Nabelek et al., 2012). Of importance to the question of how UHT rocks get hot, it is critical to understand that thermal diffusivity

(and thermal conductivity, but less so) of rocks decreases with increasing temperature (e.g. Vosteen and Schellschmidt, 2003; Clauser, 2006, 2009). Thermal diffusivity of the crust is usually taken to be 1 $mm^2\ s^{-1}$ in modelling studies. However, thermal diffusivity of a range of crustal rock types decreases rapidly from about 2 to 0.7 $mm^2\ s^{-1}$ in the approximate interval 0–575 °C and decreases more slowly above about 575 °C to values of approximately 0.7–0.3 $mm^2\ s^{-1}$ for the deep crust and upper mantle (Fig. 11; Whittington et al., 2009). Thermal diffusivity and thermal conductivity are both forecast to be lowest in the deep crust (Fig. 11; e.g. Clauser, 2006, 2009), thus implying that the deep crust is the most insulating part of the crust (and crustal lithosphere; Whittington et al., 2009). Two far-reaching implications of this are that, first, rocks will stay hot for a prolonged period once they've (eventually) been heated, and second, large amounts of energy are required in order to heat rocks in the lower crust. However, the converse is that there is significant impediment to rocks reaching extreme temperatures (>900–1000 °C) as conduction does not favour high temperatures due to the flow of heat from hotter to colder materials.

8.2. Buffering of temperature by partial melting

Adding to the impeding effect from the inherent thermal properties of lower crustal rocks is that prograde reactions and particularly partial melting reactions also hinder the increase of mid-to-deep crustal temperatures. Prograde metamorphic mineral reactions are typically endothermic (e.g. Lyubetskaya and Ague, 2009). For partial melting more specifically, these reactions require an extensive amount of heat energy to proceed (e.g. Bea, 2012). Consequently, partial melting, or the latent heat of fusion, results in a buffering of crustal temperatures (Bridgwater et al., 1974; O'Hara et al., 1978; Vielzeuf et al., 1990; Stüwe, 1995; Thompson and Connolly, 1995; Depine et al., 2008; Brown and Korhonen, 2009; Bea, 2012), such that temperature increases are impeded while major melt-producing reactions proceed. The absolute magnitude or extent of thermal buffering provided by partial melting reactions is a matter of some debate (e.g. Vielzeuf et al., 1990; Thompson and Connolly, 1995; Brown and Korhonen, 2009). Nevertheless, Vielzeuf et al. (1990) eloquently argued that pre-conditioning, or fertility, of the crust is a vital factor in whether or not UHT conditions can be achieved. In detail, it is argued that fertile mid- to deep-crustal rocks/terranes going through their first metamorphic event have far less potential to reach UHT conditions because of the thermal buffering effect of partial melting; but that rocks/terranes melted in a previous metamorphic cycle (or a long-lived single cycle) are less fertile (more 'mature') and therefore less prone to melt-related thermal buffering in consequent events. That is, melt-depleted, residual source rocks/terranes have the most potential to reach UHT conditions (e.g. Vielzeuf et al., 1990; Brown and Korhonen, 2009; Clark et al., 2011). It is interesting to note that three classic regional UHT terranes, the Napier Complex in Antarctica, Eastern Ghats Province in India and In Ouzzal terrane in Algeria are characterised by sapphirine + quartz and orthopyroxene + sillimanite + quartz rocks that are more typically gneissic, rather than migmatitic (Sandiford and Wilson, 1984, 1986; Sandiford, 1985a; Osanai et al., 1999; Ouzegane et al., 2003b; Clark et al., 2013). If the logic of Vielzeuf et al. (1990) and Clark et al. (2011) is correct, this could imply that the crust of at least these three terranes was pre-conditioned before the UHT metamorphic event; or alternatively that the crust was 'pre-conditioned' during a very long single event (Korhonen et al., 2013b), where the heat source for thermally extreme metamorphism was maintained for a sufficiently long timescale (Brown and Korhonen, 2009).

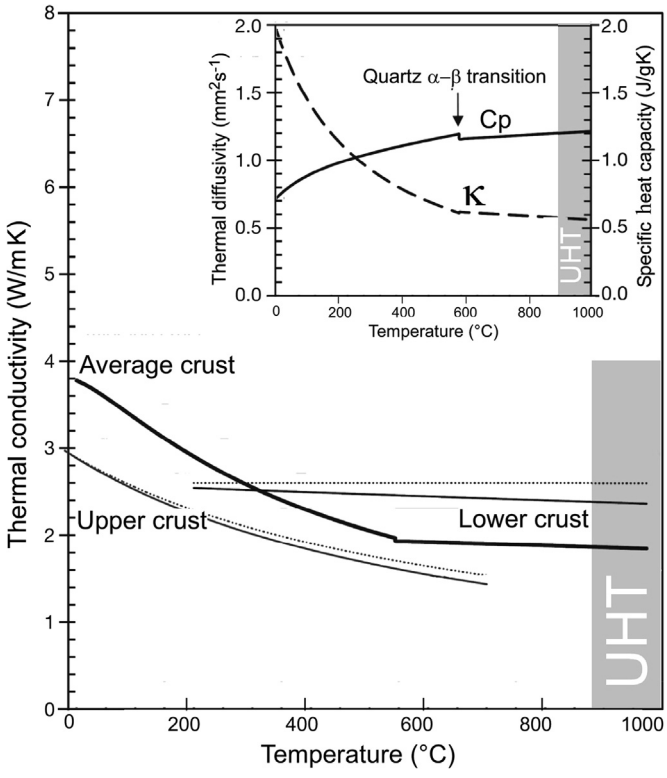

Figure 11. Summary of thermal conductivity, thermal diffusivity and heat capacity of upper, lower and average crust. The lower crust has low thermal conductivity and diffusivity meaning that it is difficult to heat but once heated is slow to cool. The temperature realm of UHT granulites is shaded grey. Adapted from Whittington et al. (2009).

8.3. Heat sources for UHT metamorphism

The majority of UHT localities and terranes are characterised by apparent thermal gradients >>75 °C $kbar^{-1}$ (Pattison et al., 2003; Brown, 2006, 2007a,b). The conductive limit of crustal metamorphism is in the vicinity of about 100 °C $kbar^{-1}$ (Jaeger, 1964; Sandiford and Hand, 1998a; Stüwe, 2007; Brown, 2008b), implying that for many occurrences of UHT (and lower temperature granulite) metamorphism (e.g. Pattison et al., 2003; Brown, 2006) it is improbable that the heat source is purely conductive, assuming modest to low crustal heat production (approximately less than 1.5–2 $\mu W\ m^{-3}$) and mantle heat flow of approximately 30 $mW\ m^{-2}$. In combination with *P–T* constraints from UHT rocks, such steep thermal gradients imply that the crust cannot be substantially thicker than the depths recorded by many UHT rocks due to the limit imposed by the dry peridotite solidus (e.g. Harley, 2004). In such situations advective mantle heat sources have been widely invoked to generate the very high apparent thermal gradients (Ellis, 1980; Wells, 1980; Sandiford, 1985a; Bohlen, 1987, 1991; Sandiford et al., 1987; Huppert and Sparks, 1988; Bohlen and Mezger, 1989; Harley, 1989; Vielzeuf et al., 1990; Sandiford and Powell, 1991; Brown, 1993; Collins, 2002; Brandt et al., 2007; Stüwe, 2007). However, curiously, numerous regional UHT/granulite terranes, at least at the current level of exposure, are not characterised by voluminous, syn-metamorphic mafic or ultramafic rocks (e.g. Ellis, 1980; Collins, 2002; Harley, 2004; Baldwin and Brown, 2008; Clark et al., 2011; Smithies et al., 2011). In rare cases coeval mantle magmatism is directly linked to granulite formation (Yoshino and Okudaira, 2004; Kemp et al., 2007; Maidment et al., 2013). In some other instances mafic magmatism was not coeval with regional granulite facies metamorphism (e.g. Barboza et al., 1999), but resulted in a contact aureole superimposed on

the regional event (Barboza and Bergantz, 2000). The apparent absence of syn-metamorphic mafic and/or ultramafic rocks from many UHT terranes could be due to hydridization of mafic magmas with crustal-sourced magmas (e.g. Vielzeuf et al., 1990; Collins and Richards, 2008; Smithies et al., 2011) or remelting of (depleted?) mafic rocks (Collins and Richards, 2008).

Other heat sources that have been proposed for generating regionally hot/UHT temperatures, either in isolation but more probably in concert (see Brown and Korhonen (2009) for review), are radiogenic crustal heat production (e.g. England and Thompson, 1984; Chamberlain and Sonder, 1990; Jamieson et al., 1998; Sandiford and Hand, 1998b; Kramers et al., 2001; Andreoli et al., 2006; Clark et al., 2011; Bea, 2012), elevated mantle heat flow (England and Thompson, 1984; Collins, 2002; Hyndman et al., 2005; Currie and Hyndman, 2006; Hyndman et al., 2009; Hyndman and Currie, 2011) and local or pervasive strain (viscous) heating (e.g. Kincaid and Silver, 1996; Stüwe, 1998; Burg and Gerya, 2005; Nabelek et al., 2010; Duretz et al., 2014). In the landmark study of England and Thompson (1984), UHT conditions at appropriate depths were simulated using elevated values for mantle heat flow as well as radiogenic crustal heat production, and low crustal thermal conductivity. The first study to specifically address how UHT conditions can be generated in continental crust, through quantitatively predicting (using a 1D heat flow equation) the coupled temperature effect of radiogenic heat production, mechanical (strain) heating and chemical (e.g. melting) heating, was that of Clark et al. (2011). In order to generate regional UHT conditions for rocks instantaneously buried to the deep (40 km) crust, Clark et al. (2011) found that the following were required: (1) (very) elevated ($\geq$3.5 $\mu W\ m^{-3}$) upper-crustal radiogenic heat production; (2) slow ($\leq$0.05 $mm\ y^{-1}$) erosion rates; (3) suppression of partial melting ('pre-conditioning' of crust as per Vielzeuf et al., 1990); and (4) a suitable and volumetrically large enough (tectonic) setting (see next section) that allows for incubation of the lower crust for long periods of time. Scenarios that were not found to generate UHT conditions for probable ranges of input parameters were mechanical heating—as rock strength decreases rapidly with increasing temperature—and thickening of back-arc basins in crust with low to average upper-crustal radiogenic heat production.

9. Timescales and tectonic settings of regional UHT/granulite metamorphism

9.1. Timescales and geochronometers

For many UHT terranes/localities, the petrological framework and *P–T* evolution have been adequately determined. One of the most exciting areas of research with respect to UHT metamorphism over the past seven years has been to much more comprehensively understand the timescales of UHT metamorphism. Crucially, timescale information provides critical data for ideas on tectonic settings of UHT metamorphism. The vast increase in geochronological data sets over the past decade or so is largely due to increased availability of SIMS and LA–ICP–MS, and this has meant that detailed research into the time-dependence of crustal processes, as well as trace element thermometry and REE partitioning between minerals, can now be done as part of routine terrane analysis with high analytical precision and resolution. Where geochronological data can be linked to *P–T* point or *P–T* path segment information (e.g. Goncalves et al., 2004; Tomkins et al., 2005; Kelsey et al., 2007; Drüppel et al., 2013; Bhowmick et al., 2014), for example via studying Y + REE partitioning between zircon and/or monazite and garnet and/or orthopyroxene (e.g. Hermann and Rubatto, 2003; Möller et al., 2003; Hokada and Harley, 2004; Kelly and Harley, 2005; Tomkins et al., 2005; Kelly et al., 2006; Harley and Kelly, 2007b; Baldwin and Brown, 2008; Clark et al., 2009; Kotková and Harley, 2010; Kelly et al., 2012), it provides important constraint on timescales of (UHT) metamorphic processes; and in turn the *P–T–t* information can be used to better constrain possible tectonic settings. As this integration of multi-disciplinary data has increased, the timescales over which regional UHT metamorphism occurs are now better understood.

Before discussing in more detail the constraints on timescales of regional UHT metamorphism, it is first worth considering in more general terms that timescale is dependent on a multitude of interconnected factors including tectonic setting, particle path vectors (especially *P–t* paths) of an analysed rock, the type and duration of heat source(s), erosion rate and thermo-physical properties of rocks such as thermal diffusivity. *P–t* paths are potentially more informative about tectonic settings/processes of UHT metamorphism than *P–T* paths because *P–T* path shapes are not unique to tectonic setting (e.g. Bohlen, 1991; Stüwe and Sandiford, 1995; Brown, 2007a; Stüwe, 2007) and as such they do not provide an easily accessible absolute-time-integrated view of the physical passage of a rock through an orogen (Stüwe, 2007; Jamieson and Beaumont, 2013). In addition, the question of 'what is the duration of metamorphism?' has two aspects to it. The first relates to the timescale of metamorphism at the scale of the orogen, which is reflected by the duration of the heat source causing the metamorphism. The second is the duration of metamorphism as recorded by a specific hand specimen-sized rock sample within that orogen. The timescales are unlikely to be one and the same (even when assuming the ideal scenario with uninhibited geochronometer mineral growth). The probability that a single rock will preserve the entirety of the duration of the orogen-scale heat source is strongly dependent on the *P–T–t* loop a rock follows within an orogen. For rocks that exhume rapidly, recording the duration of the orogen-scale heat source is less probable since the exhuming rocks will carry some of the heat from deep in the crust with them, but there is no necessity that the orogen-scale heat source must get simultaneously exhumed. By contrast, rocks that near-isobarically cool stand a far greater chance of recording the timescale because they stay within the orogen. Therefore, the *P–T–t* loop can play a critically important role in controlling whether rocks at Earth's surface are more or less likely to record a small fragment of the total duration (i.e. very much a minimum duration) versus a more complete duration of the orogenic-scale heat source driving metamorphism.

The U–Pb isotopic decay systems in the accessory minerals zircon ($ZrSiO_4$) and monazite [(LREE,Y,Th,U,Ca](Si,P)O_4] are the most commonly used geochronometers for obtaining age constraints on granulite and UHT metamorphism. Geochronology is now routinely carried out in situ to preserve the microstructural content of the geochronometer in thin sections of rock specimens. Zircon is typically considered to be less reactive than monazite, including within melt-bearing rocks (e.g. Högdahl et al., 2012; Rubatto et al., 2013), suggesting that the concomitant use of the two geochronometers from the same rock has the potential to provide insight into the temporal evolution of a terrane that one geochronometer (zircon) in isolation may not provide (e.g. Kelsey et al., 2008). Indeed, combined zircon and monazite geochronology, perhaps coupled with trace element (i.e. REE) partitioning/distribution data to determine whether equilibrium existed between zircon (or monazite) and major minerals occurred (e.g. Rubatto, 2002; Whitehouse, 2003; Whitehouse and Platt, 2003; Foster et al., 2004; Kelly and Harley, 2005; Harley and Kelly, 2007b; Harley et al., 2007; Rubatto et al., 2013), and phase diagrams where possible (Spear, 2010; Spear and Pyle, 2010; Kelsey and Powell, 2011; Cubley et al., 2013; Yakymchuk and Brown,

2014a), currently provides the most thorough approach to interpreting U–Pb age data sets. However, there are five primary complications in using and interpreting zircon and monazite U–Pb age data to constrain timescales of UHT metamorphism.

First, the Pb closure temperature in zircon and monazite is close to, or even exceeded by, temperatures >900 °C, depending on the size of the zircon or monazite grain, the heating and/or cooling rate of the rocks/terrane, the amount of melt present and the amount of strain leading to recrystallisation (e.g. Ashwal et al., 1999; Cherniak and Watson, 2001; Cherniak et al., 2004; Sajeev et al., 2010; Halpin et al., 2012; Wawrzenitz et al., 2012; Williams and Jercinovic, 2012; Ayers et al., 2013). In some cases, favoured by 'dry' rock compositions, U–Pb age data have been interpreted to either record protracted growth of zircon or monazite over (very) long timescales at UHT conditions (Korhonen et al., 2013b; Walsh et al., 2014) or provide evidence that monazite (or zircon) U–Pb systematics are capable of remaining closed to diffusion even when temperatures are exceedingly high (approximately 1050 °C; Black et al., 1986; Harley and Black, 1997; Hacker et al., 2000; Kelly and Harley, 2005; Sajeev et al., 2010).

Second, temperatures >900 °C may exceed that at which zircon and/or monazite (completely) dissolve into melt during heating along the prograde path (Watson and Harrison, 1983; Rapp and Watson, 1986; Rapp et al., 1987; Kelsey et al., 2008; Spear, 2010; Spear and Pyle, 2010; Kelsey and Powell, 2011; Stepanov et al., 2012; Boehnke et al., 2013; Yakymchuk and Brown, 2014a). The important implication is that zircon and/or monazite ages may not record growth at the thermal peak of metamorphism but may instead only record (part of) the retrograde evolution (e.g. Roberts and Finger, 1997; Kelsey et al., 2008; Yakymchuk and Brown, 2014a).

Third, uranogenic Pb in zircon can be locally and patchily distributed at scales similar to SIMS analytical volumes, leading to erroneously old $^{207}Pb/^{206}Pb$ ages (Hinton and Long, 1979; Kusiak et al., 2013a,b). The development of patchy Pb distribution occurs during UHT metamorphism and thus far has been identified in UHT rocks of the Napier Complex and Southern Granulite Terrane, India (Whitehouse et al., 2014; Williams et al., 1984; Black et al., 1986; Harley and Black, 1997; Kelly and Harley, 2005; Kusiak et al., 2013a,b). Patchy distribution of uranogenic Pb is identified in UHT rocks on the basis of unusual sputtering behaviour of Pb during U–Pb analysis of zircon with SIMS, as well as with high resolution scanning ion imaging and/or tomography (Whitehouse et al., 2014; Williams et al., 1984; Kelly and Harley, 2005; Kusiak et al., 2013a,b). The patchy distribution of uranogenic Pb is not spatially related to cracks, primary radiation damage, concentration of U or Th in zircon, nor inclusions (Whitehouse et al., 2014; Kusiak et al., 2013a,b). Because patchy Pb distribution affects $^{207}Pb/^{206}Pb$ ages, an important implication is that attempts to constrain the timescale of UHT metamorphism with affected data are hampered.

Fourth, it is well documented that (late) low-temperature fluid ingression and/or metasomatism can have a major impact on monazite stability, leading to dissolution–precipitation and resetting of its U–Pb(–Th) isotope system (e.g. DeWolf et al., 1993; Teufel and Heinrich, 1997; Zhu et al., 1997; Townsend et al., 2000; Seydoux-Guillaume et al., 2002; Zeh et al., 2003; Budzyń et al., 2011; Harlov et al., 2011; Williams et al., 2011; Janots et al., 2012; Kelly et al., 2012; Ondrejka et al., 2012; Seydoux-Guillaume et al., 2012; Sindern et al., 2012; Upadhyay and Pruseth, 2012; Didier et al., 2013). Zircon U–Pb systematics can also be affected by (late-stage) fluid that induces dissolution and reprecipitation (e.g. Vavra and Schaltegger, 1999; Carson et al., 2002; Kirkland et al., 2009; Kooijman et al., 2011).

The four preceding complications can and do result in discordant age analyses. Monazite older than approximately 100 Ma should not be reversely discordant as U–Pb ages will not be plagued by excess ^{206}Pb related to decay of ^{230}Th (Schärer, 1984). In such cases where reverse discordancy occurs in old (approximately >100 Ma) monazite, $^{207}Pb/^{235}U$ ages are typically considered more reliable (e.g. Corfu, 2013). Patchy uranogenic Pb in zircon results in reverse discordance (Williams et al., 1984; Black et al., 1986; Kelly and Harley, 2005; Kusiak et al., 2013a,b), but, depending on the difference in age between zircon growth and Pb mobilization ('Pb gain'), analyses can smear along concordia to give the effect of continuous growth and/or Pb loss.

Fifth, the systematic growth and dissolution behaviour of zircon and monazite as a function of rock composition, pressure, temperature and silicate phase assemblage evolution remains incompletely known (e.g. Janots et al., 2007; Janots et al., 2008; Kelsey et al., 2008; Spear, 2010; Spear and Pyle, 2010; Kelsey and Powell, 2011; Yakymchuk and Brown, 2014a). Therefore, the specific detail of exactly where zircon and monazite grow along a *P–T* path in a specific rock remains subject to debate, but in detail is critical to improving the resolution with which we understand timescales of (UHT) metamorphism. Without this resolution, it is not necessarily clear from geochronological ± corresponding trace element data sets how long a particular rock (or terrane) remained in the UHT 'window'.

Each of the above five issues can make the interpretation of U–Pb age data sets from zircon and/or monazite problematic (e.g. Halpin et al., 2012; Korhonen et al., 2013b). An interesting case in point is the classic Napier Complex, Antarctica, where, despite many studies, the extreme temperatures of UHT metamorphism have prevented clear-cut estimations of timescale and even specific timing of the UHT event (e.g. see Horie et al., 2012 for overview).

Interpreting zircon U–Pb age data from high-temperature metamorphic rocks has traditionally been somewhat plagued also by the internal morphology (seen using cathodoluminescence, CL) of zircon, which can be extremely complex (e.g. Hoskin and Schaltegger, 2003; Kelly and Harley, 2005; Halpin et al., 2012; Corfu, 2013). To help in the interpretation of zircon ages as either 'metamorphic' or 'magmatic' when CL imaging reveals complex internal zoning, the Th/U ratio at the spot of age analysis has commonly been called upon. Traditionally, Th/U ratios <0.1 were interpreted to indicate 'metamorphic' zircon, and commonly, the corresponding part of the zircon was characterised by a featureless CL response (e.g. Williams and Claesson, 1987; Williams et al., 1996; Rubatto, 2002; Hermann and Rubatto, 2003). However, Th/U ratios <0.1 cannot, unfortunately, be used as a robust indicator of metamorphically-grown zircon, for the reason that the Th/U ratio is strongly controlled by the presence (and coexistence) of other Th-bearing minerals such as monazite, allanite, xenotime and/or fluid/melt (e.g. Kelly and Harley, 2005; Högdahl et al., 2012). If phases with a strong affinity for Th are present along with zircon, this will more probably result in low Th/U ratios in zircon, regardless of whether the zircon is of magmatic or metamorphic origin. Therefore, in such situations the Th/U ratio cannot uniquely define zircon as having a metamorphic origin (e.g. Whitehouse and Kamber, 2002; Möller et al., 2003; Bingen et al., 2004; Harley and Kelly, 2007b; Harley et al., 2007; Högdahl and Lundqvist, 2009; Corfu, 2013). The UHT rocks of the classic Napier Complex provide a useful example of Th/U >>0.1 in zircon when there are no phases present with a strong affinity for Th (Harley and Black, 1997; Kelly and Harley, 2005). Zircons in the study of Kelly and Harley (2005) have a large range of U concentrations (approximately 100–6400 ppm U) but Th/U is commonly >>0.1 due to zircon being the main sink of Th, regardless of the type of zoning for the corresponding part of the zircon.

In addition to the complicating issues outlined above, processes such as melt loss can lead to different ages being recorded in different rocks in the same terrane because melt loss elevates the

solidus temperature of residual rock (e.g. White and Powell, 2002). Using the results and logic of Kelsey et al. (2008), monazite ages in numerous studies have been interpreted to approximate the age at which the elevated solidus was crossed during cooling (e.g. Brown and Korhonen, 2009; Kali et al., 2010; Warren et al., 2011; Baba et al., 2012; Clark et al., 2012; Jian et al., 2012; Reno et al., 2012; Korhonen et al., 2013a,b; Weinberg et al., 2013; Morrissey et al., 2014). However, Stepanov et al. (2012) argued that the rate of monazite dissolution with increasing temperature is overestimated in the Kelsey et al. (2008) study. Stepanov et al. (2012) stated that temperature, and not melt composition (cf. Kelsey et al., 2008), is a stronger control on monazite dissolution. The experimental data of Stepanov et al. (2012) indicated that monazite will survive to higher temperatures than predicted by Kelsey et al. (2008; see also Yakymchuk and Brown, 2014a), implying that it is not necessarily so trivial to tie monazite age data from partially melted rocks to the down-temperature crossing of the elevated solidus. In addition, the growth rate of zircon and monazite with cooling in melt-bearing systems is known to be non-linear (Watson, 1996; Williams, 2001; Harrison et al., 2007; Kelsey et al., 2008; Yakymchuk and Brown, 2014a). However, in melt-depleted rocks such as UHT granulites monazite geochronology may effectually represent the age at which the elevated solidus was crossed upon cooling (Reno et al., 2012; Korhonen et al., 2013b; Yakymchuk and Brown, 2014a).

Lu–Hf garnet geochronology presents an additional or alternative avenue for chronometry of granulite and UHT rocks. However, at present it has seen little application to granulite facies rocks (Choi et al., 2006; Kelly et al., 2011; Smit et al., 2013). This chronometric method requires garnet grains to be separated from the rock and analysed as a bulk separate with either the whole-rock or a separate of at least one other Lu–Hf-bearing mineral (e.g. rutile or ilmenite). In garnet, the diffusivity of Lu is one to two orders of magnitude higher than that of Hf at about 900 °C (Kohn, 2009) but net diffusive loss of Lu is not expected due to its strong affinity for garnet (Smit et al., 2013). Conversely, Hf is incompatible in garnet and its closure temperature is calculated to exceed 900 °C for a range of grain sizes if cooling rates are sufficiently fast (approximately >20 °C Ma^{-1}; Smit et al., 2013).

If garnet has been partially resorbed, back-diffusion of Lu (analogous to Mn) has the effect of causing Lu/Hf ratios to become higher, resulting in Lu–Hf ages younger (so-called 'apparent ages') than the actual age of garnet crystallisation (Kelly et al., 2011). The difference between apparent and actual ages increases with the extent of resorption and with increasing time between initial isotopic decay (after growth) and resorption (Kelly et al., 2011). Possible contamination of garnet from sub-microscopic zircon and/or rutile and/or ilmenite inclusions (Smit et al., 2013) can additionally reduce Lu–Hf age precision, particularly if the inclusions are much older or younger than host garnet (Scherer et al., 2000). Nevertheless, Lu–Hf geochronology is expected to be most successful in application to fast-cooled granulite/UHT rocks as well as garnet that has not been significantly resorbed. In these instances Lu–Hf garnet ages will more probably indicate growth rather than apparent ages (Smit et al., 2013).

Overall, the somewhat blurred resolution we have for matching age data sets to specific/exact parts of the *P–T* evolution of UHT rocks (in particular) means that, in some respects, order-of-magnitude estimates on the timescales of UHT metamorphism are possibly about as precise as timescale estimates can be. Indeed, most researchers are cautious about proposing timescales of UHT metamorphism as a result of the multitude of factors introducing uncertainty to the interpretation of U–Pb age data. Nevertheless, from the available data (Table 2, Fig. 12) there appears to be, broadly and simplistically, a continuum in the timescales over which UHT

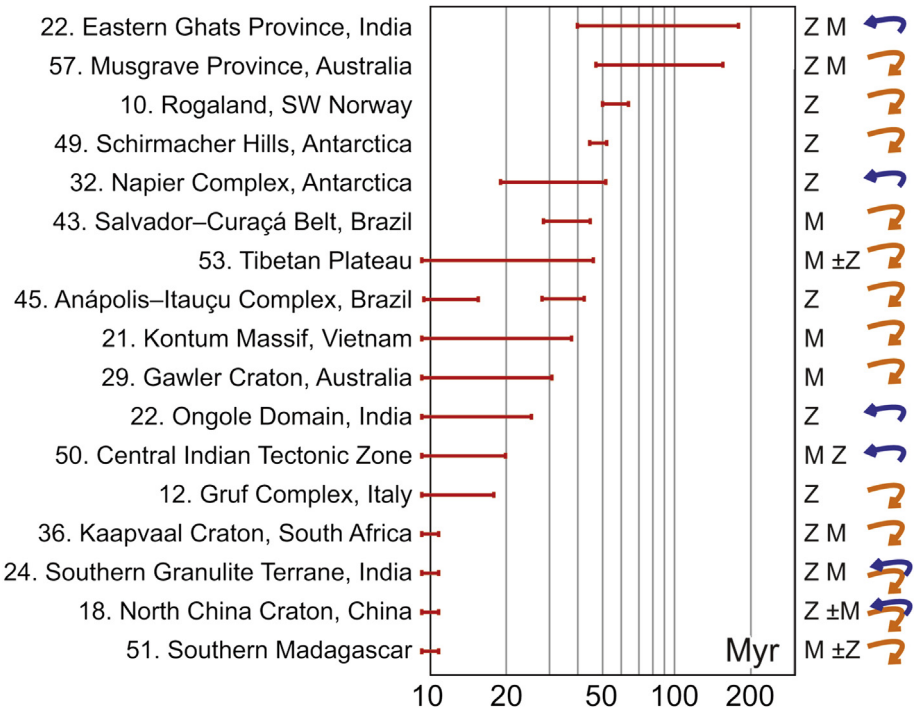

Figure 12. Summary of timescales proposed for UHT metamorphism in numerous terranes/localities. Timescale ranges for most terranes/localities are very approximate (see Table 2 for references for each terrane/locality) owing to issues regarding geochronological data from UHT rocks outlined in the main text. Proposed timescales of <5–10 Myr are depicted with a span just exceeding 10 Myr. The geochronometer used for constraining the timescale of UHT metamorphism is denoted by Z (zircon) and/or M (monazite). Schematic *P–T* paths shown for each terrane/locality are based on reported *P–T* trajectories or are here interpreted on the basis of reported paragenetic sequence. The 'clockwise' (orange) vs. 'anticlockwise' (blue) notation is defined on the basis of pressure increasing up the page and temperature increasing from left to right and indicates that *P–T* path shape is independent of timescale.

metamorphism has been classified, ranging from 'short', of the order of approximately <5–40 Myr (Table 2; Schmitz and Bowring, 2003; Baldwin and Brown, 2008; Clark et al., 2009; Leite et al., 2009; Santosh et al., 2009c, 2012, 2013; Schmitz et al., 2009; Brandt et al., 2011; Cutts et al., 2011a; Galli et al., 2011; Giustina et al., 2011; Jöns and Schenk, 2011; Orejana et al., 2011; Guo et al., 2012; Xiang et al., 2012; Nakano et al., 2013; Bhowmick et al., 2014; Sarkar et al., 2014); and 'long', of the order of approximately ≥40 Myr (Baba et al., 2010; Das et al., 2011; Korhonen et al., 2011; Smithies et al., 2011; Drüppel et al., 2013; Korhonen et al., 2013b; Walsh et al., 2014). The timescale of UHT metamorphism for a particular locality/terrane will be dependent on the longevity of the heat source as well as numerous other factors discussed earlier (see section 8) that comprise the total geologic and tectonic system (Brown and Korhonen 2009). The concept that metamorphism of the deep crust can take place over timescales of >>40 Ma, and be recorded by minerals such as zircon and monazite, is not necessarily a new concept (e.g. O'Hara et al., 1978; Chardon et al., 2009; Smithies et al., 2011), especially in light of the importance of factors such as elevated crustal heat production and slow erosion rates (Clark et al., 2011) that aid in generating and sustaining UHT conditions in the crust, but is possibly one that is not widely accepted for UHT metamorphism.

9.2. Tectonic settings of regional UHT/HT granulite metamorphism

Unequivocally deciphering the tectonic setting of regional UHT metamorphism based on field study is commonly not possible since the old age and/or intensity of deformation and erosional removal of overlying crust has typically removed the original geologic and tectonic context in which UHT metamorphism of the deep crust occurred (cf. Pownall et al., 2014). However, particle path vectors, i.e. P–T paths and/or P–t paths, derived through integrating careful petrographic analysis with calculated pseudosections and geochronology provide the primary basis for mounting discussions on potential tectonic settings. This is because temporal variations in P and T in a metamorphic terrane are primarily a function of heat source, heat transfer mechanisms and the interaction between crustal loading and Airy (and/or thermal) isostatic response (England and Richardson, 1977; Wells, 1980; Sandiford, 1985a; Harley, 1989; Brown, 1993; Hyndman and Currie, 2011). For example, a granulite/UHT terrane formed in thickened crust will probably be exhumed more rapidly than one formed in relatively normal thickness crust near Airy or thermal isostatic equilibrium and thus be (likely) characterized by a different P–T ($-t$) path. Interestingly, most UHT terranes that have evolved over timescales of >>50 Myr (above and Table 2) are characterized by P–T paths involving near-isobaric cooling (Baba et al., 2010; Korhonen et al., 2011; Korhonen et al., 2013a,b) that evolve down-temperature close to parallel with the apparent thermal gradient (e.g. Walsh et al., 2014), regardless of whether the overall P–T path is interpreted to be clockwise or anticlockwise. The one current exception is the c. 1000 Ma Sveconorwegian Orogen in Rogaland, which is interpreted to have involved a strongly decompressive clockwise P–T path (Drüppel et al., 2013). However, as forward numerical modelling approaches become more geologically realistic through testing against rock-based P–T–t data (Jamieson and Beaumont, 2013), P–T–t path data derived from regional metamorphic terranes are likely to become increasingly compared to these forward models of large-scale geodynamic processes to understand and/or infer the setting of UHT (and other types of) metamorphism.

As summarised in earlier sections, UHT metamorphism is characterized by elevated thermal gradients and the main sources of heat for establishing such gradients are considered to be radiogenic crustal heat production and/or advective and/or conductive mantle heat, coupled with slow erosion and reduced fertility (pre-conditioning) of crust (e.g. Vielzeuf et al., 1990; Currie and Hyndman, 2006; Clark et al., 2011). The tectonic setting(s) responsible for the formation of granulite/UHT metamorphism has long been a topic of debate. However, as established by Brown (2007a,b) there are principally two types of orogenic systems that characterise the Archean through to modern Earth: accretionary and collisional. As granulite/UHT metamorphism appears to be punctuated throughout Earth history (Brown, 2006, 2007a), this may limit the tectonic/geodynamic possibilities for granulite/UHT formation.

Prior to the early- to mid-1980s the broader geologic/geodynamic context of granulite (or 'Archaean high grade gneiss terrane') formation, when broached, appears to have been largely interpreted to occur in active subduction–accretion ("Cordilleran") type settings, with regionally extensive sub-horizontal fabrics–with recumbent isoclinal folds–generated through crustal-scale thrust-stacking related processes (e.g. Bridgwater et al., 1974; Windley and Smith, 1976; Tarney and Windley, 1977; James and Black, 1981; Park, 1981), including at arcs (Windley and Smith, 1976), or by prolonged lower-crustal laminar flow (e.g. Holland and Lambert, 1969). Interestingly, Park (1981) proposed that crustal thinning followed by compression/thickening could produce granulite facies metamorphism and sub-horizontal fabrics. However, by and large, accretionary-related processes were largely ignored as mechanisms for granulite/UHT formation until the early 2000s.

Tectonic models proposed for granulite formation from the late 1970s through to the 1990s (approximately) were mostly based on collisional orogenic systems and were probably largely driven by a combination of: (1) the landmark England and Richardson (1977) and England and Thompson (1984) papers on the generation of 'clockwise'[3] P–T paths in erosion-influenced continent–continent collision settings; (2) a large number of granulite terranes being characterized by 'clockwise' P–T paths (e.g. summary in Harley, 1989); and (3) the total modern day crustal thickness in regions of exposed granulites being of 'normal' (approximately 35 km) thickness. The third point mostly fell out of favour towards the end of the 1980s as it was based on the incorrect assumption that ancient (usually inferred to be Archean) crustal thickness was the sum of depths inferred from granulite facies mineral assemblage barometry and modern day crustal thickness in exposed granulite terranes. This invalid summation of crustal thicknesses led to the common interpretation that ancient crust was of the order of approximately 50–80 km thick. Consequently, the prevailing tectonic interpretation for most granulite formation was within substantially over-thickened crust, based on Tibetan Plateau-style continental collision models (England and Richardson, 1977; Ellis, 1980, 1987; Park, 1981; England and Bickle, 1984; Bohlen, 1987; Newton, 1987; Harley, 1989; Harley and Fitzsimons, 1991; Harley, 1995). In some of these models, granulite facies conditions were interpreted to occur as a result of extensional collapse of the plateau and/or lithospheric delamination which brought the asthenosphere closer to the Moho and also helped to explain P–T paths with the retrograde part characterized by steep isothermal decompression (mafic magmatic underplating; Ellis, 1980, 1987; Housman et al., 1981; Sonder et al., 1987; Harley, 1988, 1989; Sandiford, 1989; Harley and Fitzsimons, 1991; Platt and England, 1993; Gibson and Ireland, 1995; Platt et al., 1998). Nevertheless, it appears necessary to invoke tectonic thinning processes that operate on shorter timescales than erosion to explain the geometry

[3] Clockwise is used here in the sense of P increasing up page and T increasing from left to right. Anticlockwise is used herein with the same reference frame.

of near-isothermal decompression paths and the high temperatures at which decompression typically occurs (e.g. Harley 1989). To add to the complexity, near-isobaric cooling (IBC) *P–T* paths and/or regionally sub-horizontal fabrics (e.g. Napier Complex) were sometimes also proposed to reflect possible extensional collapse of Tibetan-style thickened crust (England and Thompson, 1986; Sonder et al., 1987; Harley, 1989; Sandiford, 1989).

More commonly, granulites featuring near-IBC along 'anticlockwise' *P–T* paths have historically been interpreted to develop in regions of large-scale, synchronous (mantle) magmatism that either underplates or 'overaccretes' (Hensen and Green, 1973; Ellis, 1980; Wells, 1980; Sandiford and Powell, 1986a; Bohlen, 1987, 1991; Bohlen and Mezger, 1989; Harley, 1989, 2000; Motoyoshi and Hensen, 1989; Hensen and Motoyoshi, 1992; Brandt et al., 2007; Wan et al., 2013). Less commonly, granulites—specifically including UHT granulites—were considered to form in regions of lithospheric extension (Vielzeuf and Kornprobst, 1984; Weber, 1984; Wickham and Oxburgh, 1985; Sandiford and Powell, 1986a; Ellis, 1987; Harley, 1989; Sandiford, 1989; Zen, 1995) on the basis of near-IBC *P–T* paths, recumbent gneissic fabrics (James and Black, 1981; Sandiford and Wilson, 1984; Sandiford, 1985a; Harley, 1989; Bohlen, 1991), *P–T* estimates that indicate metamorphism at the base of approximately normal thickness crust and geochronology that indicated long crustal residence times and thus low erosion rates (Grew and Manton, 1979; James and Black, 1981; DePaolo et al., 1982; Black et al., 1983a,b; Sandiford, 1985b, 1989; Sandiford and Powell, 1991). In these cases, the main heat source causing UHT metamorphism is stated or implied to be mafic mantle magmatism. The above conjecture regarding IBC-dominated *P–T* paths (see also Harley (1989) for the many and varied mechanisms for IBC-path development), sometimes by the same authors, highlights the limitations that *P–T* paths in isolation have for delineating tectonic setting (Stüwe, 2007; Jamieson and Beaumont, 2013).

The above conjecture about the tectonics of granulite facies metamorphism was at a time when regional temperatures of approximately 900–1000 °C in the deep crust were mostly being doubted as a result of the use of conventional thermobarometric techniques to retrieve temperature estimates of granulite formation (see Kelsey, 2008). This was despite the robust results of experimental studies conducted chiefly by Hensen and Green (1970, 1971, 1972, 1973) where diagnostic UHT mineral assemblages were found to develop at extreme (>900 °C) temperatures. Because temperatures estimated by conventional thermometers were in the vicinity of 700 °C (see Frost and Chacko, 1989; Harley, 1989), the follow-on implication was that apparent thermal gradients were not required to be as high as had been suggested for granulites, particularly those of the Napier Complex, Labwor Hills and Lewisian Complex which were viewed as 'anomalous'. In this context, it is not surprising that tectonic models for granulite facies metamorphism focused on achieving lower temperatures (approximately 700–800 °C) in the mid- to deep-crust and that tectonic models trying to explain (rare) localities such as the more thermally-extreme Napier Complex were, for the most part, not pursued. However, in the 1990s and early 2000s the significance of the seminal experimental work of (e.g.) Hensen and Green was revisited in light of a series of new petrological experiments conducted for Mg–Al-rich UHT mineral assemblages (Bertrand et al., 1991; Motoyoshi et al., 1993; Audibert et al., 1995; Carrington, 1995; Carrington and Harley, 1995a,b; Das et al., 2001, 2003; Hollis and Harley, 2003; Brigida et al., 2007; Fockenberg, 2008; Podlesskii et al., 2008). These experiments lead to resurgence in belief that the crust could achieve extreme thermal conditions (>900 °C) on a regional scale during 'normal' tectonic processes. As a consequence, there was renewed interest in trying to understand what tectonic settings can lead to relatively common UHT crustal metamorphism.

Surface heat flow data from the actively extending Basin and Range Province, USA, was used by Lachenbruch and Sass (1978) and Lachenbruch (1978) to quantify lower crustal temperatures (at ~30 km depth) in the range of 700–900 °C below most of the Province, and locally higher than 1000 °C. This, as well as active felsic and basaltic volcanism in the Province (Christiansen and Lipman, 1972), was used by Sandiford and Powell (1986a) and Sandiford et al. (1987) to reinforce their assertion that continental extension is a valid setting for generating granulite metamorphism, and to propose that the extensional Basin and Range Province could be a useful contemporary analogue for exposed and unexposed (non-exhumed) ancient granulite—particularly UHT—terranes that have *P–T* paths characterized by near-IBC trajectories (e.g. Napier Complex, Labwor Hills, Namaqualand and eastern Australian Tasmanides), even if there is an absence of high-volume, syn-metamorphic mafic magmatic rocks in these terranes. Nevertheless, these studies represent crucial research that ultimately led to (extensional) accretionary orogenic systems being more widely invoked as regions of UHT/granulite formation (e.g. Collins, 2002; Hyndman et al., 2005; Currie and Hyndman, 2006; Brown, 2007a; Hyndman et al., 2009; Santosh et al., 2009a; Dasgupta et al., 2013). Collins (2002) argued that granulites are more commonly developed in extensional rather than collisional settings, citing the long-lived subduction–accretion Tasmanide system of eastern Australia as the type example. Collins (2003) and Brown (2003) stated that granulites formed in 'extensional accretionary systems' would be characterized by near-IBC retrograde paths and could have either 'clockwise' or 'anticlockwise' prograde paths generated during transient thickening. Lateral accretion of crustal material has the benefit that total radiogenic heat production will be increased when the accreted material is thickened (e.g. Jamieson and Beaumont, 2013). Hyndmann et al. (2005), Currie and Hyndmann (2006) and Hyndman and Currie (2011) showed that circum-Pacific continental back-arcs are regions of high surface heat flow and thin crust. This led to the widespread inference that a number of ancient UHT occurrences/terranes could represent closure and thickening of former back-arcs, especially (but not only) those with clockwise *P–T* paths (e.g. Brown, 2006, 2007a; Clark et al., 2009; Clark et al., 2011); or at the very least, could represent thickening of formerly extended crust (Park, 1981; Thompson, 1989; Bohlen, 1991; De Yoreo et al., 1991; Thompson and Connolly, 1995). However, Clark et al. (2011) cautioned that in the absence of voluminous, syn-metamorphic, mafic magmatism closure and thickening of back-arcs will only produce UHT metamorphic conditions if there is above-average radiogenic crustal heat production in the thickened pile, slow erosion rates and if the fertility of the crust has been reduced by earlier dehydration through melt loss.

More recently, the theme of generating UHT metamorphic conditions by thickening of (extended) back-arcs has been returned to through sophisticated 2-D geodynamic forward models (Sizova et al., 2014). The models were formulated to investigate Proterozoic versus Phanerozoic tectonic regimes. UHT conditions are predicted in continental crust by 'Proterozoic-like' models that, in comparison to modern Earth, feature elevated crustal heat production, hotter (by 80–150 °C) ambient upper mantle temperatures, thicker lithosphere and a greater density contrast between mantle lithosphere and asthenospheric mantle, all of which are necessary to generate regional UHT conditions in thin crust that is later thickened in convergence. The models predict shallow slab break-off and syn-extensional magmatism in very hot back-arcs, produced as a result of decompressional melting of hydrated asthenospheric mantle. Therefore, granulite formation is tied to

crust-formation processes in these models (e.g. see Kemp et al., 2007). Clockwise *P–T* paths are predicted for the metamorphic evolution of the back-arc during extension (Sizova et al., 2014). With renewed convergence, not shown in their published figures, near-IBC *P–T* paths are predicted as a consequence of collisional thickening of the hot back-arc (Sizova et al., 2014). The Eastern Ghats Province, India, with its near-IBC 'anticlockwise' *P–T* path (e.g. Sengupta et al., 1990; Korhonen et al., 2013a; Korhonen et al., 2014), and Musgrave Province, Australia, with its retrograde *P–T* path more or less parallel to the apparent thermal gradient (Walsh et al., 2014) and voluminous A-type magmatism (Smithies et al., 2011) have been proposed as potential candidates of the slab break-off model. Curiously, however, the timescale of orogenesis in these two terranes is far longer (>100 Myr; Smithies et al., 2011; Korhonen et al., 2013b; Walsh et al., 2014) than the very short timescale for UHT metamorphism implied by the geodynamic models (Sizova et al., 2014). The widths of back-arc regions in Sizova et al. (2014) are approximately 150–400 km prior to renewed convergence and, depending on the magnitude of renewed convergence, support the notion that wide orogenic plateau—albeit with subdued or negative topography—are probably required to facilitate long-lived UHT conditions (Clark et al., 2011; cf. Chardon et al., 2009) such as in the Eastern Ghats and Musgrave Provinces.

Gorczyk et al. (2015) has used sophisticated 2-D geodynamic forward models to explore the long-lived magmatic and UHT metamorphic history of the Musgrave Province in more detail. This is the only study to date to have specifically investigated the geodynamic evolution of a single UHT terrane. The models predict voluminous crustal melting, lower volume mantle melting and crustal UHT metamorphism at appropriate length, depth and time scales (Smithies et al., 2011; Kirkland et al., 2013; Walsh et al., 2014) by commencing simulations with the Musgrave Province as a hot, thin and wide back-arc. Moreover, the tight clockwise *P–T* paths recorded by UHT rocks (Walsh et al., 2014) are replicated (Gorczyk et al., 2015).

In all the above models proposing thickened back-arcs as sites of UHT metamorphism, 'pre-conditioning' of the crust to allow it to attain temperatures >900–1000 °C occurs during the same event that produces UHT metamorphism. That is, thermal buffering effects resulting from melting are included (Sizova et al., 2010; Jamieson and Beaumont, 2013). However, the observation that classic regional UHT terranes (e.g. Napier Complex) are severely dehydrated rather than hydrated has been used to challenge the above models (Santosh and Kusky, 2010; Santosh et al., 2011). Santosh and Kusky (2010) and Santosh et al. (2011) argued that the low water content of UHT granulites is not readily explicable by thickening of back-arcs that are wet as a result of hydration from fluids released from the subducting slab (e.g. Hyndmann et al., 2005; Sizova et al., 2014). In order to account for the dehydrated nature of UHT granulites, but still account for high heat flux, UHT metamorphism as a result of ridge subduction and subduction slab windows is proposed (Brown, 1998a,b, 2001; Santosh and Kusky, 2010; Santosh et al., 2011, 2012). In such models, subduction of an actively spreading ocean ridge results in a 'window' between the subducting slabs that widens with depth in the subduction channel (Bradley et al., 2003) and allows upwelling hot asthenosphere to come in contact with the base of the over-riding plate. This location in the arc will be magmatically inactive and thus not characterised by H_2O-rich fluids derived from slab dehydration (Bradley et al., 2003; Santosh and Kusky, 2010; Santosh et al., 2011). CO_2-rich fluid inclusions in UHT granulites (e.g. Tsunogae et al., 2002; Sarkar et al., 2003b; Santosh and Omori, 2008) have been inferred to be evidence for slab window-type settings (Santosh and Kusky, 2010; Santosh et al., 2011, 2012). Slab window models carry two implications. First, pre-conditioning of the crust to allow it to generate UHT mineral assemblages must either occur earlier than—i.e. temporally unrelated to—the UHT event or it occurs during a sufficiently long-lived slab window-related event such that trace of H_2O-rich fluids (as inclusions) in crust are 'displaced' by CO_2-rich fluids. Second, UHT metamorphism will (approximately) be spatially restricted to the width of the slab window, and as such, could help to explain the 'localised' nature of numerous Gondwana-related (e.g.) UHT localities.

Large–hot orogens (Beaumont et al., 2006) have not been explored in a forward (geodynamic) modelling sense specifically for the generation of UHT metamorphic conditions (e.g. Jamieson and Beaumont, 2013). As a result, geodynamic models for large–hot orogens do not predict UHT conditions in regions of the deep crust where crust is interpreted to be weak and characterized by homogeneous or heterogeneous ductile flow (Jamieson and Beaumont, 2013). However, the type example, the India–Asia collision (Tibetan Plateau), is capable of generating UHT conditions at approximately 30–50 km depth in an orogenic plateau setting on the basis of <15 Ma UHT metapelitic granulite xenoliths (Hacker et al., 2000) erupted in mafic volcanic flows. The presence of young hot and dry xenoliths in the deep crust seems to indicate that there is (or was) pre-conditioned deep crust underlying a large part of Tibet (Hacker et al., 2000), crust that is now incapable of generating significant amounts of melt. The time at which the deep crust became pre-conditioned by extensive dehydration is unconstrained, and therefore could be as old as c. 45 Ma (Hacker et al., 2000). Large–hot orogens with substantially over-thickened crust have the added capacity of allowing for ductile flow of the deep crust along pressure gradients, which could be argued to explain sub-horizontal fabrics with recumbent isoclinal folds that characterize some regional granulite/UHT terranes (Bridgwater et al., 1974; James and Black, 1981; Park, 1981; Sandiford and Wilson, 1984; Dumond et al., 2010). However, this is a non-unique resolution to the question of the origin of such fabrics and the thickening implied by large–hot orogens is not necessarily compatible with pressure estimates retrieved from deep crustal UHT granulites (e.g. Napier Complex; Sandiford, 1985a).

The occurrence of UHT xenoliths from Tibet establishes that UHT metamorphism remains an ongoing crustal process in (modern) Earth. Other examples of age-unconstrained UHT xenoliths from young (Miocene and younger) volcanic and subvolcanic fields in Mexico (Hayob et al., 1989; Hayob and Essene, 1990; Ortega-Gutiérrez et al., 2012) could represent Tertiary, Mesozoic or Proterozoic UHT metamorphism. Pownall et al. (2014) recently reported exhumed 16 Ma UHT granulites from Seram, Indonesia. UHT mineral assemblages were generated as a result of juxtaposition of mantle lithosphere against crustal rocks and slab-rollback-induced extension that caused core complex-style exhumation of the UHT rocks (Pownall et al., 2014). This occurrence of UHT metamorphism is extremely important as it affords a very rare opportunity to directly constrain the tectonic setting of metamorphism and thus, potentially, provide a contemporary analogue for more ancient examples where the boundary conditions are no longer preserved.

Where mafic magmatism has been demonstrated to be synchronous with large-scale granulite/UHT metamorphism (e.g. Sandiford and Powell, 1986a; Kemp et al., 2007; Peng et al., 2010; Pownall et al., 2014), either solely through extension or via lithospheric mantle delamination or slab window-related processes, there is no necessity to invoke later thickening of extended crust to generate UHT conditions. When granulite/UHT metamorphism is caused directly by mafic magmatism, granulite formation is tied to mantle differentiation processes and crustal growth (e.g. Kemp et al., 2007).

In summary, UHT metamorphism is postulated to occur in collisional and accretionary orogens. It is interesting that the early ideas regarding tectonic setting for granulite formation in the 1970s (see Park, 1981, for summary) have not been superceded and in fact remain highly relevant and insightful synopses. Further, the range of settings covered above is almost identical to those outlined many years ago by De Yoreo et al. (1991) for occurrences of high-temperature–low-pressure metamorphic belts. Importantly, the majority of examples above require that long-lived, regional UHT metamorphic conditions be achieved only when already hot, extended crust is thickened, as this is the mechanism by which crustal radiogenic heat production is concentrated and thus increased through lateral accretion. However, more fundamentally, all quantitatively proposed tectonic settings for regional granulite/UHT metamorphism are related to the major Earth recycling and crust-generation process of subduction. No doubt due to this strong connection with subduction-related processes, UHT metamorphism was recognized by Brown (2006, 2007a,b) as showing an apparent temporal relationship to supercontinent assembly. Even though *P–T* path shapes are not diagnostic of tectonic setting it appears that a range of possible tectonic settings are required to allow for the non-exhumation of near-IBC-type UHT granulites versus the near-isothermal decompression and exhumation path followed by other UHT granulites (e.g. Brown, 2003; Collins, 2003). Overall, granulite/UHT metamorphism in continental crust is most effectually explained by the amount, distribution and redistribution of heat-producing elements before, during and after convergence (or extension in wholly non-convergent situations), high mantle heat flux, enhanced by low erosion rates and preconditioning of the crust to reduce melt fertility. The energetics of heating in dry/mature crust means that UHT metamorphism should be preferentially favoured in terranes that have previously (including earlier in same event) undergone partial melting or contain large volumes of comparatively low-H_2O igneous rocks. Due to slow conductive heating and cooling rates, regional UHT metamorphism is best categorized as a long-lived (approximately $\geq$40 Myr, Table 2, Fig. 12) crustal process if erosion rates are sufficiently slow to enable survival of the radiogenic-dominated heat source.

10. Conclusion

UHT crustal metamorphism is now accepted as a relatively common deep-crustal process. The past seven years or so has seen a large increase in interest in UHT metamorphism, which, in concert with analytical and computational advances, has resulted in significant progress in our interrogation and understanding of UHT metamorphic processes. To wit, trace element thermometry has opened up an entirely new way with which to recognise UHT metamorphism in otherwise non-diagnostic rocks and terranes, and timescales for regional UHT metamorphism in some terranes are now understood to exceed 100 Myr. As geodynamic forward models of large-scale orogenic and taphrogenic crustal processes become more sophisticated it will become increasingly possible and accessible to tie petrography-based *P–T–t* constraints from the metamorphic record to such models. Overall, there is very much still a requirement to understand metamorphic systems from a field-, petrography- and pressure–temperature-based platform, possibly more so than ever in light of the always improving and seemingly limitless analytical capabilities! Not surprisingly, the main advances in our understanding of UHT metamorphism have come from analytical (geochronology, trace element work) and computational directions. Extrapolating along these directions into the future will likely see increased ease and ability to extract depth–time information from the metamorphic rock record, which in turn will provide unprecedented insight into rates and timescales of tectonic processes. Such information is critical for understanding the role of deep crustal processes in the full context of the Earth system. We hope that this document provides motivation to promote continued recognition, context, significance and study of UHT/HT metamorphism.

Acknowledgements

Prof. M. Santosh is thanked for his warm hospitality and the invitation to write an updated review of progress on UHT metamorphism while DEK was on a research visit to China University of Geosciences, Beijing, in September 2013 funded by Australia's Group of Eight (Go8) and in China by the China Science and Technology Exchange Center (CSTEC). Thorough and constructive reviews by M. Brown and F. Korhonen were warmly welcomed.

References

Ackermand, D., Herd, R.K., Reinhardt, M., Windley, B.F., 1987. Sapphirine parageneses from the Caraiba complex, Bahia, Brazil: the influence of Fe^{2+}–Fe^{3+} distribution on the stability of sapphirine in natural assemblages. Journal of Metamorphic Geology 5, 323–339.

Ackermand, D., Seifert, F., Schreyer, W., 1975. Instability of sapphirine at high pressures. Contributions to Mineralogy and Petrology 50, 79–92.

Adjerid, Z., Godard, G., Ouzegane, K.H., Kienast, J.-R., 2013. Multistage progressive evolution of rare osumilite-bearing assemblages preserved in ultrahigh-temperature granulites from In Ouzzal (Hoggar, Algeria). Journal of Metamorphic Geology 31, 505–524.

Ague, J.J., Eckert Jr., J.O., 2012. Precipitation of rutile and ilmenite needles in garnet: implications for extreme metamorphic conditions in the Acadian Orogen, U.S.A. American Mineralogist 97, 840–855.

Ague, J.J., Eckert Jr., J.O., Chu, X., Baxter, E.F., Chamberlain, C.P., 2013. Discovery of ultrahigh-temperature metamorphism in the Acadian orogen, Connecticut, USA. Geology 41, 271–274.

Aït-Djafer, S., Adjerid, Z., Badani, A., Ouzegane, K., Kienast, J.-R., 2009. Spinel–quartz high temperature paragenesis in Al–Fe granulites from the Ihouhaouene area (NW Hoggar, Algeria). Journal of African Earth Sciences 55, 79–91.

Aleksandrov, S.M., Troneva, M.A., 2006. Composition, mineral assemblages, and genesis of serendibite-bearing magnesian skarns. Geochemistry International 44, 665–680.

Altenberger, U., Mejia Jimenez, D.M., Günter, C., Sierra Rodriguez, G.I., Scheffler, F., Oberhänsli, R., 2012. The Garzón Massif, Colombia-a new ultrahigh-temperature metamorphic complex in the Early Neoproterozoic of northern South America. Mineralogy and Petrology 105, 171–185.

Anderson, J.R., Kelsey, D.E., Hand, M., Collins, W.J., 2013. Conductively driven, high-thermal gradient metamorphism in the Anmatjira Range, Arunta region, central Australia. Journal of Metamorphic Geology 31, 1003–1026.

Andreoli, M.A.G., Hart, R.J., Ashwal, L.D., Coetzee, H., 2006. Correlations between U, Th content and metamorphic grade in the Western Namaqualand Belt, South Africa, with implications for radioactive heating of the crust. Journal of Petrology 47, 1095–1118.

Annersten, H., Seifert, F., 1981. Stability of the assemblage orthopyroxene–sillimanite–quartz in the system MgO–FeO–Fe_2O_3–Al_2O_3–SiO_2–H_2O. Contributions to Mineralogy and Petrology 77, 158–165.

Anovitz, L.M., 1991. Al zoning in pyroxene and plagioclase: window on the late prograde to early retrograde *P–T* paths in granulite terrains. American Mineralogist 76, 1328–1343.

Aranovich, L.Y., Berman, R.G., 1997. A new garnet–orthopyroxene thermometer based on reversed Al_2O_3 solubility in FeO–Al_2O_3–SiO_2 orthopyroxene. American Mineralogist 82, 345–353.

Aranovich, L.Y., Podlesskii, K.K., 1989. Geothermometry of high-grade metapelites: simultaneously operating reactions. In: Daly, J.S., Cliff, R.A., Yardley, B.W.D. (Eds.), Evolution of Metamorphic Belts, Geological Society Special Publication, London, vol. 43, pp. 45–62.

Arima, M., Gower, C.F., 1991. Osumilite-bearing granulites in the eastern Grenville Province, eastern Labrador, Canada – mineral parageneses and metamorphic conditions. Journal of Petrology 32, 29–61.

Arima, M., Onuma, K., 1977. The solubility of alumina in enstatite and the phase equilibria in the join $MgSiO_3$—$MgAl_2SiO_6$ at 10–25 kbar. Contributions to Mineralogy and Petrology 61, 251–265.

Ashwal, L.D., Tucker, R.D., Zinner, E.K., 1999. Slow cooling of deep crustal granulites and Pb-loss in zircon. Geochimica et Cosmochimica Acta 63, 2839–2851.

Ashworth, J.R., 1993. Fluid-absent diffusion kinetics of Al inferred from retrograde metamorphic coronas. American Mineralogist 78, 331–337.

Ashworth, J.R., Birdi, J.J., 1990. Diffusion modelling of coronas around olivine in an open system. Geochimica et Cosmochimca Acta 54, 2389–2401.

Ashworth, J.R., Birdi, J.J., Emmett, T.F., 1992. Diffusion in coronas around clinopyroxene: modelling with local equilibrium and steady state, and a non-steady-

state modification to account for zoned actinolite-hornblende. Contributions to Mineralogy and Petrology 109, 307–325.
Ashworth, J.R., Sheplev, V.S., 1997. Diffusion modelling of metamorphic layered coronas with stability criterion and consideration of affinity. Geochimica et Cosmochimica Acta 61, 3671–3689.
Ashworth, J.R., Sheplev, V.S., Bryxina, N.A., Kolobov, V.Y., Reverdatto, V.V., 1998. Diffusion-controlled corona reaction and overstepping of equilibrium in a garnet granulite, Yenisey Ridge, Siberia. Journal of Metamorphic Geology 16, 231–246.
Audibert, N., Hensen, B.J., Bertrand, P., 1995. Experimental study of phase relations involving osumilite in the system K_2O–FeO–MgO–Al_2O_3–SiO_2–H_2O at high pressure and temperature. Journal of Metamorphic Geology 13, 331–344.
Austrheim, H., 1987. Eclogitization of lower crustal granulites by fluid migration through shear zones. Earth and Planetary Science Letters 81, 221–232.
Ayers, J.C., Crombie, S., Loflin, M., Miller, C.F., Luo, Y., 2013. Country rock monazite response to intrusion of the searchlight Pluton, southern Nevada. American Journal of Science 313, 345–394.
Ayres, M., Harris, N., 1997. REE fractionation and Nd-isotope disequilibrium during crustal anatexis: constraints from Himalayan leucogranites. Chemical Geology 139, 249–269.
Baba, S., 2003. Two stages of sapphirine formation during prograde and retrograde metamorphism in the Palaeoproterozoic Lewisian complex in South Harris, NW Scotland. Journal of Petrology 44, 329–354.
Baba, S., Dunkley, D.J., Hokada, T., Horie, K., Suzuki, K., Shiraishi, K., 2012. New SHRIMP U–Pb zircon ages and CHIME monazite ages from South Harris granulites, Lewisian Complex, NW Scotland: implications for two stages of zircon formation during Palaeoproterozoic UHT metamorphism. Precambrian Research 200-203, 104–128.
Baba, S., Grew, E.S., Shearer, C.K., Sheraton, J.W., 2000. Surinamite: a high-temperature metamorphic beryllosilicate from Lewisian sapphirine-bearing kyanite–orthopyroxene–quartz–potassium feldspar gneiss at South Harris, N.W. Scotland. American Mineralogist 85, 1474–1484.
Baba, S., Hokada, T., Kaiden, H., Dunkley, D.J., Owada, M., Shiraishi, K., 2010. SHRIMP zircon U–Pb dating of sapphirine-bearing granulite and biotite–hornblende gneiss in the Schirmacher Hills, east Antarctica: implications for Neoproterozoic ultrahigh-temperature metamorphism predating the assembly of Gondwana. Journal of Geology 118, 621–639.
Baba, S., Owada, M., Grew, E.S., Shiraishi, K., 2006. Sapphirine granulite from Schirmacher Hills, central Dronning Maud Land. In: Fütterer, D.K., Damaske, D., Kleinschmidt, G., Miller, H., Tessensohn, F. (Eds.), Antarctic Contributions to Global Earth Science. Springer, Berlin, pp. 37–44.
Baba, S., Shinjo, R., Windley, B.F., 2008. Origin of sapphirine-bearing garnet–orthopyroxene granulites: possible hydrothermally altered ocean floor. Polar Science 2, 87–107.
Balasubrahmanyan, M.N., 1976. Significance of sapphirine and kornerupine-bearing cordierite rocks from around Kiranur, Tiruchirapalli district, Tamil-Nadu. Journal of the Geological Society of India 17, 158–158.
Baldwin, J.A., Brown, M., 2008. Age and duration of ultrahigh-temperature metamorphism in the Anápolis–Itauçu Complex, Southern Brasília Belt, central Brazil – constraints from U–Pb geochronology, mineral rare earth element chemistry and trace-element thermometry. Journal of Metamorphic Geology 26, 213–233.
Baldwin, J.A., Brown, M., Schmitz, M.D., 2007a. First application of titanium-in-zircon thermometry to ultrahigh-temperature metamorphism. Geology 35, 295–298.
Baldwin, J.A., Powell, R., Brown, M., Moraes, R., Fuck, R.A., 2005. Modelling of mineral equilibria in ultrahigh-temperature metamorphic rocks from the Anápolis–Itauçu Complex, central Brazil. Journal of Metamorphic Geology 23, 511–531.
Baldwin, J.A., Powell, R., Williams, M.L., Goncalves, P., 2007b. Formation of eclogite, and reaction during exhumation to mid-crustal levels, Snowbird tectonic zone, western Canadian Shield. Journal of Metamorphic Geology 25, 953–974.
Barboza, S.A., Bergantz, G.W., 2000. Metamorphism and anatexis in the mafic complex contact aureole, Ivrea zone, northern Italy. Journal of Petrology 41, 1307–1327.
Barboza, S.A., Bergantz, G.W., Brown, M., 1999. Regional granulite facies metamorphism in the Ivrea zone: is the Mafic Complex the smoking gun or a red herring? Geology 27, 447–450.
Bea, F., 2012. The sources of energy for crustal melting and the geochemistry of heat-producing elements. Lithos 153, 278–291.
Beaumont, C., Nguyen, M.H., Jamieson, R.A., Ellis, S., 2006. Crustal flow modes in large hot orogens. In: Law, R.D., Searle, M.P., Godin, L. (Eds.), Channel Flow, Ductile Extrusion and Exhumation of Lower Mid-crust in Continental Collision Zones, Geological Society, London, Special Publication, vol. 268, pp. 91–145.
Belyanin, G.A., Rajesh, H.M., Sajeev, K., Van Reenen, D.D., 2012a. Orthopyroxene + sillimanite predating sapphirine + quartz: a rare case of ultrahigh-temperature metamorphism from the Central Zone, Limpopo Complex, South Africa. The Canadian Mineralogist 50, 1153–1163.
Belyanin, G.A., Rajesh, H.M., Sajeev, K., Van Reenen, D.D., 2012b. Ultrahigh-temperature metamorphism from an unusual corundum+orthopyroxene intergrowth bearing Al–Mg granulite from the Southern Marginal Zone, Limpopo Complex, South Africa. Contributions to Mineralogy and Petrology 164, 457–475.
Belyanin, G.A., Rajesh, H.M., van Reenen, D.D., Mouri, H., 2010. Corundum + orthopyroxene ± spinel intergrowths in an ultrahigh-temperature Al–Mg granulite from the Southern Marginal Zone, Limpopo Belt, South Africa. American Mineralogist 95, 196–199.
Berg, J.H., 1977. Dry granulite mineral assemblages in the contact aureoles of the Nain Complex, Labrador. Contributions to Mineralogy and Petrology 64, 33–52.
Berg, J.H., Wheeler, E.P., 1976. Osumilite of deep-seated origin in the contact aureole of the anorthositic Nain Complex, Labrador. American Mineralogist 61, 29–37.
Berger, J., Féménias, O., Ohnenstetter, D., Plissart, G., Mercier, J.-C.C., 2010. Origin and tectonic significance of corundum–kyanite–sapphirine amphibolites from the Variscan French Massif Central. Journal of Metamorphic Geology 28, 341–360.
Berman, R.G., 1988. Internally consistent thermodynamic data for minerals in the system Na_2O–K_2O–CaO–MgO–FeO–Fe_2O_3–Al_2O_3–SiO_2–TiO_2–H_2O–CO_2. Journal of Petrology 29, 445–522.
Berman, R.G., Brown, T.H., Greenwood, H.J., 1985. An internally consistent thermodynamic data base for minerals in the system Na_2O–K_2O–CaO–MgO–FeO–Fe_2O_3–Al_2O_3–SiO_2–TiO_2–H_2O–CO_2. Atomic Energy Commission of Canada Ltd. Technical Report 377, 62p.
Berman, R.G., Brown, T.H., Perkins, E.H., 1987. GEØ-CALC: software for calculation and display of *P–T–X* phase diagrams. American Mineralogist 72, 861–862.
Bertrand, P., Ellis, D.J., Green, D.H., 1991. The stability of sapphirine–quartz and hypersthene–sillimanite–quartz assemblages: an experimental investigation in the system FeO–MgO–Al_2O_3–SiO_2 under H_2O and CO_2 conditions. Contributions to Mineralogy and Petrology 108, 55–71.
Bhandari, A., Pant, N.C., Bhowmick, S.K., Goswami, S., 2011. ~1.6 Ga ultrahigh-temperature granulite metamorphism in the Central Indian Tectonic Zone: insights from metamorphic reaction history, geothermobarometry and monazite chemical ages. Geological Journal 46, 198–216.
Bhowmick, S.K., Wilde, S.A., Bhandari, A., Sarbadhikari, B., 2014. Zoned monazite and zircon as monitors for the thermal history of granulite terranes: an example from the Central Indian Tectonic Zone. Journal of Petrology 55, 585–621.
Bingen, B., Austrheim, H., Whitehouse, M., 2001. Ilmenite as a source for zirconium during high-grade metamorphism? Textural evidence from the Caledonides of Western Norway and implications for zircon geochronology. Journal of Petrology 42, 355–375.
Bingen, B., Austrheim, H., Whitehouse, M.J., Davis, W.J., 2004. Trace element signature and U-Pb geochronology of eclogite-facies zircon, Bergen Arcs, Caledonides of W Norway. Contributions to Mineralogy and Petrology 147, 671–683.
Birch, F., Clark, H., 1940a. The thermal conductivity of rocks and its dependence upon temperature and composition. Part I. American Journal of Science 238, 529–558.
Birch, F., Clark, H., 1940b. The thermal conductivity of rocks and its dependence upon temperature and composition. Part II. American Journal of Science 238, 613–635.
Black, L.P., James, P.R., Harley, S.L., 1983a. Geochronology and geological evolution of metamorphic rocks in the Field Islands area, East Antarctica. Journal of Metamorphic Geology 1, 277–303.
Black, L.P., James, P.R., Harley, S.L., 1983b. Geochronology and structure of the early Archaean rocks at Fyfe Hills, Enderby Land, Antarctica. Precambrian Research 21, 197–222.
Black, L.P., Williams, I.S., Compston, W., 1986. Four zircon ages from one rock: the history of a 3930 Ma-old granulite from Mount Sones, Enderby Land, Antarctica. Contributions to Mineralogy and Petrology 94, 427–437.
Blackburn, T., Bowring, S.A., Schoene, B., Mahan, K., Dudas, F., 2011. U–Pb thermochronology: creating a temporal record of lithosphere thermal evolution. Contributions to Mineralogy and Petrology 162, 479–500.
Blackburn, T., Shimuzu, N., Bowring, S.A., Schoene, B., Mahan, K.H., 2012. Zirconium in rutile speedometry: new constraints on lower crustal cooling rates and residence temperatures. Earth and Planetary Science Letters 317, 231–240.
Boehnke, P., Watson, E.B., Trail, D., Harrison, T.M., Schmitt, A.K., 2013. Zircon saturation re-revisited. Chemical Geology 351, 324–334.
Boger, S.D., White, R.W., 2003. The metamorphic evolution of metapelitic granulites from Radok Lake, northern Prince Charles Mountains, east Antarctica; evidence for an anticlockwise *P–T* path. Journal of Metamorphic Geology 21, 285–298.
Boger, S.D., White, R.W., Schulte, B., 2012. The importance of iron speciation (Fe^{+2}/Fe^{+3}) in determining mineral assemblages: an example from the high-grade aluminous metapelites of southeastern Madagascar. Journal of Metamorphic Geology 30, 997–1018.
Bohlen, S.R., 1987. Pressure-temperature-time paths and a tectonic model for the evolution of granulites. Journal of Geology 95, 617–632.
Bohlen, S.R., 1991. On the formation of granulites. Journal of Metamorphic Geology 9, 223–229.
Bohlen, S.R., Mezger, K., 1989. Origin of granulite terranes and the formation of the lowermost continental crust. Science 244, 326–329.
Borfecchia, E., Mino, L., Gianolio, D., Groppo, C., Malaspina, N., Martinez-Criado, G., Sans, J.A., Poli, S., Castelli, D., Lamberti, C., 2012. Iron oxidation state in garnet from a subduction setting: a micro-XANES and electron microprobe ("flank method") comparative study. Journal of Analytical Atomic Spectroscopy 27, 1725–1733.
Bose, S., Das, K., 2007. Sapphirine+quartz assemblage in contrasting textural modes from the Eastern Ghats Belt, India: implications for stability relations in UHT metamorphism and retrograde processes. Gondwana Research 11, 492–503.
Bose, S., Das, K., Dasgupta, S., Miura, H., Fukuoka, M., 2006. Exsolution textures in orthopyroxene in aluminous granulites as indicators of UHT metamorphism: new evidence from the Eastern Ghats Belt, India. Lithos 92, 506–523.
Bose, S., Fukuoka, M., Sengupta, P., Dasgupta, S., 2000. Evolution of high-Mg–Al granulites from Sunkarametta, Eastern Ghats, India: evidence for a lower

crustal heating–cooling trajectory. Journal of Metamorphic Geology 18, 223–240.
Bowman, J.R., Moser, D.E., Valley, J.W., Wooden, J.L., Kita, N.T., Mazdab, F.K., 2011. Zircon U-Pb isotope, $\delta^{18}O$ and trace element response to 80 m.y. of high temperature metamorphism in the lower crust: sluggish diffusion and new records of Archean craton formation. American Journal of Science 311, 719–772.
Bradley, D.C., Kusky, T.M., Haeussler, P., Rowley, D.C., Goldfarb, R., Nelson, S., 2003. Geologic signature of early ridge subduction in the accretionary wedge, forearc basin, and magmatic arc of south-central Alaska. In: Sisson, V.B., Roeske, S., Pavlis, T.L. (Eds.), Geology of a Transpressional Orogen Developed During a Ridge – Trench Interaction along the North Pacific Margin, Geological Society of America, Special Paper, vol. 371, pp. 19–50.
Brandt, S., Klemd, R., Okrusch, M., 2003. Ultrahigh-temperature metamorphism and multistage evolution of garnet–orthopyroxene granulites from the Proterozoic Epupa Complex, NW Namibia. Journal of Petrology 44, 1121–1144.
Brandt, S., Schenk, V., Raith, M.M., Appel, P., Gerdes, A., Srikantappa, C., 2011. Late Neoproterozoic *P–T* evolution of HP–UHT granulites from the Palni Hills (South India): new constraints from phase diagram modelling, LA–ICP–MS zircon dating and in-situ EMP monazite dating. Journal of Petrology 52, 1813–1856.
Brandt, S., Will, T.M., Klemd, R., 2007. Magmatic loading in the Proterozoic Epupa Complex, NW Namibia, as evidenced by ultrahigh-temperature sapphirine-bearing orthopyroxene–sillimanite–quartz granulites. Precambrian Research 153, 143–178.
Braun, I., Cenki-Tok, B., Paquette, J.-L., Tiepolo, M., 2007. Petrology and U–Th–Pb geochronology of the sapphirine–quartz-bearing metapelites from Rajapalayam, Madurai Block, Southern India: evidence for polyphase Neoproterozoic high-grade metamorphism. Chemical Geology 241, 129–147.
Bridgwater, D., McGregor, V.R., Myers, J.S., 1974. A horizontal tectonic regime in the Archaean of Greenland and its implications for early crustal thickening. Precambrian Research 1, 179–197.
Brigida, C., Poli, S., Valle, M., 2007. High-temperature phase relations and topological constraints in the quaternary system $MgO–Al_2O_3–SiO_2–Cr_2O_3$: an experimental study. American Mineralogist 92, 735–747.
Brovarone, A.V., Agard, P., 2013. True metamorphic isograds or tectonically sliced metamorphic sequence? New high-spatial resolution petrological data for the New Caledonia case study. Contributions to Mineralogy and Petrology 166, 451–469.
Brown, G.C., Fyfe, W.S., 1970. The production of granitic melts during ultrametamorphism. Contributions to Mineralogy and Petrology 28, 310–318.
Brown, M., 1993. *P–T–t* evolution of orogenic belts and the causes of regional metamorphism. Journal of the Geological Society, London 150, 227–241.
Brown, M., 1994. The generation, segregation, ascent and emplacment of granite magma: the migmatite-to-crustally-derived granite connection in thickened orogens. Earth-Science Reviews 36, 83–130.
Brown, M., 1998a. Ridge-trench interactions and high-*T*–low-*P* metamorphism, with particular reference to the Cretaceous evolution of the Japanese Islands. In: Treloar, P.J., O'Brien, P.J. (Eds.), What Drives Metamorphism and Metamorphic Reactions?, Geological Society, London, Special Publication, vol. 138, pp. 131–163.
Brown, M., 1998b. Unpairing metamorphic belts: *P–T* paths and a tectonic model for the Ryoke Belt, southwest Japan. Journal of Metamorphic Geology 16, 3–22.
Brown, M., 2001. From microscope to mountain belt: 150 years of petrology and its contribution to understanding geodynamics, particularly the tectonics of orogens. Journal of Geodynamics 32, 115–164.
Brown, M., 2002. Retrograde processes in migmatites and granulites revisited. Journal of Metamorphic Geology 20, 25–40.
Brown, M., 2003. Hot orogens, tectonic switching, and creation of continental crust: comment and reply: COMMENT. Geology. http://dx.doi.org/10.1130/0091-7613-31.1.e9. Forum 31.
Brown, M., 2004. The mechanism of melt extraction from lower continental crust of orogens. Transactions of the Royal Society of Edinburgh: Earth Sciences 95, 34–48.
Brown, M., 2006. Duality of thermal regimes is the distinctive characteristic of plate tectonics since the Neoarchean. Geology 34, 961–964.
Brown, M., 2007a. Metamorphic conditions in orogenic belts: a record of secular change. International Geology Review 49, 193–234.
Brown, M., 2007b. Metamorphism, plate tectonics, and the supercontinent cycle. Earth Science Frontiers 14, 1–18.
Brown, M., 2008a. Granites, migmatites and residual granulites. In: Sawyer, E.W., Brown, M. (Eds.), Working with Migmatites, Short Course Series, vol. 38. Mineralogical Association of Canada, Quebec City, pp. 97–144.
Brown, M., 2008b. Metamorphic conditions in orogenic belts: a record of secular change. In: Ernst, W.G., Rumble III, D. (Eds.), Metamorphic Conditions along Convergent Plate Junctions: Mineralogy, Petrology, Geochemistry and Tectonics—The J.G. Liou Volume, International book series, vol. 10. Bellweather Publishing, Ltd. for the Geological Society of America, pp. 24–65.
Brown, M., 2010a. Melting of the continental crust during orogenesis: the thermal, rheological, and compositional consequences of melt transport from lower to upper continental crust. Canadian Journal of Earth Sciences 47, 655–694.
Brown, M., 2010b. Metamorphic patterns in orogenic systems and the geological record. In: Cawood, P.A., Kröner, A. (Eds.), Earth Accretionary Systems in Space and Time, Geological Society, London, Special Publication, vol. 318, pp. 37–74.
Brown, M., 2014. The contribution of metamorphic petrology to understanding lithosphere evolution and geodynamics. Geoscience Frontiers 5, 553–569.
Brown, M., Korhonen, F.J., 2009. Some remarks on melting and extreme metamorphism of crustal rocks. In: Gupta, A.K., Dasgupta, S. (Eds.), Physics and Chemistry of the Earth's interior: Crust, Mantle and Core. Springer, New Delhi, pp. 67–87.
Brown, M., Raith, M., 1996. First evidence of ultrahigh-temperature decompression from the granulite province of southern India. Journal of the Geological Society 153, 819–822.
Brown, M., Rushmer, T. (Eds.), 2006. Evolution and Differentiation of the Continental Crust. Cambridge University Press, p. 553.
Budzyń, B., Harlov, D.E., Williams, M.L., Jercinovic, M.J., 2011. Experimental determination of stability relations between monazite, fluorapatite, allanite, and REE-epidote as a function of pressure, temperature, and fluid composition. American Mineralogist 96, 1547–1567.
Burg, J.-P., Gerya, T.V., 2005. The role of viscous heating in Barrovian metamorphism of collisional orogens: thermomechanical models and application to the Lepontine Dome in the Central Alps. Journal of Metamorphic Geology 23, 75–95.
Bushmin, S.A., Dolivo-Dobrovolsky, D.V., Lebedeva, Y.M., 2007. Infiltration metasomatism under high-pressure granulite-facies conditions based on orthopyroxene–sillimanite rocks in shear zones of the Lapland granulite belt. Doklady Earth Sciences 412, 106–109.
Caddick, M.J., Konopásek, J., Thompson, A.B., 2010. Preservation of garnet growth zoning and the duration of prograde metamorphism. Journal of Petrology 51, 2327–2347.
Caddick, M.J., Thompson, A.B., 2008. Quantifying the tectono-metamorphic evolution of pelitic rocks from a wide range of tectonic settings: mineral compositions in equilibrium. Contributions to Mineralogy and Petrology 156, 177–195.
Caporuscio, F.A., Morse, S.A., 1978. Occurrence of sapphirine plus quartz at Peekskill, New York. American Journal of Science 278, 1334–1342.
Carlson, W.D., 2002. Scales of disequilibrium and rates of equilibration during metamorphism. American Mineralogist 87, 185–204.
Carrington, D.P., 1995. The relative stability of garnet–cordierite and orthopyroxene–sillimanite–quartz assemblages: experimental data. European Journal of Mineralogy 7, 949–960.
Carrington, D.P., Harley, S.L., 1995a. Partial melting and phase relations in high-grade metapelites: an experimental petrogenetic grid in the KFMASH system. Contributions to Mineralogy and Petrology 120, 270–291.
Carrington, D.P., Harley, S.L., 1995b. The stability of osumilite in metapelitic granulites. Journal of Metamorphic Geology 13, 613–625.
Carrington, D.P., Harley, S.L., 1996. Cordierite as a monitor of fluid and melt H_2O contents in the lower crust: an experimental calibration. Geology 24, 647–650.
Carson, C.J., Ague, J.J., Coath, C.D., 2002. U–Pb geochronology from Tonagh Island, East Antarctica: implications for the timing of ultra-high temperature metamorphism of the Napier Complex. Precambrian Research 116, 237–263.
Carson, C.J., Powell, R., Clarke, G.L., 1999. Calculated mineral equilibria for eclogites in $CaO–Na_2O–FeO–MgO–Al_2O_3–SiO_2–H_2O$: application to the Pouébo Terrane, Pam Peninsula, New Caledonia. Journal of Metamorphic Geology 17, 9–24.
Carson, C.J., Powell, R., Wilson, C.J.L., Dirks, P., 1997. Partial melting during tectonic exhumation of a granulite terrane: an example from the Larsemann hills, east Antarctica. Journal of Metamorphic Geology 15, 105–126.
Carswell, D.A., Cuthbert, S.J., Ravna, E.J.K., 1999. Ultrahigh-pressure metamorphism in the Western Gneiss Region of the Norwegian Caledonides. International Geology Review 41, 955–966.
Chamberlain, C.P., Sonder, L.J., 1990. Heat producing elements and the thermal and baric patterns of metamorphic belts. Science 250, 763–769.
Chardon, D., Gapais, D., Cagnard, F., 2009. Flow of ultra-hot orogens: a view from the Precambrian, clues for the Phanerozoic. Tectonophysics 477, 105–118.
Chatterjee, N., Ghose, N.C., 2010. Metamorphic evolution of the Naga Hills eclogite and blueschist, Northeast India: implications for early subduction of the Indian plate under the Burma microplate. Journal of Metamorphic Geology 28, 209–225.
Chatterjee, N.D., Schreyer, W., 1972. The reaction $enstatite_{ss}$ + sillimanite = $sapphirine_{ss}$ + quartz in the system $MgO–Al_2O_3–SiO_2$. Contributions to Mineralogy and Petrology 36, 49–62.
Chen, H.L., Li, Z.L., Yang, S.F., Dong, C.W., Xiao, W.J., Tainosho, Y., 2006. Mineralogical and geochemical study of a newly discovered mafic granulite, northwest China: implications for tectonic evolution of the Altay Orogenic Belt. Island Arc 15, 210–222.
Cherniak, D.J., Manchester, J., Watson, E.B., 2007a. Zr and Hf diffusion in rutile. Earth and Planetary Science Letters 261, 267–279.
Cherniak, D.J., Watson, E.B., 2001. Pb diffusion in zircon. Chemical Geology 172, 5–24.
Cherniak, D.J., Watson, E.B., 2007. Ti diffusion in zircon. Chemical Geology 242, 470–483.
Cherniak, D.J., Watson, E.B., Grove, M., Harrison, T.M., 2004. Pb diffusion in monazite: a combined RBS/SIMS study. Geochimica et Cosmochimica Acta 68, 829–840.
Cherniak, D.J., Watson, E.B., Wark, D.A., 2007b. Ti diffusion in quartz. Chemical Geology 236, 65–74.
Chinner, G.A., Fox, J.S., 1974. The origin of cordierite–anthophyllite rocks in the Land's End aureole. Geological Magazine 111, 397–408.
Chinner, G.A., Sweatman, T.R., 1968. A former association of enstatite and kyanite. Mineralogical Magazine 36, 1052–1060.
Choi, S.H., Mukasa, S.B., Andronikov, A.V., Osanai, Y., Harley, S.L., Kelly, N.M., 2006. Lu–Hf systematics of the ultra-high temperature Napier Metamorphic Complex

in Antarctica: evidence for the early Archean differentiation of Earth's mantle. Earth and Planetary Science Letters 246, 305–316.
Christiansen, R.L., Lipman, P.W., 1972. Cenozoic volcanism and plate tectonic evolution of the Eastern United States, II. Late Cenozoic. Philosophical Transactions of the Royal Society of London. Series A, Mathematical and Physical Sciences 271, 249–284.
Christy, A.G., 1989. The effect of composition, temperature and pressure on the stability of the 1Tc and 2M polytypes of sapphirine. Contributions to Mineralogy and Petrology 103, 203–215.
Clark, C., Collins, A.S., Santosh, M., Taylor, R., Wade, B.P., 2009. The *P–T–t* architecture of a Gondwanan suture: REE, U–Pb and Ti-in-zircon thermometric constraints from the Palghat Cauvery shear system, South India. Precambrian Research 174, 129–144.
Clark, C., Fitzsimons, I.C.W., Healy, D., Harley, S.L., 2011. How does the continental crust get really hot? Elements 7, 235–240.
Clark, C., Hand, M., Brown, M., Gupta, S., Nanda, J., Fitzsimons, I., 2013. Field guide to the Ultrahigh Temperature granulites of the Eastern Ghats Province 11–15 January 2013. Granulites and Granulites conference, p. 78.
Clark, C., Kinny, P.D., Harley, S.L., 2012. Sedimentary provenance and age of metamorphism of the Vestfold Hills, East Antarctica: evidence for a piece of Chinese Antarctica? Precambrian Research 196–197, 23–45.
Clarke, G.L., Daczko, N.R., Nockolds, C., 2001. A method for applying matrix corrections to X-ray intensity maps using the Bence–Albee algorithm and Matlab. Journal of Metamorphic Geology 19, 635–644.
Clarke, G.L., Powell, R., Fitzherbert, J.A., 2006. The lawsonite paradox: a comparison of field evidence and mineral equilibria modelling. Journal of Metamorphic Geology 24, 715–725.
Clarke, G.L., Powell, R., Guiraud, M., 1989. Low-pressure granulite facies metapelitic assemblages and corona textures from MacRobertson Land, east Antarctica: the importance of Fe_2O_3 and TiO_2 in accounting for spinel-bearing assemblages. Journal of Metamorphic Geology 7, 323–335.
Clauser, C., 2006. Geothermal Energy. In: Heinloth, K. (Ed.), Landolt–Börnstein, Group VIII: "Advanced Materials and Technologies", vol. 3 "Energy Technologies", subvol. C: "Renewable Energies". Springer Verlag, Heidelberg, pp. 493–604.
Clauser, C., 2009. Heat transport processes in the Earth's crust. Surveys in Geophysics 30, 163–191.
Clemens, J.D., 1990. The granulite – granite connexion. In: Vielzeuf, D., Vidal, P. (Eds.), Granulites and Crustal Evolution. NATO Scientific Publication. Kluwer Academic Publishers, Dordrecht, pp. 25–36.
Clemens, J.D., Vielzeuf, D., 1987. Constraints on melting and magma production in the crust. Earth and Planetary Science Letters 86, 287–306.
Clifford, T.N., Stumpfl, E.F., Burger, A.J., McCarthy, T.S., Rex, D.C., 1981. Mineral–chemical and isotopic studies of Namaqualand granulites, South Africa: a Grenville analogue. Contributions to Mineralogy and Petrology 77, 225–250.
Collins, A.S., Clark, C., Plavsa, D., 2014. Peninsular India in Gondwana: the tectonothermal evolution of the Southern Granulite Terrain and its Gondwanan counterparts. Gondwana Research 25, 190–203.
Collins, W.J., 2002. Hot orogens, tectonic switching, and creation of continental crust. Geology 30, 535–538.
Collins, W.J., 2003. Hot orogens, tectonic switching, and creation of continental crust: comment and reply: REPLY. Geology. http://dx.doi.org/10.1130/0091-7613-31.1.e10. Forum 31.
Collins, W.J., Richards, S.W., 2008. Geodynamic significance of S-type granites in circum-Pacific orogens. Geology 36, 559–562.
Connolly, J.A.D., 1990. Multivariable phase diagrams: an algorithm based on generalized thermodynamics. American Journal of Science 290, 666–718.
Connolly, J.A.D., 1995. Phase diagram methods for graphitic rocks and application to the system C–O–H–FeO–TiO_2–SiO_2. Contributions to Mineralogy and Petrology 119, 94–116.
Connolly, J.A.D., 2005. Computation of phase equilibria by linear programming: a tool for geodynamic modeling and its application to subduction zone decarbonation. Earth and Planetary Science Letters 236, 524–541.
Connolly, J.A.D., Petrini, K., 2002. An automated strategy for calculation of phase diagram sections and retrieval of rock properties as a function of physical conditions. Journal of Metamorphic Geology 20, 697–708.
Corfu, F., 2013. A century of U–Pb geochronology: the long quest towards concordance. Geological Society of America Bulletin 125, 33–47.
Corvino, A.F., Boger, S.D., Wilson, C.J.L., 2007. Metamorphic Conditions During Formation of a Metapelitic Sillimanite–garnet Gneiss from Clemence Massif, Prince Charles Mountains, East Antarctica. U.S. Geological Survey and The National Academies; USGS OF-2007-1047, Short Research Paper 062. http://dx.doi.org/10.3133/of2007-1047.srp062.
Creighton, S., Stachel, T., Eichenberg, D., Luth, R.W., 2010. Oxidation state of the lithospheric mantle beneath Diavik diamond mine, central Slave craton, NWT, Canada. Contributions to Mineralogy and Petrology 159, 645–657.
Creighton, S., Stachel, T., Matveev, S., Höfer, H., McCammon, C., Luth, R.W., 2009. Oxidation of the Kaapvaal lithospheric mantle driven by metasomatism. Contributions to Mineralogy and Petrology 157, 491–504.
Crowe, W.A., Osanai, Y., Toyoshima, T., Owada, M., 2002. SHRIMP geochronology of a mylonite zone on Tonagh Island: characterisation of the last high-grade tectonothermal event in the Napier Complex, East Antarctica. Polar Geoscience 15, 17–36.
Cubley, J.F., Pattison, D.R.M., Tinkham, D.K., Fanning, C.M., 2013. U–Pb geochronological constraints on the timing of episodic regional metamorphism and rapid high-*T* exhumation of the Grand Forks complex, British Columbia. Lithos 156–159, 241–267.
Currie, C.A., Hyndman, R.D., 2006. The thermal structure of subduction zone back arcs. Journal of Geophysical Research 111, B08404. http://dx.doi.org/10.01029/02005JB004024.
Currie, K.L., Gittins, J., 1988. Contrasting sapphirine parageneses from Wilson Lake, Labrador and their tectonic implications. Journal of Metamorphic Geology 6, 603–622.
Cutts, K., Hand, M., Kelsey, D.E., 2011a. Evidence for early Mesoproterozoic (ca. 1590 Ma) ultrahigh-temperature metamorphism in southern Australia. Lithos 124, 1–16.
Cutts, K.A., Hand, M., Kelsey, D.E., Strachan, R.A., 2009. Orogenic versus extensional settings for regional metamorphism: Knoydartian events in the Moine Supergroup revisited. Journal of the Geological Society, London 166, 201–204.
Cutts, K.A., Hand, M., Kelsey, D.E., Strachan, R.A., 2011b. *P–T* constraints and timing of Barrovian metamorphism in the Shetland Islands, Scottish Caledonides: implications for the structural setting of the Unst ophiolite. Journal of the Geological Society, London 168, 1265–1284.
Cutts, K.A., Kelsey, D.E., Hand, M., 2013. Evidence for late Paleoproterozoic (ca 1690–1665 Ma) high- to ultrahigh-temperature metamorphism in southern Australia: implications for Proterozoic supercontinent models. Gondwana Research 23, 617–640.
Cutts, K.A., Kinny, P.D., Strachan, R.A., Hand, M., Kelsey, D.E., Emery, M., Friend, C.R.L., Leslie, A.G., 2010. Three metamorphic events recorded in a single garnet: integrated phase modelling, *in situ* LA–ICPMS and SIMS geochronology from the Moine Supergroup, NW Scotland. Journal of Metamorphic Geology 28, 249–267.
Cutts, K.A., Stevens, G., Hoffmann, J.E., Buick, I.S., Frei, D., Münker, C., 2014. Paleo- to Mesoarchean polymetamorphism in the Barberton Granite–Greenstone Belt, South Africa: constraints from U–Pb monazite and Lu–Hf garnet geochronology on the tectonic processes that shaped the belt. Geological Society of America Bulletin 126, 251–270.
Das, K., Bose, S., Karmakar, S., Dunkley, D.J., Dasgupta, S., 2011. Multiple tectonometamorphic imprints in the lower crust: first evidence of *ca.* 950 Ma (zircon U–Pb SHRIMP) compressional reworking of UHT aluminous granulites from the Eastern Ghats Belt, India. Geological Journal 46, 217–239.
Das, K., Dasgupta, S., Miura, H., 2001. Stability of osumilite coexisting with spinel solid solution in metapelitic granulites at high oxygen fugacity. American Mineralogist 86, 1423–1434.
Das, K., Dasgupta, S., Miura, H., 2003. An experimentally constrained petrogenetic grid in the silica-saturated portion of the system KFMASH at high temperatures and pressures. Journal of Petrology 44, 1055–1075.
Dasgupta, S., Bose, S., Das, K., 2013. Tectonic evolution of the Eastern Ghats Belt, India. Precambrian Research 227, 247–258.
Dasgupta, S., Ehl, J., Raith, M.M., Sengupta, P., Sengupta, P., 1997. Mid-crustal contact metamorphism around the Chimakurthy mafic–ultramafic complex, Eastern Ghats Belt, India. Contributions to Mineralogy and Petrology 129, 182–197.
Dasgupta, S., Sanyal, S., Sengupta, P., Fukuoka, M., 1994. Petrology of granulites from Anakapalle – evidence for Proterozoic decompression in the Eastern Ghats, India. Journal of Petrology 35, 433–459.
Dasgupta, S., Sengupta, P., 1995. Ultrametamorphism in Precambrian granulite terranes: evidence from Mg–Al granulites and calc-silicate granulites of the Eastern Ghats, India. Geological Journal 30, 307–318.
Dasgupta, S., Sengupta, P., Ehl, J., Raith, M., Bardhan, S., 1995. Reaction textures in a suite of spinel granulites from the Eastern Ghats Belt, India: evidence for polymetamorphism, a partial petrogenetic grid in the system KFMASH and the roles of ZnO and Fe_2O_3. Journal of Petrology 36, 435–461.
Dawson, J.B., Harley, S.L., 2009. Some post-equilibrium reactions in kimberlite-derived eclogites paper A-00081. Lithos 112S, 1025–1031.
de Capitani, C., Brown, T.H., 1987. The computation of chemical equilibrium in complex systems containing non-ideal solutions. Geochimica et Cosmochimica Acta 51, 2639–2652.
de Capitani, C., Petrakakis, K., 2010. The computation of equilibrium assemblage diagrams with Theriak/Domino software. American Mineralogist 95, 1006–1016.
De Paoli, M.C., Clarke, G.L., Daczko, N.R., 2012. Mineral equilibria modeling of the granulite–eclogite transition: effects of whole-rock composition on metamorphic facies assemblages. Journal of Petrology 53, 949–970.
De Yoreo, J.J., Lux, D.R., Guidotti, C.V., 1991. Thermal modelling in low-pressure/high-temperature metamorphic belts. Tectonophysics 188, 209–238.
DePaolo, D.J., Manton, W., Grew, E.S., Halpern, M., 1982. Sm–Nd, Rb–Sr, and U–Th–Pb systematics of granulite facies gneisses from Fyfe Hills, Enderby Land, Antarctica. Nature 298, 614–618.
Depine, G.V., Andronicos, C.L., Phipps-Morgan, J., 2008. Near-isothermal conditions in the middle and lower crust induced by melt migration. Nature 452, 80–83.
DeWolf, C.P., Belshaw, N.S., O'Nions, R.K., 1993. A metamorphic history from micron-scale $^{207}Pb/^{206}Pb$ chronometry of Archean monazite. Earth and Planetary Science Letters 120, 207–220.
Dharma Rao, C.V., Chmielowski, R.M., 2011. New constraints on the metamorphic evolution of the Eastern Ghats Belt, India, based on relict composite inclusions

in garnet from ultrahigh-temperature sapphirine granulites. Geological Journal 46, 240–262.
Dharma Rao, C.V., Santosh, M., Chmielowski, R.M., 2012. Sapphirine granulites from Panasapattu, Eastern Ghats belt, India: ultrahigh-temperature metamorphism in a Proterozoic convergent plate margin. Geoscience Frontiers 3, 9–31.
Didier, A., Bosse, V., Boulvais, P., Bouloton, J., Paquette, J.-L., Montel, J.-M., Devidal, J.-L., 2013. Disturbance versus preservation of U–Th–Pb ages in monazite during fluid–rock interaction: textural, chemical and isotopic in situ study in micro-granites (Velay Dome, France). Contributions to Mineralogy and Petrology 165, 1051–1072.
Diener, J.F.A., Powell, R., 2010. Influence of ferric iron on the stability of mineral assemblages. Journal of Metamorphic Geology 28, 599–613.
Diener, J.F.A., Powell, R., 2012. Revised activity–composition models for clinopyroxene and amphibole. Journal of Metamorphic Geology 30, 131–142.
Diener, J.F.A., Powell, R., White, R.W., 2008a. Quantitative phase petrology of cordierite-orthoamphibole gneisses and related rocks. Journal of Metamorphic Geology 26, 795–814.
Diener, J.F.A., White, R.W., Link, K., Dreyer, T.S., Moodley, A., 2013. Clockwise, low-*P* metamorphism of the Aus granulite terrain, southern Namibia, during the Mesoproterozoic Namaqua Orogeny. Precambrian Research 224, 629–652.
Diener, J.F.A., White, R.W., Powell, R., 2008b. Granulite facies metamorphism and subsolidus fluid-absent reworking, Strangways Range, Arunta Block, central Australia. Journal of Metamorphic Geology 26, 603–622.
Dolivo-Dobrovol'skii, D.V., Skublov, S.G., Glebovitskii, V.A., Astaf'ev, B.Y., Voinova, O.A., Shcheglova, T.P., 2013. Age (U–Pb, SHRIMP-II), geochemistry of zircon, and conditions of the formation of sapphirine-bearing rocks of the Central Kola Granulite–Gneiss area. Doklady Earth Sciences 453, 1121–1126.
Doroshev, A.M., Malinovskiy, I.Y., 1974. Upper pressure limit of stability of sapphirine. Doklady Akademiia Nauk SSSR 219, 136–138.
Droop, G.T.R., 1987. A general equation for estimating Fe^{3+} concentrations in ferromagnesian silicates and oxides from microprobe analyses, using stoichiometric criteria. Mineralogical Magazine 51, 431–435.
Droop, G.T.R., 1989. Reaction history of garnet–sapphirine granulites and conditions of Archaean high-pressure granulite facies metamorphism in the Central Limpopo Mobile Belt, Zimbabwe. Journal of Metamorphic Geology 7, 383–403.
Droop, G.T.R., Brodie, K.H., 2012. Anatectic melt volumes in the thermal aureole of the Etive Complex, Scotland: the roles of fluid-present and fluid-absent melting. Journal of Metamorphic Geology 30, 843–864.
Droop, G.T.R., Bucher-Nurminen, K., 1984. Reaction textures and metamorphic evolution of sapphirine-bearing granulites from the Gruf Complex, Italian Central Alps. Journal of Petrology 25, 766–803.
Drüppel, K., Elsäßer, L., Brandt, S., Gerdes, A., 2013. Sveconorwegian mid-crustal ultrahigh-temperature metamorphism in Rogaland, Norway: U–Pb LA–ICP–MS geochronology and pseudosections of sapphirine granulites and associated paragneisses. Journal of Petrology 54, 305–350.
Dumond, G., Goncalves, P., Williams, M.L., Jercinovic, M.J., 2010. Subhorizontal fabric in exhumed continental lower crust and implications for lower crustal flow: Athabasca granulite terrane, western Canadian Shield. Tectonics 29, TC2006. http://dx.doi.org/10.1029/2009TC002514.
Dunkley, D.J., Clarke, G.L., Harley, S.L., 1999. Diffusion metasomatism in silica-undersaturated sapphirine-bearing granulite from Rumdoodle Peak, Framnes Mountains, East Antarctica. Contributions to Mineralogy and Petrology 134, 264–276.
Duretz, T., Schmalholz, S.M., Podladchikov, Y.Y., Yuen, D.A., 2014. Physics-controlled thickness of shear zones caused by viscous heating: implications for crustal shear localization. Geophysical Research Letters 41, 4904–4911.
Dziggel, A., Diener, J.F.A., Stolz, N.B., Kolb, J., 2012. Role of H_2O in the formation of garnet coronas during near-isobaric cooling of mafic granulites: the Tasiusarsuaq terrane, southern West Greenland. Journal of Metamorphic Geology 30, 957–972.
Ellis, D.J., 1980. Osumilite–sapphirine–quartz granulites from Enderby Land, Antarctica: *P–T* conditions of metamorphism, implications for garnet–cordierite equilibria and the evolution of the deep crust. Contributions to Mineralogy and Petrology 74, 201–210.
Ellis, D.J., 1987. Origin and evolution of granulites in normal and thickened crusts. Geology 15, 167–170.
Ellis, D.J., Green, D.H., 1985. Garnet-forming reactions in mafic granulites from Enderby Land, Antarctica—implications for geothermometry and geobarometry. Journal of Petrology 26, 633–662.
Ellis, D.J., Sheraton, J.W., England, R.N., Dallwitz, W.B., 1980. Osumilite–sapphirine–quartz granulites from Enderby Land, Antarctica – mineral assemblages and reactions. Contributions to Mineralogy and Petrology 72, 123–143.
Ellis, D.J., Thompson, A.B., 1986. Subsolidus and partial melting reactions in the quartz-excess CaO + MgO + Al_2O_3 + SiO_2 + H_2O system under water-excess and water-deficient conditions to 10 kb: some implications for the origin of peraluminous melts from mafic rocks. Journal of Petrology 27, 91–212.
Elvevold, S., Gilotti, J.A., 2000. Pressure–temperature evolution of retrogressed kyanite eclogites, Weinschenk Island, north-east Greenland Caledonides. Lithos 53, 127–147.
England, P.C., Bickle, M., 1984. Continental thermal and tectonic regimes during the Archaean. Journal of Geology 92, 123–143.
England, P.C., Richardson, R.W., 1977. The influence of erosion upon the mineral facies of rocks from different metamorphic environments. Journal of the Geological Society, London 134, 201–213.
England, P.C., Thompson, A.B., 1984. Pressure–Temperature–time paths of regional metamorphism I. Heat transfer during the evolution of regions of thickened continental crust. Journal of Petrology 25, 894–928.
England, P.C., Thompson, A.B., 1986. Some thermal and tectonic models for crustal melting in continental collision zones. In: Coward, M.P., Ries, A.C. (Eds.), Collision Tectonics, Geological Society, London, Special Publication, vol. 19, pp. 83–94.
Engvik, A.K., Austrheim, H., 2010. Formation of sapphirine and corundum in scapolitised and Mg-metasomatised gabbro. Terra Nova 22, 166–171.
Engvik, A.K., Mezger, K., Wortelkamp, S., Bast, R., Corfu, F., Korneliussen, A., Ihlen, P., Bingen, B., Austrheim, H., 2011. Metasomatism of gabbro – mineral replacement and element mobilization during the Sveconorwegian metamorphic event. Journal of Metamorphic Geology 29, 399–423.
Evans, T., 2004. A method for calculating effective bulk composition modification due to crystal fractionation in garnet-bearing schist: implications for isopleth thermobarometry. Journal of Metamorphic Geology 22, 547–557.
Ewing, T.A., Hermann, J., Rubatto, D., 2013. The robustness of the Zr-in-rutile and Ti-in-zircon thermometers during high-temperature metamorphism (Ivrea–Verbano Zone, northern Italy). Contributions to Mineralogy and Petrology 165, 757–779.
Fei, Y.W., Saxena, S.K., 1990. Internally consistent thermodynamic data and equilibrium phase-relations for compounds in the system MgO–SiO_2 at high-pressure and high-pressure and high-temperature. Journal of Geophysical Research 95 (B5), 6915–6928.
Ferriss, E.D.A., Essene, E.J., Becker, U., 2008. Computational study of the effect of pressure on the Ti-in-zircon geothermometer. European Journal of Mineralogy 20, 745–755.
Ferry, J.M., Watson, E.B., 2007. New thermodynamic models and revised calibrations for the Ti-in-zircon and Zr-in-rutile thermometers. Contributions to Mineralogy and Petrology 154, 429–437.
Fialin, M., Bézos, A., Wagner, C., Magnien, V., Humler, E., 2004. Quantitative electron microprobe analysis of $Fe^{3+}/\Sigma Fe$: Basic concepts and experimental protocol for glasses. American Mineralogist 89, 654–662.
Fialin, M., Wagner, C., Métrich, N., Humler, E., Galoisy, L., Bézos, A., 2001. $Fe^{3+}/\Sigma Fe$ vs. Fe$L\alpha$ peak energy for minerals and glasses: recent advances with the electron microprobe. American Mineralogist 86, 456–465.
Fisher, G.W., 1973. Nonequilibrium thermodynamics as a model for diffusion-controlled metamorphic processes. American Journal of Science 273, 897–924.
Fitton, J.G., Gill, R.C.O., 1970. The oxidation of ferrous iron in rocks during mechanical grinding. Geochimica et Cosmochimica Acta 34, 518–524.
Fitzherbert, J.A., Clarke, G.L., Powell, R., 2005. Preferential retogression of high-*P* metasediments and the preservation of blueschist to eclogite faceis metabasite during exhumation, Diahot terrane, NE New Caledonia. Lithos 83, 67–96.
Fitzsimons, I.C.W., Harley, S.L., 1994. The influence of retrograde cation-exchange on granulite *P–T* estimates and a convergence technique for the recovery of peak metamorphic conditions. Journal of Petrology 35, 543–576.
Florence, F.P., Spear, F.S., 1991. Effects of diffusional modification of garnet growth zoning on P–T path calculations. Contributions to Mineralogy and Petrology 107, 487–500.
Fockenberg, T., 2008. Pressure–temperature stability of pyrope in the system MgO–Al_2O_3–SiO_2–H_2O. European Journal of Mineralogy 20, 735–744.
Forbes, C.J., Giles, D., Hand, M., Betts, P.G., Suzuki, K., Chalmers, N., Dutch, R., 2011. Using *P–T* paths to interpret the tectonothermal setting of prograde metamorphism: an example from the northeastern Gawler Craton, South Australia. Precambrian Research 185, 65–85.
Foster, G., Parrish, R.R., Horstwood, M.S.A., Chenery, S., Pyle, J., Gibson, H.D., 2004. The generation of prograde P–T–t points and paths; a textural, compositional, and chronological study of metamorphic monazite. Earth and Planetary Science Letters 228, 125–142.
Frey, M., de Capitani, C., Liou, G., 1991. A new petrogenetic grid for low-grade metabasites. Journal of Metamorphic Geology 9, 497–509.
Friedman, G.M., 1960. Chemical analyses of rocks with the petrographic microscope. American Mineralogist 45, 69–78.
Frost, B.R., Chacko, T., 1989. The granulite uncertainty principle: limitations on thermobarometry in granulites. Journal of Geology 97, 435–450.
Fu, B., Page, F.Z., Cavosie, A.J., Fournelle, J., Kita, N.T., Lackey, J.S., Wilde, S.A., Valley, J.W., 2008. Ti-in-zircon thermometry: applications and limitations. Contributions to Mineralogy and Petrology 156, 197–215.
Fyfe, W.S., 1973a. The generation of batholiths. Tectonophysics 17, 273–283.
Fyfe, W.S., 1973b. The granulite facies, partial melting and the Archaean crust. Philosophical Transactions of the Royal Society of London, Series A: Mathematical and Physical Sciences 247, 457–461.
Gaidies, F., Abart, R., de Capitani, C., Schuster, R., Connolly, J.A.D., Reusser, E., 2006. Characterization of polymetamorphism in the Austroalpine basement east of the Tauern Window using garnet isopleth thermobarometry. Journal of Metamorphic Geology 24, 451–475.
Gaidies, F., de Capitani, C., Abart, R., 2008. THERIA_G: a software program to numerically model prograde garnet growth. Contributions to Mineralogy and Petrology 155, 657–671.
Gaidies, F., Pattison, D.R.M., de Capitani, C., 2011. Toward a quantitative model of metamorphic nucleation and growth. Contributions to Mineralogy and Petrology 162, 975–993.

Galli, A., Le Bayon, B., Schmidt, M.W., Burg, J.-P., Caddick, M.J., Reusser, E., 2011. Granulites and charnockites of the Gruf Complex: evidence for Permian ultra-high temperature metamorphism in the Central Alps. Lithos 124, 17–45.

Galli, A., Le Bayon, B., Schmidt, M.W., Burg, J.-P., Reusser, E., Sergeev, S.A., Larionov, A., 2012. U–Pb zircon dating of the Gruf Complex: disclosing the late Variscan granulitic lower crust of Europe stranded in the Central Alps. Contributions to Mineralogy and Petrology 163, 353–378.

Gardien, V., Thompson, A.B., Grujic, D., Ulmer, P., 1995. Experimental melting of biotite plus plagioclase plus quartz or minus muscovite assemblages and implications for crustal melting. Journal of Geophysical Research 100 (B8), 15581–15591.

Gardien, V., Thompson, A.B., Ulmer, P., 2000. Melting of biotite + plagioclase + quartz gneisses: the role of H_2O in the stability of amphibole. Journal of Petrology 41, 651–666.

Gibson, G.M., Ireland, T.R., 1995. Granulite formation during continental extension in Fiordland, New Zealand. Nature 375, 479–482.

Giustina, M.E.S.D., Pimental, M.M., Filho, C.F.F., de Hollanda, M.H.B.M., 2011. Dating coeval mafic magmatism and ultrahigh temperature metamorphism in the Anápolis–Itauçu Complex, Central Brazil. Lithos 124, 82–102.

Gnos, E., Kurz, D., 1994. Sapphirine–quartz and sapphirine–corundum assemblages in metamorphic rocks associated with the Semail Ophiolite (United-Arab-Emirates). Contributions to Mineralogy and Petrology 116, 398–410.

Godard, G., Mabit, J.-L., 1998. Peraluminous sapphirine formed during retrogression of a kyanite-bearing eclogite from Pays de Léon, Armorican Massif, France. Lithos 43 (1), 15–29.

Goergen, E.T., Whitney, D.L., 2012a. Corona networks as three-dimensional records of transport scale and pathways during metamorphism. Geology 40, 183–186.

Goergen, E.T., Whitney, D.L., 2012b. Long length scales of element transport during reaction texture development in orthoamphibole–cordierite gneiss: Thor–Odin dome, British Columbia, Canada. Contributions to Mineralogy and Petrology 163, 337–352.

Goncalves, P., Nicollet, C., Montel, J.M., 2004. Petrology and in situ U–Th–Pb monazite geochronology of ultrahigh-temperature metamorphism from the Andriamena mafic unit, north-central Madagascar. Significance of a petrographical *P–T* path in a polymetamorphic context. Journal of Petrology 45, 1923–1957.

Gorczyk, W., Smithies, H., Korhonen, F., Howard, H., Quentin de Gromard, R., 2015. Ultra-hot Mesoproterozoic evolution of intracontinental central Australia. Geoscience Frontiers 6, 23–37.

Goscombe, B., 1992. Silica-undersaturated sapphirine, spinel and kornerupine granulite facies rocks, NE Strangways Range, Central Australia. Journal of Metamorphic Geology 10, 181–201.

Gottschalk, M., 1997. Internally consistent thermodynmaic data for rock-forming minerals. European Journal of Mineralogy 9, 175–223.

Green, E.C.R., Holland, T.J.B., Powell, R., 2012. A thermodynamic model for silicate melt in $CaO–MgO–Al_2O_3–SiO_2$ to 50 kbar and 1800 °C. Journal of Metamorphic Geology 30, 579–597.

Greenfield, J.E., Clarke, G.L., Bland, M., Clark, D.J., 1996. *In-situ* migmatite and hybrid diatexite at Mt Stafford, central Australia. Journal of Metamorphic Geology 14, 413–426.

Grew, E.S., 1980. Sapphirine + quartz association from Archean rocks in Enderby Land, Antarctica. American Mineralogist 65, 821–836.

Grew, E.S., 1982a. Osumilite in the sapphirine–quartz terrane of Enderby Land, Antarctica: implications for osumilite petrogenesis in the granulite facies. American Mineralogist 67, 762–787.

Grew, E.S., 1982b. Sapphirine, kornerupine, and sillimanite + orthopyroxene in the charnockitic region of South India. Journal of the Geological Society of India 23, 469–505.

Grew, E.S., 1983a. A grandidierite–sapphirine association from India. Mineralogical Magazine 47, 401–403.

Grew, E.S., 1983b. Note on sapphirine and kornerupine in South-India. Journal of the Geological Society of India 24, 378–379.

Grew, E.S., Manton, W., 1979. Archean rocks in Antarctica: 2.5 billion year uranium–lead ages of pegmatites in Enderby Land. Science 206, 443–445.

Grew, E.S., Yates, M., Marquez, N., Berezkin, V.I., Kitsul, V.I., 1989. Secondary grandidierite in kornerupine–sapphirine rocks of the Aldan Shield. Doklady Akademii Nauk SSSR 309, 423–428.

Grew, E.S., Yates, M.G., Konilov, A.N., Marquez, N., 1992. Kornerupine from the Archean Kola Series at Sholt-Yavr, Kola Peninsula, Russia. Mineralogical Magazine 56, 247–251.

Groppo, C., Lombardo, B., Rolfo, F., Pertusati, P., 2007. Clockwise exhumation path of granulitized eclogites from the Ama Drime range (Eastern Himalayas). Journal of Metamorphic Geology 25, 51–75.

Groppo, C., Rolfo, F., Indares, A., 2012. Partial melting in the higher Himalayan crystallines of eastern Nepal: the effect of decompression and implications for the channel flow model. Journal of Petrology 53, 1057–1088.

Grujic, D., Stipp, M., Wooden, J.L., 2011. Thermometry of quartz mylonites: importance of dynamic recrystallization on Ti-in-quartz reequilibration. Geochemistry Geophysics Geosystems 12, Q06012. http://dx.doi.org/10.01029/02010GC003368.

Guernina, S., Sawyer, E.W., 2003. Large-scale melt depletion in granulite terranes: an example from the Archean Ashuanipi Subprovince of Quebec. Journal of Metamorphic Geology 21, 181–201.

Guiraud, M., Kienast, J.-R., Ouzegane, K., 1996a. Corundum–quartz-bearing assemblage in the Ihouhaouene area (In Ouzzal, Algeria). Journal of Metamorphic Geology 14, 755–761.

Guiraud, M., Kienast, J.R., Rahmani, A., 1996b. Petrological study of high-temperature granulites from In Ouzzal, Algeria: some implications on the phase relationships in the FMASTOCr system. European Journal of Mineralogy 8, 1375–1390.

Guiraud, M., Powell, R., Rebay, G., 2001. H_2O in metamorphism and unexpected behaviour in the preservation of metamorphic mineral assemblages. Journal of Metamorphic Geology 19, 445–454.

Guo, J.-H., Peng, P., Chen, Y., Jiao, S., Windley, B.F., 2012. UHT sapphirine granulite metamorphism at 1.93–1.92 Ga caused by gabbronorite intrusions: implications for tectonic evolution of the northern margin of the North China Craton. Precambrian Research 222–223, 124–142.

Hacker, B.R., Gnos, E., Ratschbacher, L., Grove, M., McWilliams, M.O., Sobolev, S.V., Wan, J., Wu, Z., 2000. Hot and dry deep crustal xenoliths from Tibet. Science 287, 2463–2466.

Hagen, B., Hoernes, S., Rötzler, J., 2008. Geothermometry of the ultrahigh-temperature Saxon granulites revisited. Part II: thermal peak conditions and cooling rates inferred from oxygen-isotope fractionations. European Journal of Mineralogy 20, 1117–1133.

Halpin, J.A., Clarke, G.L., White, R.W., Kelsey, D.E., 2007a. Contrasting *P–T–t* paths for Neoproterozoic metamorphism in MacRobertson and Kemp Lands, east Antarctica. Journal of Metamorphic Geology 25, 683–701.

Halpin, J.A., Daczko, N.R., Milan, L.A., Clarke, G.L., 2012. Decoding near-concordant U–Pb zircon ages spanning several hundred million years: recrystallisation, metamictisation or diffusion? Contributions to Mineralogy and Petrology 163, 67–85.

Halpin, J.A., White, R.W., Clarke, G.L., Kelsey, D.E., 2007b. The Proterozoic *P–T–t* evolution of the Kemp Land coast, east Antarctica; Constraints from Si-saturated and Si-undersaturated metapelites. Journal of Petrology 48, 1321–1349.

Harley, S.L., 1984. The solubility of alumina in orthopyroxene coexisting with garnet in $FeO–MgO–Al_2O_3–SiO_2$ and $CaO–FeO–MgO–Al_2O_3–SiO_2$. Journal of Petrology 25, 665–696.

Harley, S.L., 1985. Garnet–orthopyroxene bearing granulites from Enderby Land, Antarctica: metamorphic pressure–temperature–time evolution of the Archaean Napier Complex. Journal of Petrology 26, 819–856.

Harley, S.L., 1986. A sapphirine–cordierite–garnet–sillimanite granulite from Enderby Land, Antarctica: implications for FMAS petrogenetic grids in the granulite facies. Contributions to Mineralogy and Petrology 94, 452–460.

Harley, S.L., 1988. Proterozoic granulites from the Rauer Group, east Antarctica .1. Decompressional pressure temperature paths deduced from mafic and felsic gneisses. Journal of Petrology 29, 1059–1095.

Harley, S.L., 1989. The origins of granulites: a metamorphic perspective. Geological Magazine 126, 215–247.

Harley, S.L., 1993. Sapphirine granulites from the Vestfold Hills, East Antarctica: geochemical and metamorphic evolution. Antarctic Science 5, 389–402.

Harley, S.L., 1995. Upwardly mobile hot crust. Nature 375, 451–452.

Harley, S.L., 1998a. An appraisal of peak temperatures and thermal histories in ultrahigh-temperature (UHT) crustal metamorphism; the significance of aluminous orthopyroxene. In: Motoyoshi, Y., Shiraishi, K. (Eds.), Origin and Evolution of Continents; Proceedings of the International Symposium, Memoirs of National Institute of Polar Research. Special Issue, vol. 53. National Institute of Polar Research, Tokyo, Japan, pp. 49–73.

Harley, S.L., 1998b. On the occurrence and characterization of ultrahigh-temperature crustal metamorphism. In: Treloar, P.J., O'Brien, P.J. (Eds.), What Drives Metamorphism and Metamorphic Relations?, Geological Society, London, Special Publication, vol. 138, pp. 81–107.

Harley, S.L., 1998c. Ultrahigh temperature granulite metamorphism (1050 °C, 12 kbar) and decompression in garnet (Mg70)–orthopyroxene–sillimanite gneisses from the Rauer Group, East Antarctica. Journal of Metamorphic Geology 16, 541–562.

Harley, S.L., 2000. Crust–mantle relations in Antarctica: the evolution of the east Antarctic shield and tectonic settings of UHT metamorphism Crust–Mantle Interactions. Proceedings of the International School Earth and Planetary Sciences, Sienna 261–274.

Harley, S.L., 2004. Extending our understanding of ultrahigh temperature crustal metamorphism. Journal of Mineralogical and Petrological Sciences 99, 140–158.

Harley, S.L., 2008. Refining the *P–T* records of UHT crustal metamorphism. Journal of Metamorphic Geology 26, 125–154.

Harley, S.L., Black, L.P., 1997. A revised Archaean chronology for the Napier Complex, Enderby Land, from SHRIMP ion-microprobe studies. Antarctic Science 9, 74–91.

Harley, S.L., Fitzsimons, I.C.W., 1991. Pressure–temperature evolution of metapelitic granulites in a polymetamorphic terrane: the Rauer Group, East Antarctica. Journal of Metamorphic Geology 9, 231–243.

Harley, S.L., Green, D.H., 1982. Garnet–orthopyroxene barometry for granulites and peridotites. Nature 300, 697–701.

Harley, S.L., Hensen, B.J., 1990. Archaean and Proterozoic high-grade terranes of East Antarctica (40–80°E); a case study of diversity in granulite facies metamorphism. In: Ashworth, J.R., Brown, M. (Eds.), High-temperature Metamorphism and Crustal Anatexis. Mineralogical Society of Great Britain, The Mineralogical Society Series, vol. 2. Unwin Hyman, London, pp. 320–370.

Harley, S.L., Hensen, B.J., Sheraton, J.W., 1990. Two-stage decompression in orthopyroxene–sillimanite granulites from Forefinger Point, Enderby Land,

Antarctica; implications for the evolution of the Archaean Napier Complex. Journal of Metamorphic Geology 8, 591–613.
Harley, S.L., Kelly, N.M., 2007a. Ancient Antarctica: the Archaean of the east Antarctic Shield. In: Van Kranendonk, M.J., Smithies, R.H., Bennett, V.C. (Eds.), Earth's Oldest Rocks, Developments in Precambrian Geology, vol. 15. Elsevier B. V., The Netherlands, pp. 149–186.
Harley, S.L., Kelly, N.M., 2007b. The impact of zircon–garnet REE distribution data on the interpretation of zircon U–Pb ages in complex high-grade terrains: an example from the Rauer Islands, East Antarctica. Chemical Geology 241, 62–87.
Harley, S.L., Kelly, N.M., Möller, A., 2007. Zircon behaviour and the thermal histories of mountain chains. Elements 3, 25–30.
Harlov, D.E., Newton, R.C., 1993. Reversal of the metastable kyanite + corundum + quartz and andalusite + corundum + quartz equilibria and the enthalpy of formation of kyanite and andalusite. American Mineralogist 78, 594–600.
Harlov, D.E., Wirth, R., Hetherington, C.J., 2011. Fluid-mediated partial alteration in monazite: the role of coupled dissolution–reprecipitation in element redistribution and mass transfer. Contributions to Mineralogy and Petrology 162, 329–348.
Harrison, T.M., Watson, E.B., Aikman, A.B., 2007. Temperature spectra of zircon crystallization in plutonic rocks. Geology 35, 635–638.
Hasan, S.E., 1978. Thermophysical Properties of Rocks. Proceedings 19th US Symposium on Rock Mechanics 1, pp. 210–214.
Hayden, L.A., Watson, E.B., Wark, D.A., 2008. A thermobarometer for sphene (titanite). Contributions to Mineralogy and Petrology 155, 529–540.
Hayob, J.L., Essene, E.J., 1990. High-temperature granulites – reply. Nature 347, 133–134.
Hayob, J.L., Essene, E.J., Ruiz, J., Ortega-Gutiérrez, F., Aranda-Gómez, J.J., 1989. Young high-temperature granulites from the base of the crust in central Mexico. Nature 342, 265–268.
Hensen, B.J., 1971. Theoretical phase relations involving cordierite and garnet in the system MgO–FeO–Al_2O_3–SiO_2. Contributions to Mineralogy and Petrology 33, 191–214.
Hensen, B.J., 1972a. Cordierite–garnet Equilibrium as a Function of Pressure, Temperature, and Iron–magnesium Ratio. Carnegie Institution of Washington Year Book 71, pp. 418–421.
Hensen, B.J., 1972b. Phase Relations Involving Pyrope, $Enstatite_{ss}$ and $Sapphirine_{ss}$ in the System MgO–Al_2O_3–SiO_2. Carnegie Institution of Washington Year Book 71, pp. 421–427.
Hensen, B.J., 1977. The stability of osumilite in high grade metamorphic rocks. Contributions to Mineralogy and Petrology 64, 197–204.
Hensen, B.J., 1986. Theoretical phase relations involving cordierite and garnet revisited: the influence of oxygen fugacity on the stability of sapphirine and spinel in the system Mg–Fe–Al–Si–O. Contributions to Mineralogy and Petrology 92, 362–367.
Hensen, B.J., 1987. P–T grids for silica-undersaturated granulites in the systems MAS (n + 4) and FMAS (n + 3)—tools for the derivation of P–T paths of metamorphism. Journal of Metamorphic Geology 5, 255–271.
Hensen, B.J., 1988. Chemical potential diagrams and chemographic projections; applications to sapphirine-granulites from Kiranur and Ganguvarpatti, Tamil Nadu; evidence for rapid uplift in part of the South Indian Shield? Neues Jahrbuch für Mineralogie, Abhandlungen 158, 193–210.
Hensen, B.J., Essene, E.J., 1971. Stability of pyrope–quartz in the system MgO–Al_2O_3–SiO_2. Contributions to Mineralogy and Petrology 30, 72–83.
Hensen, B.J., Green, D.H., 1970. Experimental data on coexisting cordierite and garnet under high grade metamorphic conditions. Physics of the Earth and Planetary Interiors 3, 431–440.
Hensen, B.J., Green, D.H., 1971. Experimental study of the stability of cordierite and garnet in pelitic compositions at high pressures and temperatures; I, Compositions with excess alumino-silicate. Contributions to Mineralogy and Petrology 33, 309–330.
Hensen, B.J., Green, D.H., 1972. Experimental study of the stability of cordierite and garnet in pelitic compositions at high pressures and temperatures; II, Compositions without excess alumino-silicate. Contributions to Mineralogy and Petrology 35, 331–354.
Hensen, B.J., Green, D.H., 1973. Experimental study of the stability of cordierite and garnet in pelitic compositions at high pressures and temperatures III. Synthesis of experimental data and geological applications. Contributions to Mineralogy and Petrology 38, 151–166.
Hensen, B.J., Harley, S.L., 1990. Graphical analysis of P–T–X relations in granulite facies metapelites. In: Ashworth, J.R., Brown, M. (Eds.), High-temperature Metamorphism and Crustal Anatexis, The Mineralogical Society Series, vol. 2. Mineralogical Society of Great Britain, Unwin Hyman, London-Boston-Sydney-Wellington, United Kingdom, pp. 19–56.
Hensen, B.J., Motoyoshi, Y., 1992. Osumilite-producing reactions in high temperature granulites from the Napier Complex, east Antarctica: tectonic implications. In: Yoshida, H., Kaminuma, K., Shiraishi, K. (Eds.), Recent Progress in Antarctic Earth Science. Terra Scientific Publishing Company (TERRAPUB), Tokyo, pp. 87–92.
Herd, R.K., Ackermand, D., Thomas, A., Windley, B.F., 1987. Oxygen fugacity variations and mineral reactions in sapphirine-bearing paragneisses, E. Grenville province, Canada. Mineralogical Magazine 51, 203–206.
Herd, R.K., Windley, B.F., Ackermand, D., 1984. Grandidierite from a pelitic xenolith in the Haddo House Complex, NE Scotland. Mineralogical Magazine 48, 401–406.
Herd, R.K., Windley, B.F., Ghisler, M., 1969. The mode of occurrence and petrogenesis of the sapphirine-bearing and associated rocks of west Greenland. Rapport Grønlands Geologiske Undersøgelse 24, 1–44.
Hermann, J., Rubatto, D., 2003. Relating zircon and monazite domains to garnet growth zones: age and duration of granulite facies metamorphism in the Val Malenco lower crust. Journal of Metamorphic Geology 21, 833–852.
Hiess, J., Nutman, A.P., Bennett, V.C., Holden, P., 2008. Ti-in-zircon thermometry applied to contrasting Archean metamorphic and igneous systems. Chemical Geology 247, 323–338.
Hinton, R.W., Long, J.V.P., 1979. High-resolution ion-microprobe measurement of lead isotopes: variations within single zircons from Lac Seul, northwestern Ontario. Earth and Planetary Science Letters 45, 309–325.
Hofmann, A.E., Baker, M.B., Eiler, J.M., 2014. Sub-micron-scale trace-element distributions in natural zircons of known provenance: implications for Ti-in-zircon thermometry. Contributions to Mineralogy and Petrology 168, 1057. http://dx.doi.org/10.1007/s00410-014-1057-8.
Hofmann, A.E., Baker, M.B., Eiler, J.M., 2013. An experimental study of Ti and Zr partitioning among zircon, rutile, and granitic melt. Contributions to Mineralogy and Petrology 166, 235–253.
Hofmann, A.E., Valley, J.W., Watson, E.B., Cavosie, A.J., Eiler, J.M., 2009. Sub-micron scale distributions of trace elements in zircon. Contributions to Mineralogy and Petrology 158, 317–335.
Högdahl, K., Lundqvist, T., 2009. Discussion on "Successive ~1.94 Ga plutonism and ~1.92 Ga deformation and metamor- phism south of the Skellefte district, northern Sweden: substantiation of the marginal basin accretion hypothesis of Svecofennian evolution" by Skiöld T., Rutland R.W.R., Precambrian Res 148:181–204, 2006. Precambrian Research 168, 330–334.
Högdahl, K., Majka, J., Sjöström, H., Nilsson, K.P., Claesson, S., Konečný, P., 2012. Reactive monazite and robust zircon growth in diatexites and leucogranites from a hot, slowly cooled orogen: implications for the Palaeoproterozoic tectonic evolution of the central Fennoscandian Shield, Sweden. Contributions to Mineralogy and Petrology 163, 167–188.
Hokada, T., 2007. Perrierite in sapphirine–quartz gneiss: geochemical and geochronological features and implications for accessory-phase paragenesis of UHT metamorphism. Journal of Mineralogical and Petrological Sciences 102, 44–49.
Hokada, T., Harley, S.L., 2004. Zircon growth in UHT leucosome: constraints from zircon–garnet rare earth elements (REE) relations in Napier Complex, East Antarctica. Journal of Mineralogical and Petrological Sciences 99, 180–190.
Hokada, T., Misawa, K., Shiraishi, K., Suzuki, S., 2003. Mid to late Archaean (3.3–2.5 Ga) tonalitic crustal formation and high-grade metamorphism at Mt. Riiser-Larsen, Napier Complex, East Antarctica. Precambrian Research 127, 215–228.
Hokada, T., Motoyoshi, Y., Suzuki, S., Ishikawa, M., Ishizuka, A., 2008. Geodynamic evolution of Mt. Riiser Larsen, Napier Complex, Antarctica, with reference to the UHT mineral associations and their reaction relations. In: Satish-Kumar, M., Motoyoshi, Y., Osanai, Y., Hiroi, Y., Shiraishi, K. (Eds.), Geodynamic Evolution of East Antarctica: a Key to the East–West Gondwana Connection, Geological Society Special Publication, London, vol. 308, pp. 253–282.
Holland, J.G., Lambert, R.S.J., 1969. Structural regimes and metamorphic facies. Tectonophysics 7, 197–218.
Holland, T.J.B., Powell, R., 1985. An internally consistent thermodynamic dataset with uncertainties and correlations: 2. Data and results. Journal of Metamorphic Geology 3, 343–370.
Holland, T.J.B., Powell, R., 1990. An enlarged and updated internally consistent thermodynamic dataset with uncertainties and correlations: the system K_2O–Na_2O–CaO–MgO–MnO–FeO–Fe_2O_3–Al_2O_3–TiO_2–SiO_2–C–H_2–O_2. Journal of Metamorphic Geology 8, 89–124.
Holland, T.J.B., Powell, R., 1998. An internally consistent thermodynamic data set for phases of petrological interest. Journal of Metamorphic Geology 16, 309–343.
Holland, T.J.B., Powell, R., 2001. Calculation of phase relations involving haplogranitic melts using an internally-consistent thermodynamic data set. Journal of Petrology 42, 673–683.
Holland, T.J.B., Powell, R., 2011. An improved and extended internally consistent thermodynamic dataset for phases of petrological interest, involving a new equation of state for solids. Journal of Metamorphic Geology 29, 333–383.
Hollis, J., Harley, S.L., 2002. New evidence for the peak temperatures and the near-peak pressure–temperature evolution of the Napier Complex. Royal Society of New Zealand Bulletin 35, 19–29.
Hollis, J., Harley, S.L., 2003. Alumina solubility in orthopyroxene coexisting with sapphirine and quartz. Contributions to Mineralogy and Petrology 144, 473–483.
Hollis, J.A., Harley, S.L., White, R.W., Clarke, G.L., 2006. Preservation of evidence for prograde metamorphism in ultrahigh-temperature, high-pressure kyanite-bearing granulites, South Harris, Scotland. Journal of Metamorphic Geology 24, 263–279.
Holness, M.B., Cesare, B., Sawyer, E.W., 2011. Melted rocks under the microscope: microstructures and their interpretation. Elements 7, 247–252.
Horai, K., Simmons, G., 1969. Thermal conductivity of rock-forming minerals. Earth and Planetary Science Letters 6, 359–368.
Horie, K., Hokada, T., Hiroi, Y., Motoyoshi, Y., Shiraishi, K., 2012. Contrasting Archaean crustal records in western part of the Napier Complex, East Antarctica: new constraints from SHRIMP geochronology. Gondwana Research 21, 829–837.

Hoskin, P.W.O., Schaltegger, U., 2003. The composition of zircon and igneous and metamorphic petrogenesis. In: Hanchar, J.M., Hoskin, P.W.O. (Eds.), Zircon, Reviews in Mineralogy and Geochemistry, vol. 53. Mineralogical Society of America, pp. 27–62.
Housman, G.A., McKenzie, D.P., Molnar, P., 1981. Convective instability of a thickened boundary layer and its relevance for the thermal evolution of convergent belts. Journal of Geophysical Research 86, 6115–6132.
Huang, R., Audétat, A., 2012. The titanium-in-quartz (TitaniQ) thermobarometer: a critical examination and re-calibration. Geochimica et Cosmochimica Acta 84, 75–89.
Huppert, H.E., Sparks, S.J., 1988. The generation of granitic magmas by intrusion of basalt into continental crust. Journal of Petrology 29, 599–624.
Hyndman, R.D., Currie, C.A., 2011. Why is the North America Cordillera high? Hot backarcs, thermal isostasy, and mountain belts. Geology 39, 783–786.
Hyndman, R.D., Currie, C.A., Mazzotti, S., 2005. Subduction zone backarcs, mobile belts, and orogenic heat. GSA Today 15, 4–10.
Hyndman, R.D., Currie, C.A., Mazzotti, S., Frederiksen, A., 2009. Temperature control of continental lithosphere elastic thickness, *Te* vs *Vs*. Earth and Planetary Science Letters 277, 539–548.
Indares, A., White, R.W., Powell, R., 2008. Phase equilibria modelling of kyanite-bearing anatectic paragneisses from the central Grenville Province. Journal of Metamorphic Geology 26, 815–836.
Inger, S., Harris, N., 1993. Geochemical constraints on leucogranite magmatism in the Langtang Valley, Nepal, Himalaya. Journal of Petrology 34, 345–368.
Ishii, S., Tsunogae, T., Santosh, M., 2006. Ultrahigh-temperature metamorphism in the Achankovil Zone: implications for the correlation of crustal blocks in southern India. Gondwana Research 10, 99–114.
Iwamura, S., Tsunogae, T., Kato, M., Koizumi, T., Dunkley, D.J., 2013. Petrology and phase equilibrium modelling of spinel–sapphirine-bearing mafic granulite from Akarui Point, Lützow–Holm Complex, East Antarctica: implications for the *P–T* path. Journal of Mineralogical and Petrological Sciences 108, 345–350.
Jaeger, J.C., 1964. Thermal effects of intrusions. Reviews of geophysics 2, 443–466.
James, P.R., Black, L.P., 1981. A review of the structural evolution and geochronology of the Archaean Napier Complex of Enderby Land, Australian Antarctic Territory. In: Glover, J.E., Groves, D.I. (Eds.), Archaean Geology: Second International Symposium, Perth, 1980, Geological Society of Australia Special Publication, Perth, vol. 7, pp. 71–83.
Jamieson, R.A., Beaumont, C., 2013. On the origin of orogens. Geological Society of America Bulletin 125, 1671–1702.
Jamieson, R.A., Beaumont, C., Fullsack, P., Lee, B., 1998. Barrovian Metamorphism: where's the heat? In: Treloar, P.J., O'Brien, P.J. (Eds.), What drives Metamorphism and Metamorphic Reactions?, Geological Society Special Publication, London, vol. 138, pp. 23–51.
Jamieson, R.A., Beaumont, C., Nguyen, M.H., Lee, B., 2002. Interaction of metamorphism, deformation and exhumation in large convergent orogens. Journal of Metamorphic Geology 20 (1), 9–24.
Janák, M., Ravna, E.J.K., Kullerud, K., 2012. Constraining peak *P–T* conditions in UHP eclogites: calculated phase equilibria in kyanite- and phengite-bearing eclogite of the Tromsø Nappe, Norway. Journal of Metamorphic Geology 30, 377–396.
Janots, E., Berger, A., Gnos, E., Whitehouse, M., Lewin, E., Pettke, T., 2012. Constraints on fluid evolution during metamorphism from U–Th–Pb systematics in Alpine hydrothermal monazite. Chemical Geology 326-327, 61–71.
Janots, E., Brunet, F., Goffé, B., Poinssot, C., Burchard, M., Cemič, L., 2007. Thermochemistry of monazite-(La) and dissakisite-(La): implications for monazite and allanite stability in metapelites. Contributions to Mineralogy and Petrology 154, 1–14.
Janots, E., Engi, M., Berger, J., Allaz, J., Schwarz, O., Spandler, C., 2008. Prograde metamorphic sequence of REE minerals in pelitic rocks of the Central Alps: implications for allanite–monazite–xenotime phase relations from 250 to 6110 °C. Journal of Metamorphic Geology 26, 509–526.
Jian, P., Kröner, A., Zhou, G., 2012. SHRIMP zircon U–Pb ages and REE partition for high-grade metamorphic rocks in the North Dabie complex: insight into crustal evolution with respect to Triassic UHP metamorphism in east-central China. Chemical Geology 328, 49–69.
Jiao, S., Guo, J.-H., Harley, S.L., Peng, P., 2013a. Geochronology and trace element geochemistry of zircon, monazite and garnet from the garnetite and/or associated other high-grade rocks: implications for Palaeoproterozoic tectonothermal evolution of the Khondalite Belt, North China Craton. Precambrian Research 237, 78–100.
Jiao, S., Guo, J., 2011. Application of the two-feldspar geothermometer to ultrahigh-temperature (UHT) rocks in the Khondalite belt, North China craton and its implications. American Mineralogist 96, 250–260.
Jiao, S., Guo, J., Harley, S.L., Windley, B.F., 2013b. New constraints from garnetite on the *P–T* path of the Khondalite Belt: implications for the tectonic evolution of the North China Craton. Journal of Petrology 54, 1725–1758.
Jiao, S., Guo, J., Mao, Q., Zhao, R., 2011. Application of Zr-in-rutile thermometry: a case study from ultrahigh-temperature granulites of the Khondalite belt, North China Craton. Contributions to Mineralogy and Petrology 162, 379–393.
Joesten, R., 1977. Evolution of mineral assemblage zoning in diffusion metasomatism. Geochimica et Cosmochimica Acta 41, 649–670.
Johnson, T., Brown, M., 2004. Quantitative constraints on metamorphism in the variscides of southern Brittany – a complementary pseudosection approach. Journal of Petrology 45, 1237–1259.
Johnson, T.E., Brown, M., 2005. The granulite facies, crustal melting, and prograde and retrograde phase equilibria in metapelites at the amphibolite to granulite facies transition. In: Thomas, H. (Ed.), Metamorphism and Crustal Evolution. Atlantic Publishers and Distributors, New Delhi, pp. 3–27.
Johnson, T.E., Brown, M., Gibson, R., Wing, B., 2004. Spinel–cordierite symplectites replacing andalusite: evidence for melt-assisted diapirism in the Bushveld Complex, South Africa. Journal of Metamorphic Geology 22, 529–545.
Johnson, T.E., Brown, M., White, R.W., 2010. Petrogenetic modelling of strongly residual metapelitic xenoliths within the southern Platreef, Bushveld Complex, South Africa. Journal of Metamorphic Geology 26, 269–291.
Johnson, T.E., Fischer, S., White, R.W., Brown, M., Rollinson, H.R., 2012. Archaean intracrustal differentiation from partial melting of metagabbro—field and geochemical evidence from the Central Region of the Lewisian Complex, NW Scotland. Journal of Petrology 53, 2115–2138.
Johnson, T.E., White, R.W., 2011. Phase equilibrium constraints on conditions of granulite-facies metamorphism at Scourie, NW Scotland. Journal of the Geological Society, London 168, 147–159.
Johnson, T.E., White, R.W., Brown, M., 2011. A year in the life of an aluminous metapelite xenolith—The role of heating rates, reaction overstep, H_2O retention and melt loss. Lithos 124, 132–143.
Jöns, N., Schenk, V., 2004. Petrology of whiteschists and associated rocks at Mautia Hill (Tanzania): fluid infiltration during high-grade metamorphism? Journal of Petrology 45, 1959–1981.
Jöns, N., Schenk, V., 2008. Relics of the Mozambique Ocean in the central East African Orogen: evidence from the Vohibory Block of southern Madagascar. Journal of Metamorphic Geology 26, 17–28.
Jöns, N., Schenk, V., 2011. The ultrahigh temperature granulites of southern Madagascar in a polymetamorphic context: implications for the amalgamation of the Gondwana supercontinent. European Journal of Mineralogy 23, 127–156.
Kali, E., Leloup, P.H., Arnaud, N., Mahéo, G., Liu, D., Boutonnet, E., Van der Woerd, J., Liu, X., Liu-Zeng, J., Li, H., 2010. Exhumation history of the deepest central Himalayan rocks, Ama Drime range: key pressure–temperature–deformation–time constraints on orogenic models. Tectonics 29, TC2014. http://dx.doi.org/10.1029/2009TC002551.
Kamineni, D.C., Rao, A.T., 1988a. Sapphirine-bearing quartzite from the Eastern Ghats terrain, Vizianagaram, India. Journal of Geology 96, 209–220.
Kamineni, D.C., Rao, A.T., 1988b. Sapphirine granulites from the Kakanuru area, Eastern Ghats, India. American Mineralogist 73, 692–700.
Kanazawa, T., Tsunogae, T., Sato, K., Santosh, M., 2009. The stability and origin of sodicgedrite in ultrahigh-temperature Mg–Al granulites: a case study from the Gondwana suture in southern India. Contributions to Mineralogy and Petrology 157, 95–110.
Kars, H., Jansen, J.B.H., Tobi, A.C., Poorter, R.P.E., 1980. The metapelitic rocks of the polymetamorphic precambrian of Rogaland, SW Norway. 2. Mineral relations between cordierite, hercynite and magnetite within the osumilite-in isograd. Contributions to Mineralogy and Petrology 74, 235–244.
Kawasaki, T., Motoyoshi, Y., 2007. Solubility of TiO_2 in Garnet and Orthopyroxene: Ti Thermometer for Ultrahigh-temperature Granulites. U.S. Geological Survey and the National Academies; USGS OF-2007-1047. Short Research Paper 038. http://dx.doi.org/10.3133/of2007-1047.srp038.
Kawasaki, T., Nakano, N., Osanai, Y., 2011. Osumilite and a spinel+quartz association in garnet–sillimanite gneiss from Rundvågshetta, Lützow-Holm Complex, East Antarctica. Gondwana Research 19, 430–445.
Kawasaki, T., Osanai, Y., 2008. Empirical thermometer of TiO_2 in quartz for ultrahigh-temperature granulites of East Antarctica. In: Satish-Kumar, M., Motoyoshi, Y., Osanai, Y., Hiroi, Y., Shiraishi, K. (Eds.), Geodynamic Evolution of East Antarctica: a Key to the East–West Gondwana Connection, Geological Society Special Publication, London, vol. 308, pp. 419–430.
Kelly, E.D., Carlson, W.D., Connelly, J.N., 2011. Implications of garnet resorption for the Lu–Hf garnet geochronometer: an example from the contact aureole of the Makhavinekh Lake Pluton, Labrador. Journal of Metamorphic Geology 29, 901–916.
Kelly, E.D., Carlson, W.D., Ketcham, R.A., 2013. Magnitudes of departures from equilibrium during regional metamorphism of porphyroblastic rocks. Journal of Metamorphic Geology 31, 981–1002.
Kelly, N.M., Clarke, G.L., Harley, S.L., 2006. Monazite behaviour and age significance in poly-metamorphic high-grade terrains: a case study from the western Musgrave Block, central Australia. Lithos 88, 100–134.
Kelly, N.M., Harley, S.L., 2004. Orthopyroxene–corundum in Mg–Al-rich granulites from the Oygarden Islands, East Antarctica. Journal of Petrology 45, 1481–1512.
Kelly, N.M., Harley, S.L., 2005. An integrated microtextural and chemical approach to zircon geochronology: refining the Archaean history of the Napier Complex, east Antarctica. Contributions to Mineralogy and Petrology 149, 57–84.
Kelly, N.M., Harley, S.L., Möller, A., 2012. Complexity in the behavior and recrystallization of monazite during high-*T* metamorphism and fluid infiltration. Chemical Geology 322–323, 192–208.
Kelsey, D.E., 2008. On ultrahigh-temperature crustal metamorphism. Gondwana Research 13, 1–29.
Kelsey, D.E., Clark, C., Hand, M., 2008. Thermobarometric modeling of zircon and monazite growth in melt-bearing systems: examples using model metapelitic and metapsammitic granulites. Journal of Metamorphic Geology 26, 199–212.
Kelsey, D.E., Hand, M., Clark, C., Wilson, C.J.L., 2007. On the application of in-situ monazite chemical geochronology to constraining *P–T–t* histories in high-

temperature (>850 °C) polymetamorphic granulites from Prydz Bay, east Antarctica. Journal of the Geological Society, London 164, 667–683.
Kelsey, D.E., Powell, R., 2011. Progress in linking accessory mineral growth and breakdown to major mineral evolution in metamorphic rocks: a thermodynamic approach in the Na_2O–CaO–K_2O–FeO–MgO–Al_2O_3–SiO_2–H_2O–TiO_2–ZrO_2 system. Journal of Metamorphic Geology 29, 151–166.
Kelsey, D.E., White, R.W., Holland, T.J.B., Powell, R., 2004. Calculated phase equilibria in K_2O–FeO–MgO–Al_2O_3–SiO_2–H_2O for sapphirine–quartz-bearing mineral assemblages. Journal of Metamorphic Geology 22, 559–578.
Kelsey, D.E., White, R.W., Powell, R., 2003a. Orthopyroxene–sillimanite–quartz assemblages: distribution, petrology, quantitative *P–T–X* constraints and *P–T* paths. Journal of Metamorphic Geology 21, 439–453.
Kelsey, D.E., White, R.W., Powell, R., 2005. Calculated phase equilibria in K_2O–FeO–MgO–Al_2O_3–SiO_2–H_2O for silica-undersaturated sapphirine-bearing mineral assemblages. Journal of Metamorphic Geology 23, 217–239.
Kelsey, D.E., White, R.W., Powell, R., Wilson, C.J.L., Quinn, C.D., 2003b. New constraints on metamorphism in the Rauer Group, Prydz Bay, east Antarctica. Journal of Metamorphic Geology 21, 739–759.
Kemp, A.I.S., Shimura, T., Hawkesworth, C.J., 2007. Linking granulites, silicic magmatism, and crustal growth in arcs: ion micoprobe (zircon) U-Pb ages from the Hidaka metamorphic belt, Japan. Geology 35, 807–810.
Kerrick, D.M., Connolly, J.A.D., 2001. Metamorphic devolatilization of subducted oceanic metabasalts: implications for seismicity, arc magmatism and volatile recycling. Earth and Planetary Science Letters 189, 19–29.
Kihle, J., Harlov, D.E., Frigaard, Ø., Jamtveit, B., 2010. Epitaxial quartz inclusions in corundum from a sapphirine–garnet boudin, Bamble Sector, SE Norway: SiO_2–Al_2O_3 miscibility at high *P–T* dry granulite facies conditions. Journal of Metamorphic Geology 28, 769–784.
Kincaid, C., Silver, P., 1996. The role of viscous dissipation in the orogenic process. Earth and Planetary Science Letters 142, 271–288.
Kirkland, C.L., Smithies, R.H., Woodhouse, A.J., Howard, H.M., Wingate, M.T.D., Belousova, E.A., Cliff, J.B., Murphy, R.C., Spaggiari, C.V., 2013. Constraints and deception in the isotopic record; the crustal evolution of the west Musgrave Province, central Australia. Gondwana Research 23, 759–781.
Kirkland, C.L., Whitehouse, M.J., Slagstad, T., 2009. Fluid-assisted zircon and monazite growth within a shear zone: a case study from Finnmark, Arctic Norway. Contributions to Mineralogy and Petrology 158, 637–657.
Kiseleva, I.A., 1976. Thermodynamic parameters of natural ordered sapphirine and synthetic disordered specimens. Transactions from Geokhimiya 2, 189–201.
Kohn, M.J., 2009. Models of garnet differential geochronology. Geochimica et Cosmochimica Acta 73, 170–182.
Kondou, N., Tsunogae, T., Santosh, M., Shimizu, H., 2009. Sapphirine + quartz assemblage from Ganguvarpatti: diagnostic evidence for ultrahigh-temperature metamorphism in central Madurai Block, southern India. Journal of Mineralogical and Petrological Sciences 104, 285–289.
Kooijman, E., Smit, M.A., Mezger, K., Berndt, J., 2012. Trace element systematics in granulite facies rutile: implications for Zr geothermometry and provenance studies. Journal of Metamorphic Geology 30, 397–412.
Kooijman, E., Upadhyay, D., Mezger, K., Raith, M.M., Berndt, J., Srikantappa, C., 2011. Response of the U–Pb chronometer and trace elements in zircon to ultrahigh-temperature metamorphism: the Kadavur anorthosite complex, southern India. Chemical Geology 290, 177–188.
Korhonen, F.J., Brown, M., Clark, C., Bhattacharya, S., 2013a. Osumilite–melt interactions in ultrahigh temperature granulites: phase equilibria modelling and implications for the *P–T–t* evolution of the Eastern Ghats Province, India. Journal of Metamorphic Geology 31, 881–907.
Korhonen, F.J., Brown, M., Grove, M., Siddoway, C.S., Baxter, E.F., Inglis, J.D., 2012a. Separating metamorphic events in the Fosdick migmatite-granite complex, West Antarctica. Journal of Metamorphic Geology 30, 165–191.
Korhonen, F.J., Clark, C., Brown, M., Bhattacharya, S., Taylor, R., 2013b. How long-lived is ultrahigh temperature (UHT) metamorphism? Constraints from zircon and monazite geochronology in the Eastern Ghats orogenic belt, India. Precambrian Research 234, 322–350.
Korhonen, F.J., Clark, C., Brown, M., Taylor, R.J.M., 2014. Taking the temperature of Earth's hottest crust. Earth and Planetary Science Letters 408, 341–354.
Korhonen, F.J., Powell, R., Stout, J.H., 2012b. Stability of sapphirine + quartz in the oxidized rocks of the Wilson Lake terrane, Labrador: calculated equilibria in NCKFMASHTO. Journal of Metamorphic Geology 30, 21–36.
Korhonen, F.J., Saito, S., Brown, M., Siddoway, C.S., 2010. Modeling multiple melt loss events in the evolution of an active continental margin. Lithos 116, 230–248.
Korhonen, F.J., Saw, A.K., Clark, C., Brown, M., Bhattacharya, S., 2011. New constraints on UHT metamorphism in the Eastern Ghats Province through the application of phase equilibria modelling and *in situ* geochronology. Gondwana Research 20, 764–781.
Korhonen, F.J., Stout, J.H., 2004. Low-variance sapphirine-bearing assemblages from Wilson Lake, Grenville Province of Labrador. In: Tollo, R.P., Corriveau, L., McLelland, J., Bartholomew, M.J. (Eds.), Proterozoic Tectonic Evolution of the Grenville Orogen in North America, vol. 197. Geological Society of America Memoir, Boulder, Colorado, pp. 81–103.
Kotková, J., Harley, S.L., 2010. Anatexis during high-pressure crustal metamorphism: evidence from garnet–whole-rock REE relationships and zircon–rutile Ti–Zr thermometry in leucogranulites from the Bohemian Massif. Journal of Petrology 51, 1967–2001.
Kramers, J.D., Kreissig, K., Jones, M.Q.W., 2001. Crustal heat production and style of metamorphism: a comparison between two Archean high grade provinces in the Limpopo Belt, southern Africa. Precambrian Research 112, 149–163.
Kriegsman, L.M., Schumacher, J.C., 1999. Petrology of sapphirine-bearing and associated granulites from central Sri Lanka. Journal of Petrology 40, 1211–1239.
Krogh, E.J., 1977. Origin and metamorphism of iron formations and associated rocks, Lofoten-Vesterålen, N. Norway. I. The Vestpolltind Fe–Mn deposit. Lithos 10, 243–255.
Kruckenberg, S.C., Whitney, D.L., 2011. Metamorphic evolution of sapphirine- and orthoamphibole–cordierite-bearing gneiss, Okanogan dome, Washington, USA. Journal of Metamorphic Geology 29, 425–449.
Kusiak, M.A., Whitehouse, M.J., Wilde, S.A., Dunkley, D.J., Menneken, M., Nemchin, A.A., Clark, C., 2013a. Changes in zircon chemistry during Archean UHT metamorphism in the Napier Complex, Antarctica. American Journal of Science 313, 933–967.
Kusiak, M.A., Whitehouse, M.J., Wilde, S.A., Nemchin, A.A., Clark, C., 2013b. Mobilization of radiogenic Pb in zircon revealed by ion imaging: implications for early Earth geochronology. Geology 41, 291–294.
Lachenbruch, A.H., 1978. Heat flow in the Basin and Range Province and thermal effects of tectonic extension. Pure and Applied Geophysics 117, 34–50.
Lachenbruch, A.H., Sass, J.H., 1978. Models of an extending lithosphere and heat flow in the Basin and Range province. Geological Society of America Memoir 152, 209–250.
Lal, R.K., Ackermand, D., Raith, M., Raase, P., Seifert, F., 1984. Sapphirine-bearing assemblages from Kiranur, Southern India: a study of chemographic relationships in the Na_2O–FeO–MgO–Al_2O_3–SiO_2–H_2O system. Neues Jahrbuch für Mineralogie, Abhandlungen 150, 121–152.
Lal, R.K., Ackermand, D., Seifert, F., Haldar, S.K., 1978. Chemographic relationships in sapphirine-bearing rocks from Sonapahar, Assam, India. Contributions to Mineralogy and Petrology 67, 169–187.
Lal, R.K., Ackermand, D., Upadhyay, H., 1987. *P–T–X* relationships deduced from corona textures in sapphirine–spinel–quartz assemblages from Paderu, southern India. Journal of Petrology 28, 1139–1168.
Lamb, W.M., Guillemette, R., Popp, R.K., Fritz, S.J., Chmiel, G.J., 2012. Determination of Fe^{3+}/Fe using the electron microprobe: a calibration for amphiboles. American Mineralogist 97, 951–961.
Lambert, I.B., Heier, K.S., 1968. Geochemical investigations of deep-seated rocks in the Australian Shield. Lithos 1, 30–53.
Le Breton, N., Thompson, A.B., 1988. Fluid-absent (dehydration) melting of biotite in metapelites in the early stages of crustal anatexis. Contributions to Mineralogy and Petrology 99, 226–237.
Lebedeva, Y.M., Glebovitskii, V.A., Bushmin, S.A., Bogomolov, E.S., Savva, E.V., Lokhov, K.I., 2010. The age of high-pressure metasomatism in shear zones during collision-related metamorphism in the Lapland Granulite Belt: the Sm–Nd method of dating the paragenesises from sillimanite–orthopyroxene rocks of Por'ya Guba Nappe. Doklady Earth Sciences 432, 602–605.
Lechler, P.J., Desilets, M.O., 1987. A review of the use of loss on ignition as a measurement of total volatiles in whole-rock analysis. Chemical Geology 63, 341–344.
Leite, C.de M.M., Barbosa, J.S.F., Goncalves, P., Nicollet, C., Sabaté, P., 2009. Petrological evolution of silica-undersaturated sapphirine-bearing granulite in the Paleoproterozoic Salvador–Curaçá Belt, Bahia, Brazil. Gondwana Research 15, 49–70.
Leong, K.M., Moore, J.M., 1972. Sapphirine-bearing rocks from Wilson Lake, Labrador. Canadian Mineralogist 11, 777–790.
Li, Z., Li, Y.L., Chen, H., Santosh, M., Xiao, W., Wang, H., 2010. SHRIMP U–Pb zircon chronology of ultrahigh-temperature spinel–orthopyroxene–garnet granulite from South Altay orogenic belt, northwestern China. Island Arc 19, 506–516.
Liu, S.J., Bai, X., Li, J.H., Santosh, M., 2011. Retrograde metamorphism of ultrahigh-temperature granulites from the khondalite belt in inner Mongolia, North China Craton: evidence from aluminous orthopyroxenes. Geological Journal 46, 263–275.
Liu, S.J., Li, J.H., Santosh, M., 2010. First application of the revised Ti-in-zircon geothermometer to Paleoproterozoic ultrahigh-temperature granulites of Tuguiwula, Inner Mongolia, North China Craton. Contributions to Mineralogy and Petrology 159, 225–235.
Liu, S.J., Tsunogae, T., Li, W., Shimizu, H., Santosh, M., Wan, Y.S., Li, J.H., 2012. Paleoproterozoic granulites from Heling'er: implications for regional ultrahigh-temperature metamorphism in the North China Craton. Lithos 148, 54–70.
Luvizotto, G.I., Zack, T., 2009. Nb and Zr behavior in rutile during high-grade metamorphism and retrogression: an example from the Ivrea–Verbano Zone. Chemical Geology 261, 303–317.
Lyubetskaya, T., Ague, J.J., 2009. Effect of metamorphic reactions on thermal evolution in collisional orogens. Journal of Metamorphic Geology 27, 579–600.
MacDonald, J.M., Wheeler, J., Harley, S.L., Mariani, E., Goodenough, K.M., Crowley, Q., Tatham, D., 2013. Lattice distortion in a zircon population and its effects on trace element mobility and U–Th–Pb isotope systematics: examples from the Lewisian Gneiss Complex, northwest Scotland. Contributions to Mineralogy and Petrology 166, 21–41.

Mahar, E.M., Baker, J.M., Powell, R., Holland, T.J.B., Howell, N., 1997. The effect of Mn on mineral stability in metapelites. Journal of Metamorphic Geology 15, 223–238.
Maidment, D.W., Hand, M., Williams, I.S., 2013. High grade metamorphism of sedimentary rocks during Palaeozoic rift basin formation in central Australia. Gondwana Research 24, 865–885.
Manning, C.E., Ingebrisen, S.E., Bird, D.K., 1993. Missing mineral zones in contact metamorphosed basalts. American Journal of Science 293, 894–938.
Marmo, B.A., Clarke, G.L., Powell, R., 2002. Fractionation of bulk rock composition due to porphyroblast growth: effects on eclogite facies mineral equilibria, Pam Peninsula, New Caledonia. Journal of Metamorphic Geology 20, 151–165.
Martinez, F.J., Reche, J., Arboleya, M.L., 2001. *P–T* modelling of the andalusite–kyanite–andalusite sequence and related assemblages in high-Al graphitic pelites. Prograde and retrograde paths in a late kyanite belt in the Variscan Iberia. Journal of Metamorphic Geology 19, 661–677.
McCarthy, T.S., 1976. Chemical interrelationships in a low-pressure granulite terrain in Namaqualand, South Africa, and their bearing on granite genesis and the composition of the lower crust. Geochimica et Cosmochimica Acta 40, 1057–1068.
McKenzie, D., Jackson, J., Priestley, K., 2005. Thermal structure of oceanic and continental lithosphere. Earth and Planetary Science Letters 233, 337–349.
McKie, D., 1963. Order-disorder in sapphirine. Mineralogical Magazine 33, 635–645.
Mehnert, K.R., 1968. Migmatites and the Origin of Granitic Rocks. Elsevier Science, New York, p. 393.
Meyer, M., John, T., Brandt, S., Klemd, R., 2011. Trace element composition of rutile and the application of Zr-in-rutile thermometry to UHT metamorphism (Epupa Complex, NW Namibia). Lithos 126, 388–401.
Meyre, C., de Capitani, C., Partzsch, J.H., 1997. A ternary solid solution model for omphacite and its application to geothermobarometry of eclogites from the Middle Adula nappe (Central Alps, Switzerland). Journal of Metamorphic Geology 15, 687–700.
Mitchell, R.K., Indares, A., Ryan, B., 2014. High to ultrahigh temperature contact metamorphism and dry partial melting of the Tasiuyak paragneiss, Northern Labrador. Journal of Metamorphic Geology 32, 535–555.
Mohan, A., Ackermand, D., Lal, R.K., 1986. Reaction textures and *P–T–X* trajectory in the sapphirine-spinel bearing granulites from Ganguvarpatti, Southern India. Neues Jahrbuch für Mineralogie, Abhandlungen 154, 1–19.
Moine, B., Sauvan, P., Jarousse, J., 1981. Geochemsitry of evaporite-bearing series: a tenative guide for the identification of meta-evaporites. Contributions to Mineralogy and Petrology 76, 401–412.
Möller, A., O'Brien, P.J., Kennedy, A., Kröner, A., 2003. Linking growth episodes of zircon and metamorphic textures to zircon chemistry: an example from the ultrahigh-temperature granulites of Rogaland (SW Norway). In: Vance, D., Müller, W., Villa, I.M. (Eds.), Geochronology: Linking the Isotopic record with Petrology and Textures, Geological Society, London, Special Publication, vol. 220, pp. 65–81.
Möller, C., 1999. Sapphirine in SW Sweden: a record of Sveconorwegian (Grenvillian) late-orogenic tectonic exhumation. Journal of Metamorphic Geology 17, 127–141.
Morfin, S., Sawyer, E.W., Bandyayera, D., 2013. Large volumes of anatectic melt retained in granulite facies migmatites: An injection complex in northern Quebec. Lithos 168, 200–218.
Morishita, T., Arai, S., Ishida, Y., Tamura, A., Gervilla, F., 2009. Constraints on the evolutionary history of aluminous mafic rocks in the Ronda peridotite massif (Spain) from trace-element compositions of clinopyroxene and garnet. Geochemical Journal 43, 191–206.
Morrissey, L.J., Hand, M., Raimondo, T., Kelsey, D.E., 2014. Long-lived high-*T*, low-*P* granulite facies metamorphism in the Arunta Region, central Australia. Journal of Metamorphic Geology 32, 25–47.
Morrissey, L.J., Hand, M., Wade, B.P., Szpunar, M., 2013. Early Mesoproterozoic metamorphism in the Barossa Complex, South Australia: links with the eastern margin of Proterozoic Australia. Australian Journal of Earth Sciences 60, 769–795.
Morse, S.A., Talley, J.H., 1971. Sapphirine reactions in deep-seated granulites near Wilson Lake, Central Labrador, Canada. Earth and Planetary Science Letters 10, 325–328.
Motoyoshi, Y., Hensen, B.J., 1989. Sapphirine–quartz–orthopyroxene symplectites after cordierite in the Archaean Napier Complex, Antarctica; evidence for a counterclockwise *P-T* path? European Journal of Mineralogy 1, 467–471.
Motoyoshi, Y., Hensen, B.J., Arima, M., 1993. Experimental study of the high-pressure stability limit of osumilite in the system K_2O–MgO–Al_2O_3–SiO_2: implications for high-temperature granulites. European Journal of Mineralogy 5, 439–445.
Motoyoshi, Y., Hensen, B.J., Matsueda, H., 1990. Metastable growth of corundum adjacent to quartz in a spinel-bearing quartzite from the Archaean Napier Complex, Antarctica. Journal of Metamorphic Geology 8, 125–130.
Mottaghy, D., Vosteen, H.-D., Schellschmidt, R., 2008. Temperature dependence of the relationship of thermal diffusivity versus thermal conductivity for crystalline rocks. International Journal of Earth Sciences 97, 435–442.
Moulas, E., Kostopoulos, D., Connolly, J.A.D., Burg, J.-P., 2013. *P–T* estimates and timing of the sapphirine-bearing metamorphic overprint in kyanite eclogites from Central Rhodope, Northern Greece. Petrology 21, 507–521.
Mouri, H., Guiraud, M., Osanai, Y., 2004. Review on "corundum plus quartz" assemblage in nature: possible indicator of ultra-high temperature conditions? Journal of Mineralogical and Petrological Sciences 99, 159–163.
Moynihan, D.P., Pattison, D.R.M., 2013. An automated method for the calculation of *P–T* paths from garnet zoning, with application to metapelitic schist from the Kootenay Arc, British Columbia, Canada. Journal of Metamorphic Geology 31, 525–548.
Nabelek, P.I., Hofmeister, A.M., Whittington, A.G., 2012. The influence of temperature-dependent thermal diffusivity on the conductive cooling rates of plutons and temperature–time paths in contact aureoles. Earth and Planetary Science Letters 317, 157–164.
Nabelek, P.I., Whittington, A.G., Hofmeister, A.M., 2010. Strain heating as a mechanism for partial melting and ultrahigh temperature metamorphism in convergent orogens: implications of temperature-dependent thermal diffusivity and rheology. Journal of Geophysical Research 115, B12417. http://dx.doi.org/10.11029/12010JB007727.
Nair, R., Chacko, T., 2002. Fluid-absent melting of high-grade semi-pelites: *P–T* constraints on orthopyroxene formation and implications for granulite genesis. Journal of Petrology 43, 2121–2142.
Nakano, N., Osanai, Y., Owada, M., 2007a. Multiple breakdown and chemical equilibrium of silicic clinopyroxene under extreme metamorphic conditions in the Kontum Massif, central Vietnam. American Mineralogist 92, 1844–1855.
Nakano, N., Osanai, Y., Owada, M., Nam, T.N., Charusiri, P., Khamphavong, K., 2013. Tectonic evolution of high-grade metamorphic terranes in central Vietnam: constraints from large-scale monazite geochronology. Journal of Asian Earth Sciences 73, 520–539.
Nakano, N., Osanai, Y., Owada, M., Ngoc Nam, T., Toyoshima, T., Tsunogae, T., Kagami, H., 2007b. Geologic and metamorphic evolution of the basement complexes in the Kontum Massif, central Vietnam. Gondwana Research 12, 438–453.
Nandakumar, V., Harley, S.L., 2000. A reappraisal of the pressure–temperature path of granulites from the Kerala Khondalite Belt, Southern India. Journal of Geology 108, 687–703.
Nasipuri, P., Bhattacharya, A., Das, S., 2009. Metamorphic reactions in dry and aluminous granulites: a Perple_X *P–T* pseudosection analysis of the influence of effective reaction volume. Contributions to Mineralogy and Petrology 157, 301–311.
Newton, R.C., 1972. An experimental determination of the high-pressure stability limits of magnesian cordierite under wet and dry conditions. Journal of Geology 80, 398–420.
Newton, R.C., 1987. Petrologic aspects of Precambrian granulite facies terrains bearing on their origins. In: Kroner, A. (Ed.), Proterozoic Lithospheric Evolution. American Geophysical Union, Geodynamic Series, Washington DC, vol. 17, pp. 11–26.
Newton, R.C., Charlu, T.V., Kleppa, O.J., 1974. A calorimetric investigation of the stability of anhydrous magnesian cordierite with application to granulite-facies metamorphism. Contributions to Mineralogy and Petrology 44, 295–311.
Nichols, G.T., Berry, R.F., Green, D.H., 1992. Internally consistent gahnitic spinel–cordierite–garnet equilibria in the FMASHZn system: geothermobarometry and applications. Contributions to Mineralogy and Petrology 111, 362–377.
Nishimiya, Y., Tsunogae, T., Santosh, M., 2010. Sapphirine+quartz corona around magnesian (X_{Mg} ~0.58) staurolite from the Palghat–Cauvery Suture Zone, southern India: evidence for high-pressure and ultrahigh-temperature metamorphism within the Gondwana suture. Lithos 114, 490–502.
Nishiyama, T., 1983. Steady diffusion model for olivine–plagioclase corona growth. Geochimica et Cosmochimica Acta 47, 283–294.
Nixon, P.H., Grew, E.S., Condliffe, E., 1984. Kornerupine in a sapphirine spinel granulite from Labwor Hills, Uganda. Mineralogical Magazine 48, 550–552.
O'Brien, P.J., 2008. Challenges in high-pressure granulite metamorphism in the era of pseudosections: reaction textures, compositional zoning and tectonic interpretation with examples from the Bohemian Massif. Journal of Metamorphic Geology 26, 235–251.
O'Hara, M.J., 1977. Thermal history of excavation of Archaean gneisses from the base of the continental crust. Journal of the Geological Society, London 134, 185–200.
O'Hara, M.J., Yarwood, G., Thompson, A.B., Brown, G.C., Watson, J.V., 1978. High pressure-temperature point on an Archaean geotherm, implied magma genesis by crustal anatexis, and consequences for garnet-pyroxene thermometry and barometry [and Discussion]. Philosophical Transactions of the Royal Society of London. Series A, Mathematical and Physical Sciences 288, 441–456.
Oh, C.W., Kusky, T., 2007. The Late Permian to Triassic Hongseong–Odesan Collision Belt in South Korea, and its tectonic correlation with China and Japan. International Geology Review 49, 636–657.
Oliver, R.L., Jones, J.B., 1965. A chlorite–corundum rock from Mount Painter, South Australia. Mineralogical Magazine 35, 140–145.
Ondrejka, M., Uher, P., Putiš, M., Broska, I., Bačík, P., Konečný, P., Schmiedt, I., 2012. Two-stage breakdown of monazite by post-magmatic and metamorphic fluids: an example from the Veporic orthogneiss, Western Carpathians, Slovakia. Lithos 142–143, 245–255.
Orejana, D., Villaseca, C., Armstrong, R.A., Jeffries, T.E., 2011. Geochronology and trace element chemistry of zircon and garnet from granulite xenoliths: constraints on the tectonothermal evolution of the lower crust under central Spain. Lithos 124, 103–116.

Ortega-Gutiérrez, F., Elías-Herrera, M., Gómez-Tuena, A., Mori, L., Reyes-Salas, M., Macías-Romo, C., Solari, L.A., 2012. Petrology of high-grade crustal xenoliths in the Chalcatzingo Miocene subvolcanic field, southern Mexico: buried basement of the Guerrero–Morelos platform and tectonostratigraphic implications. International Geology Review 54, 1597–1634.

Osanai, Y., Hamamoto, T., Maishima, O., Kagami, H., 1998. Sapphirine-bearing granulites and related high-temperature metamorphic rocks from the Higo metamorphic terrane, west-central Kyushu, Japan. Journal of Metamorphic Geology 16, 53–66.

Osanai, Y., Owada, M., Kamei, A., Hamamoto, T., Kagami, H., Toyoshima, T., Nakano, N., Nam, T.N., 2006. The Higo metamorphic complex in Kyushu, Japan as the fragment of Permo-Triassic metamorphic complexes in East Asia. Gondwana Research 9, 152–166.

Osanai, Y., Toyoshima, T., Owada, M., Tsunogae, T., Hokada, T., Crowe, W.A., 1999. Geology of ultrahigh-temperature metamorphic rocks from Tonagh Island in the Napier Complex, east Antarctica. Polar Geoscience 12, 1–28.

Osanai, Y., Toyoshima, T., Owada, M., Tsunogae, T., Hokada, T., Crowe, W.A., Kisachi, I., 2001. Ultrahigh temperature sapphirine–osumilite and sapphirine–quartz granulites from Bunt Island in the Napier Complex, East Antarctica: reconnaissance estimation of the *P–T* evolution. Polar Geoscience 14, 1–24.

Ouzegane, K., Boumaza, S., 1996. An example of ultrahigh-temperature metamorphism: orthopyroxene–sillimanite–garnet, sapphirine–quartz and spinel–quartz parageneses in Al–Mg granulites from In Hihaou, In Ouzzal, Hoggar. Journal of Metamorphic Geology 14, 693–708.

Ouzegane, K., Guiraud, M., Kienast, J.R., 2003a. Prograde and retrograde evolution in high-temperature corundum granulites (FMAS and KFMASH systems) from in Ouzzal Terrane (NW Hoggar, Algeria). Journal of Petrology 44, 517–545.

Ouzegane, K., Kienast, J.-R., Bendaoud, A., Drareni, A., 2003b. A review of Archaean and Paleoproterozoic evolution of the In Ouzzal granulitic terrane (Western Hoggar, Algeria). Journal of African Earth Sciences 37, 207–227.

Page, F.Z., Fu, B., Kita, N.T., Fournelle, J., Spicuzza, M.J., Schulze, D.J., Viljoen, F., Basei, M.A.S., Valley, J.W., 2007. Zircons from kimberlite: new insights from oxygen isotopes, trace elements, and Ti in zircon thermometry. Geochimica et Cosmochimica Acta 71, 3887–3903.

Park, R., 1981. Origin of horizontal structure in Archaean high grade terrains. In: Glover, J.E., Groves, D.I. (Eds.), Archaean Geology: Second International Symposium, Perth, 1980, Geological Society of Australia Special Publication, Perth, vol. 7, pp. 481–490.

Passchier, C., Trouw, R.A.J., 2005. Micro-tectonics, 2nd edition. Springer-Verlag, Berlin Heidelberg, p. 382.

Patiño Douce, A.E., Beard, J.S., 1995. Dehydration-melting of biotite gneiss and quartz amphibolite from 3 to 15 kbar. Journal of Petrology 36, 707–738.

Patiño Douce, A.E., Beard, J.S., 1996. Effect of $P, f(O_2)$ and Mg/Fe ratio on dehydration melting of model metagreywackes. Journal of Petrology 37, 999–1024.

Patiño Douce, A.E., Harris, N., 1998. Experimental constraints on Himalayan anatexis. Journal of Petrology 39, 689–710.

Patiño Douce, A.E., Johnston, A.D., 1991. Phase equilibria and melt productivity in the pelitic system: implications for the origin of peraluminous granitoids and aluminous granulites. Contributions to Mineralogy and Petrology 107, 202–218.

Pattison, D.R.M., Bégin, N.J., 1994. Zoning patterns in orthopyroxene and garnet in granulites: implications for geothermometry. Journal of Metamorphic Geology 12, 387–410.

Pattison, D.R.M., Chacko, T., Farquhar, J., McFarlane, C.R.M., 2003. Temperatures of granulite-facies metamorphism: constraints from experimental phase equilibria and thermobarometry corrected for retrograde exchange. Journal of Petrology 44, 867–900.

Pattison, D.R.M., de Capitani, C., Gaidies, F., 2011. Petrological consequences of variations in metamorphic reaction affinity. Journal of Metamorphic Geology 29, 953–977.

Pattison, D.R.M., Tinkham, D.K., 2009. Interplay between equilibrium and kinetics in prograde metamorphism of pelites: an example from the Nelson aureole, British Columbia. Journal of Metamorphic Geology 27, 249–279.

Peng, P., Guo, J.-H., Zhai, M., Bleeker, W., 2010. Paleoproterozoic gabbronoritic and granitic magmatism in the northern margin of the North China craton: evidence of crust–mantle interaction. Precambrian Research 183, 635–659.

Peterson, J.W., Chacko, T., Kuehner, S.M., 1991. The effects of fluorine on the vapour-absent melting of phlogopite + quartz: implications for deep-crustal processes. American Mineralogist 76, 470–476.

Peterson, J.W., Newton, R.C., 1989. Reversed experiments on biotite–quartz–feldspar melting in the system KMASH: implications for crustal anatexis. Journal of Geology 97, 465–485.

Pilugin, S.M., Fonarev, V.I., Savko, K.A., 2009. Feldspar thermometry of ultrahigh-temperature (≥1000 °C) metapelites from the Voronezh Crystalline Massif (Kursk–Besedino Granulite Block). Doklady Earth Sciences 425, 201–204.

Platt, J.P., England, P.C., 1993. Convective removal of lithosphere beneath mountain belts: thermal and mechanical consequences. American Journal of Science 293, 307–336.

Platt, J.P., Soto, J.-I., Whitehouse, M.J., Hurford, A.J., Kelley, S.P., 1998. Thermal evolution, rate of exhumation, and tectonic significance of metamorphic rocks from the floor of the Alboran extensional basin, western Mediterranean. Tectonics 17, 671–689.

Podlesskii, K.K., 2010. Stability of sapphirine-bearing mineral assemblages in the system FeO–MgO–Al_2O_3–SiO_2 and metamorphic *P–T* parameters of aluminous granulites. Petrology 18, 350–368.

Podlesskii, K.K., Aranovich, L.Y., Gerya, T.V., Kosyakova, N.A., 2008. Sapphirine-bearing assemblages in the system MgO–Al_2O_3–SiO_2: a continuing ambiguity. European Journal of Mineralogy 20, 721–734.

Powell, R., 1983. Processes in granulite facies metamorphism. In: Atherton, M.P., Gribble, C.D. (Eds.), Migmatites. Melting and Metamorphism. Shiva, London, pp. 127–139.

Powell, R., Downes, J., 1990. Garnet porphyroblast-bearing leucosomes in metapelites: mechanisms, phase diagrams and an example from Broken Hill. In: Ashworth, J.R., Brown, M. (Eds.), High-temperature Metamorphism and Crustal Anatexis, The Mineralogical Society Series, vol. 2. Mineralogical Society of Great Britain, Unwin Hyman, London, pp. 105–123.

Powell, R., Guiraud, M., White, R.W., 2005. Truth and beauty in metamorphic mineral equilibria: conjugate variables and phase diagrams. Canadian Mineralogist 43, 21–33.

Powell, R., Holland, T., 1990. Calculated mineral equilibria in the pelite system, KFMASH (K_2O–FeO–MgO–Al_2O_3–SiO_2–H_2O. American Mineralogist 75, 367–380.

Powell, R., Holland, T.J.B., 1988. An internally consistent dataset with uncertainties and correlations: 3. Applications to geobarometry, worked examples and a computer program. Journal of Metamorphic Geology 6, 173–204.

Powell, R., Holland, T.J.B., Worley, B., 1998. Calculating phase diagrams involving solid solutions via non-linear equations, with examples using THERMOCALC. Journal of Metamorphic Geology 16, 577–588.

Powell, R., Sandiford, M.J., 1988. Sapphirine and spinel phase relationships in the system FeO–MgO–Al_2O_3–TiO_2–O_2 in the presence of quartz and hypersthene. Contributions to Mineralogy and Petrology 98, 64–71.

Powell, R., White, R.W., Green, E.C.R., Holland, T.J.B., Diener, J.F.A., 2014. On parameterising thermodynamic descriptions of minerals for petrological calculations. Journal of Metamorphic Geology 32, 245–260.

Pownall, J.M., Hall, R., Armstrong, R.A., Forster, M.A., 2014. Earth's youngest-known ultrahigh-temperature granulites discovered on Seram, eastern Indonesia. Geology 42, 279–282.

Prakash, D., Arima, M., Mohan, A., 2007. Ultrahigh-temperature mafic granulites from Panrimalai, south India: constraints from phase equilibria and thermobarometry. Journal of Asian Earth Sciences 29, 41–61.

Prakash, D., Chandra Singh, P., Hokada, T., 2013. A new occurrence of sapphirine–spinel–corundum-bearing granulite from NE of Jagtiyal, Eastern Dharwar Craton, Andra Pradesh. Journal of the Geological Society of India 82, 5–8.

Prakash, D., Sharma, I.N., 2008. Reaction textures and metamorphic evolution of quartz-free granulites from Namlekonda (Karimnagar), Andhra Pradesh, Southern India. International Geology Review 50, 1008–1021.

Racek, M., Štípská, P., Powell, R., 2008. Garnet–clinopyroxene intermediate granulites in the St. Leonhard massif of the Bohemian Massif: ultrahigh-temperature metamorphism at high pressure or not? Journal of Metamorphic Geology 26, 253–271.

Raith, M., Karmakar, S., Brown, M., 1997. Ultra-high-temperature metamorphism and multistage decompressional evolution of sapphirine granulites from the Palni Hill Ranges, southern India. Journal of Metamorphic Geology 15, 379–399.

Raith, M.M., Rakotondrazafy, R., Sengupta, P., 2008. Petrology of corundum–spinel–sapphirine–anorthite rocks (sakenites) from the type locality in southern Madagascar. Journal of Metamorphic Geology 26, 647–667.

Rajesh, H.M., Santosh, M., Wan, Y., Liu, D., Liu, S.J., Belyanin, G.A., 2014. Ultrahigh temperature granulites and magnesian charnockites: evidence for Neoarchean accretion alon ghr northern margin of the Kaapvaal Craton. Precambrian Research 246, 150–159.

Rakotonandrasana, N.O.T., Arima, M., Miyawaki, R., Rambeloson, R.A., 2010. Widespread occurrences of Högbomite-2N2S in UHT metapelites from the Betroka Belt, southern Madagascar: implications on melt or fluid activity during regional metamorphism. Journal of Petrology 51, 869–895.

Rapp, R.P., Ryerson, F.J., Miller, C.F., 1987. Experimental evidence bearing on the stability of monazite during crustal anatexis. Geophysical Research Letters 14, 307–310.

Rapp, R.P., Watson, E.B., 1986. Monazite solubility and dissolution kinetics: implications for the thorium and light rare-earth chemistry of felsic magmas. Contributions to Mineralogy and Petrology 94, 304–316.

Redler, C., Johnson, T.E., White, R.W., Kunz, B.E., 2012. Phase equilibrium constraints on a deep crustal metamorphic field gradient: metapelitic rocks from the Ivrea Zone (NW Italy). Journal of Metamorphic Geology 30, 235–254.

Reinhardt, J., 1987. Cordierite–anthophyllite rocks from north-west Queensland, Australia: metamorphosed magnesian pelites. Journal of Metamorphic Geology 5, 451–472.

Reno, B.L., Piccoli, P.M., Brown, M., Trouw, R.A.J., 2012. *In situ* monazite (U–Th)–Pb ages from the Southern Brasília Belt, Brazil: constraints on the high-temperature retrograde evolution of HP granulites. Journal of Metamorphic Geology 30, 81–112.

Reverdatto, V.V., 2010. Local mineral equilibrium in metamorphism: development of D. Korzhinskii's ideas (on 110th anniversary of D.S. Korzhinskii). Russian Geology and Geophysics 51, 259–265.

Rickers, K., Raith, M., Dasgupta, S., 2001. Multistage reaction textures in xenolithic high-MgAl granulites at Anakapalle, Eastern Ghats Belt, India: examples of

contact polymetamorphism and infiltration-driven metasomatism. Journal of Metamorphic Geology 19, 561–580.
Roberts, M.P., Finger, F., 1997. Do U–Pb zircon ages from granulites reflect peak metamorphic conditions? Geology 25, 319–322.
Rosenberg, C.L., Handy, M.R., 2005. Experimental deformation of partially melted granite revisited: implications for the continental crust. Journal of Metamorphic Geology 23, 19–28.
Rötzler, J., Hagen, B., Hoernes, S., 2008. Geothermometry of the ultrahigh-temperature Saxon granulites revisited. Part I: new evidence from key mineral assemblages and reaction textures. European Journal of Mineralogy 20, 1097–1115.
Rötzler, J., Romer, R.L., 2001. *P–T–t* evolution of ultrahigh-temperature granulites from the Saxon Granulite Massif, Germany. Part I: petrology. Journal of Petrology 42, 1995–2013.
Rubatto, D., 2002. Zircon trace element geochemistry: partitioning with garnet and the link between U–Pb ages and metamorphism. Chemical Geology 184, 123–138.
Rubatto, D., Chakraborty, S., Dasgupta, S., 2013. Timescales of crustal melting in the Higher Himalayan Crystallines (Sikkim, Eastern Himalaya) inferred from trace element-constrained monazite and zircon chronology. Contributions to Mineralogy and Petrology 165, 349–372.
Rubie, D.C., 1998. Disequilibrium during metamorphism: the role of nucleation kinetics. In: Treloar, P.J., O'Brien, P.J. (Eds.), What drives Metamorphism and Metamorphic Reactions?, Geological Society, London, Special Publication, vol. 138, pp. 199–214.
Săbău, G., Alberico, A., Negulescu, E., 2002. Peraluminous sapphirine in retrogressed kyanite-bearing eclogites from the south Carpathians: status and implications. International Geology Review 44, 859–876.
Sack, R.O., Ghiorso, M.S., 1989. Importance of considerations of mixing properties in establishing an internally consistent thermodynamic database: thermochemistry of minerals in the system Mg_2SiO_4–Fe_2SiO_4–SiO_2. Contributions to Mineralogy and Petrology 102, 41–68.
Sajeev, K., Osanai, Y., 2004. Ultrahigh-temperature metamorphism (1150 °C, 12 kbar) and multistage evolution of Mg-, Al-rich granulites from the central Highland Complex, Sri Lanka. Journal of Petrology 45, 1821–1844.
Sajeev, K., Osanai, Y., Connolly, J.A.D., Suzuki, S., Ishioka, J., Kagami, H., Rino, S., 2007. Extreme crustal metamorphism during a Neoproterozoic event in Sri Lanka: a study of dry mafic granulites. The Journal of Geology 115, 563–582.
Sajeev, K., Osanai, Y., Kon, Y., Itaya, T., 2009. Stability of pargasite during ultrahigh-temperature metamorphism: a consequence of titanium and REE partitioning? American Mineralogist 94, 535–545.
Sajeev, K., Osanai, Y., Santosh, M., 2001. Ultrahigh-temperature stability of sapphirine and kornerupine in Ganguvarpatti granulite, Madurai Block, southern India. Gondwana Research 4, 762–766.
Sajeev, K., Osanai, Y., Santosh, M., 2004. Ultrahigh-temperature metamorphism followed by two-stage decompression of garnet–orthopyroxene–sillimanite granulites from Ganguvarpatti, Madurai block, southern India. Contributions to Mineralogy and Petrology 148, 29–46.
Sajeev, K., Osanai, Y., Suzuki, S., Kagami, H., 2003. Geochronological evidence for multistage-metamorphic events in ultrahigh-temperature granulites from central Highland Complex, Sri Lanka. Polar Geoscience 16, 137–148.
Sajeev, K., Williams, I.S., Osanai, Y., 2010. Sensitive high-resolution ion microprobe U–Pb dating of prograde and retrograde ultrahigh-temperature metamorphism as exemplified by Sri Lankan granulites. Geology 38, 971–974.
Sandiford, M., 1985a. The metamorphic evolution of granulites at Fyfe Hills; Implications for Archean crustal thickness in Enderby Land, Antarctica. Journal of Metamorphic Geology 3, 155–178.
Sandiford, M., 1985b. The origin of retrograde shear zones in the Napier Complex: implications for the tectonic evolution of Enderby Land, Antarctica. Journal of Structural Geology 7, 477–488.
Sandiford, M., 1989. Horizontal structures in granulite terrains: a record of mountain building or mountain collapse? Geology 17, 449–452.
Sandiford, M., 2010. Why are the continents just so...? Journal of Metamorphic Geology 28, 569–577.
Sandiford, M., Hand, M., 1998a. Australian Proterozoic high-temperature metamorphism in the conductive limit. In: Treloar, P., O'Brien, P. (Eds.), What Controls Metamorphism?, Geological Society, London, Special Publication, vol. 138, pp. 103–114.
Sandiford, M., Hand, M., 1998b. Controls on the locus of intraplate deformation in central Australia. Earth and Planetary Science Letters 162, 97–110.
Sandiford, M., Hand, M., McLaren, S., 2001. Tectonic feedback, intraplate orogeny and the geochemical structure of the crust; a central Australian perspective. In: Miller, J.A., Holdsworth, R.E., Buick, I.S., Hand, M. (Eds.), Continental Reactivation and Reworking, Geological Society, London, Special Publication, vol. 184, pp. 195–218.
Sandiford, M., McLaren, S., 2002. Tectonic feedback and the ordering of heat producing elements within the continental lithosphere. Earth and Planetary Science Letters 204, 133–150.
Sandiford, M., McLaren, S., Neumann, N., 2002. Long-term thermal consequences of the redistribution of heat-producing elements associated with large-scale granitic complexes. Journal of Metamorphic Geology 20, 87–98.
Sandiford, M., Neale, F., Powell, R., 1987. Metamorphic evolution of aluminous granulites from Labwor Hills, Uganda. Contributions to Mineralogy and Petrology 95, 217–225.
Sandiford, M., Powell, R., 1986a. Deep crustal metamorphism during continental extension: modern and ancient examples. Earth and Planetary Science Letters 79, 151–158.
Sandiford, M., Powell, R., 1986b. Pyroxene exsolution in granulites from Fyfe Hills, Enderby Land, Antarctica: evidence for 1000 °C metamorphic temperatures in Archean continental crust. American Mineralogist 71, 946–954.
Sandiford, M., Powell, R., 1991. Some Remarks on high-temperature—low-pressure metamorphism in convergent orogens. Journal of Metamorphic Geology 9, 333–340.
Sandiford, M., Wilson, C.J.L., 1984. The structural evolution of the Fyfe Hills–Khmara Bay Region, Enderby Land, East Antarctica. Australian Journal of Earth Sciences 31, 403–426.
Sandiford, M., Wilson, C.J.L., 1986. The origin of Archean gneisses in the Fyfe Hills region, Enderby Land - field occurrence, petrography and geochemistry. Precambrian Research 31, 37–68.
Santosh, M., Kusky, T., 2010. Origin of paired high pressure–ultrahigh-temperature orogens: a ridge subduction and slab window model. Terra Nova 22, 35–42.
Santosh, M., Kusky, T., Wang, L., 2011. Supercontinent cycles, extreme metamorphic processes, and changing fluid regimes. International Geology Review 53, 1403–1423.
Santosh, M., Liu, D.Y., Shi, Y.R., Liu, S.J., 2013. Paleoproterozoic accretionary orogenesis in the North China Craton: a SHRIMP zircon study. Precambrian Research 227, 29–54.
Santosh, M., Liu, S.J., Tsunogae, T., Li, J.H., 2012. Paleoproterozoic ultrahigh-temperature granulites in the North China Craton: implications for tectonic models on extreme crustal metamorphism. Precambrian Research 222-223, 77–106.
Santosh, M., Maruyama, S., Sato, K., 2009a. Anatomy of a Cambrian suture in Gondwana: Pacific-type orogeny in southern India? Gondwana Research 16, 321–341.
Santosh, M., Omori, S., 2008. CO_2 windows from mantle to atmosphere: models on ultrahigh-temperature metamorphism and speculations on the link with melting of snowball Earth. Gondwana Research 14, 82–96.
Santosh, M., Sajeev, K., 2006. Anticlockwise evolution of ultrahigh-temperature granulites within continental collision zone in southern India. Lithos 92, 447–464.
Santosh, M., Sajeev, K., Li, J.H., 2006. Extreme crustal metamorphism during Colombia supercontinent assembly: evidence from North China Craton. Gondwana Research 10, 256–266.
Santosh, M., Sajeev, K., Li, J.H., Liu, S.J., Itaya, T., 2009b. Counterclockwise exhumation of a hot orogen: the Paleoproterozoic ultrahigh-temperature granulites in the North China Craton. Lithos 110, 140–152.
Santosh, M., Tsunogae, T., Li, J.H., Liu, S.J., 2007a. Discovery of sapphirine-bearing Mg–Al granulites in the North China Craton: implications for Palaeoproterozoic ultrahigh temperature metamorphism. Gondwana Research 11, 263–285.
Santosh, M., Tsunogae, T., Ohyama, H., Sato, K., Li, J.H., Liu, S.J., 2008. Carbonic metamorphism at ultrahigh-temperatures: evidence from North China Craton. Earth and Planetary Science Letters 266, 149–165.
Santosh, M., Tsunogae, T., Tsutsumi, Y., Iwamura, M., 2009c. Microstructurally controlled monazite chronology of ultrahigh-temperature granulites from southern India: implications for the timing of Gondwana assembly. Island Arc 18, 248–265.
Santosh, M., Wan, Y., Liu, D., Chunyan, D., Li, J.H., 2009d. Anatomy of zircons from an ultrahot Orogen: the amalgamation of North China Craton within the supercontinent Columbia. Journal of Geology 117, 429–443.
Santosh, M., Wilde, S.A., Li, J.H., 2007b. Timing of Paleoproterozoic ultrahigh-temperature metamorphism in the North China Craton: evidence from SHRIMP U–Pb zircon geochronology. Precambrian Research 159, 178–196.
Sarbajna, C., Bose, S., Rajagopalan, V., Das, K., Som, A., Paul, A.K., Shivkumar, K., Umamaheswar, K., Chaki, A., 2013. U–Cr-rich high Mg–Al granulites from Karimnagar Granulite Belt, India: implications for Neoarchean–Paleoproterozoic events in southern India. Mineralogy and Petrology 107, 553–571.
Sarkar, S., Dasgupta, S., Fukuoka, M., 2003a. Petrological evolution of a suite of spinel granulites from Vizianagram, Eastern Ghats Belt, India, and genesis of sapphirine-bearing assemblages. Journal of Metamorphic Geology 21, 899–913.
Sarkar, S., Santosh, M., Dasgupta, S., Fukuoka, M., 2003b. Very high density CO_2 associated with ultrahigh-temperature metamorphism in the Eastern Ghats granulite belt, India. Geology 31, 51–54.
Sarkar, T., Schenk, V., 2014. Two-stage granulite formation in a Proterozoic magmatic arc (Ongole domain of the Eastern Ghats Belt, India): Part 1. Petrology and pressureetemperature evolution. Precambrian Research 255, 485–509.
Sarkar, T., Schenk, V., Appel, P., Berndt, J., Sengupta, P., 2014. Two-stage granulite formation in a Proterozoic magmatic arc (Ongole domain of the Eastern Ghats Belt, India): Part 2. LAeICPeMS zircon dating and texturally controlled in-situ monazite dating. Precambrian Reseach 255, 467–484.
Sato, K., Santosh, M., 2007. Titanium in quartz as a record of ultrahigh-temperature metamorphism: the granulites of Karur, southern India. Mineralogical Magazine 71, 143–154.
Sato, K., Santosh, M., Tsunogae, T., 2009. A petrologic and laser Raman spectroscopic study of sapphirine–spinel–quartz–Mg-staurolite inclusions in garnet from Kumiloothu, southern India: implications for extreme metamorphism in a collisional orogen. Journal of Geodynamics 47, 107–118.

Sawyer, E.W., 1994. Melt segregation in the continental crust. Geology 22, 1019–1022.
Sawyer, E.W., 1999. Criteria for the recognition of partial melting. Physics and Chemistry of the Earth, Part A 24, 269–279.
Sawyer, E.W., 2001. Melt segregation in the continental crust: distribution and movement of melt in anatectic rocks. Journal of Metamorphic Geology 19, 291–309.
Sawyer, E.W., 2014. The inception and growth of leucosomes: microstructure at the start of melt segregation in migmatites. Journal of Metamorphic Geology 32, 695–712.
Sawyer, E.W., Cesare, B., Brown, M., 2011. When the continental crust melts. Elements 7, 229–234.
Schafer, H.N.S., 1966. The determination of iron(II) oxide in silicate and refractory materials. The Analyst 91, 755–762.
Schärer, U., 1984. The effect of initial ^{230}Th disequilibrium on young U–Pb ages: the Makalu case, Himalaya. Earth and Planetary Science Letters 67, 191–204.
Scherer, E.E., Cameron, K.L., Blichert-Toft, J., 2000. Lu–Hf garnet geochronology; closure temperature relative to the Sm–Nd system and the effects of trace mineral inclusions. Geochimica et Cosmochimica Acta 64, 3413–3432.
Schmitz, M.D., Bowring, S.A., 2003. Ultrahigh-temperature metamorphism in the lower crust during Neoarchean Ventersdorp rifting and magmatism, Kaapvaal Craton, southern Africa. Geological Society of America Bulletin 115, 533–548.
Schmitz, S., Möller, A., Wilke, M., Malzer, W., Kanngiesser, B., Bousquet, R., Berger, A., Scheffer, S., 2009. Chemical U–Th–Pb dating of monazite by 3D-Micro X-ray fluorescence analysis with synchrotron radiation. European Journal of Mineralogy 21, 927–945.
Schreyer, W., Abraham, K., 1976. Natural boron-free kornerupine and its breakdown products in a sapphirine rock of the Limpopo Belt, southern Africa. Contributions to Mineralogy and Petrology 54, 109–126.
Schreyer, W., Seifert, F., 1969a. Compatibility relations of the aluminium silicates in the systems MgO–Al_2O_3–SiO_2–H_2O and K_2O–MgO–Al_2O_3–SiO_2–H_2O at high pressures. American Journal of Science 267, 371–388.
Schreyer, W., Seifert, F., 1969b. High-pressure phases in the system MgO–Al_2O_3–SiO_2–H_2O. American Journal of Science 267A, 407–443.
Schulters, J.C., Bohlen, S.R., 1989. The stability of hercynite and hercynite–gahnite spinels in corundum- or quartz-bearing assemblages. Journal of Petrology 30, 1017–1031.
Schumacher, J.C., Robinson, P., 1987. Mineral chemistry and metasomatic growth of aluminous enclaves in gedrite–cordierite-gneiss from southwestern New Hampshire, USA. Journal of Petrology 28, 1033–1073.
Seifert, F., 1974. Stability of sapphirine: a study of the aluminous part of the system MgO–Al_2O_3–SiO_2–H_2O. Journal of Geology 82, 173–204.
Sengupta, P., Dasgupta, S., Bhattacharya, P.K., Fukuoka, M., Chakraborti, S., Bhowmick, S., 1990. Petro-tectonic imprints in the sapphirine granulites from Anantagiri, Eastern Ghats mobile belt, India. Journal of Petrology 31, 971–996.
Sengupta, P., Karmakar, S., Dasgupta, S., Fukuoka, M., 1991. Petrology of spinel granulites from Araku, Eastern Ghats, India, and a petrogenetic grid for sapphirine-free rocks in the system FMAS. Journal of Metamorphic Geology 9, 451–459.
Sengupta, P., Sen, J., Dasgupta, S., Raith, M., Bhui, U.K., Ehl, J., 1999. Ultra-high temperature metamorphism of metapelitic granulites from Kondapalle, Eastern Ghats Belt: implications for the Indo-Antarctic correlation. Journal of Petrology 40, 1065–1087.
Seydoux-Guillaume, A.-M., Montel, J.-M., Bingen, B., Bosse, V., de Parseval, P., Paquette, J.-L., Janots, E., Wirth, R., 2012. Low-temperature alteration of monazite: fluid mediated coupled dissolution–precipitation, irradiation damage, and disturbance of the U–Pb and Th–Pb chronometers. Chemical Geology 330–331, 140–158.
Seydoux-Guillaume, A.-M., Paquette, J.-L., Wiedenbeck, M., Montel, J.-M., Heinrich, W., 2002. Experimental resetting of the U–Th–Pb systems in monazite. Chemical Geology 191, 165–181.
Sharma, I.N., Prakash, D., 2008. A new occurrence of sapphirine-bearing granulite from Podur, Andhra Pradesh, India. Mineralogy and Petrology 92, 415–425.
Shaw, R.K., Arima, M., 1998. A corundum–quartz assemblage from the Eastern Ghats Granulite Belt, India: evidence for high *P–T* metamorphism? Journal of Metamorphic Geology 16, 189–196.
Shazia, J.R., Santosh, M., Sajeev, K., 2012. Peraluminous sapphirine–cordierite pods in Mg-rich orthopyroxene granulite from southern India: implications for lower crustal processes. Journal of Asian Earth Sciences 58, 88–97.
Sheraton, J.W., 1980. Geochemistry of Precambrian metapelites from east Antarctica: secular and metamorphic variations. BMR Journal of Australian Geology & Geophysics 5, 279–288.
Sheraton, J.W., England, R.N., Ellis, D.J., 1982. Metasomatic zoning in sapphirine-bearing granulites from Antarctica. BMR Journal of Australian Geology & Geophysics 7, 269–273.
Sheraton, J.W., Offe, L.A., Tingey, R.J., Ellis, D.J., 1980. Enderby Land, Antarctica—an unusual Precambrian high-grade metamorphic terrain. Geological Society of Australia Journal 27, 1–18.
Sheraton, J.W., Tingey, R.J., Black, L.P., Offe, L.A., Ellis, D.J., 1987. Geology of an unusual Precambrian high-grade metamorphic terrane—Enderby Land and western Kemp Land, Antarctica. Bureau of Mineral Resources (BMR) Bulletin, Canberra 55.
Shimizu, H., Tsunogae, T., Santosh, M., 2009. Spinel + quartz assemblage in granulites from the Achankovil Shear Zone, southern India: implications for ultrahigh-temperature metamorphism. Journal of Asian Earth Sciences 36, 209–222.
Shimizu, H., Tsunogae, T., Santosh, M., 2013. Petrology and phase equilibrium modeling of sapphirine + quartz assemblage from the Napier Complex, East Antarctica: diagnostic evidence for Neoarchean ultrahigh-temperature metamorphism. Geoscience Frontiers 4, 655–666.
Sighinolfi, G.P., Gorgoni, C., 1978. Chemical evolution of high-grade metamorphic rocks — anatexis and remotion of material from granulite terrains. Chemical Geology 22, 157–176.
Simpson, G.D.H., Thompson, A.B., Connolly, J.A.D., 2000. Phase relations, singularities and thermobarometry of metamorphic assemblages containing phengite, chlorite, biotite, K-feldspar, quartz and H_2O. Contributions to Mineralogy and Petrology 139, 555–569.
Sindern, S., Gerdes, A., Ronkin, Y.L., Dziggel, A., Hetzel, R., Schulte, B.A., 2012. Monazite stability, composition and geochronology as tracers of Paleoproterozoic events at the eastern margin of the East European Craton (Taratash complex, Middle Urals). Lithos 132–133, 82–97.
Sizova, E., Gerya, T., Brown, M., 2014. Contrasting styles of Phanerozoic and Precambrian continental collision. Gondwana Research 25, 522–545.
Sizova, E., Gerya, T., Brown, M., Perchuk, L.L., 2010. Subduction styles in the Precambrian: insight from numerical experiments. Lithos 116, 209–229.
Skrzypek, E., Štípská, P., Cocherie, A., 2012. The origin of zircon and the significance of U–Pb ages in high-grade metamorphic rocks: a case study from the Variscan orogenic root (Vosges Mountains, NE France). Contributions to Mineralogy and Petrology 164, 935–957.
Smit, M.A., Scherer, E.E., Mezger, K., 2013. Lu–Hf and Sm–Nd garnet geochronology: chronometric closure and implications for dating petrological processes. Earth and Planetary Science Letters 381, 222–233.
Smithies, R.H., Howard, H.M., Evins, P.M., Kirkland, C.L., Kelsey, D.E., Hand, M., Wingate, M.T.D., Collins, A.S., Belousova, E., 2011. High-temperature granite magmatism, crust—mantle interaction and the Mesoproterozoic intracontinental evolution of the Musgrave Province, central Australia. Journal of Petrology 52, 931–958.
Solar, G.S., Brown, M., 2001. Petrogenesis of migmatites in Maine, USA: possible source of peraluminous leucogranite in plutons? Journal of Petrology 42, 789–823.
Sonder, L.J., England, P.C., Wernicke, B.P., Christiansen, R.L., 1987. A physical model for Cenozoic extension of western North America. In: Coward, M.P., Dewey, J.F., Hancock, P.L. (Eds.), Continental Extensional Tectonics, Geological Society, London, Special Publication, vol. 28, pp. 187–201.
Spear, F.S., 1988a. The Gibbs method and Duhem's theorem: the quantitative relationships among *P, T*, chemical potential, phase composition and reaction progress in igneous and metamorphic systems. Contributions to Mineralogy and Petrology 99, 249–256.
Spear, F.S., 1988b. Thermodynamic projection and extrapolation of high-variance mineral assemblages. Contributions to Mineralogy and Petrology 98, 346–351.
Spear, F.S., 1991. On the interpretation of peak metamorphic temperatures in light of garnet diffusion during cooling. Journal of Metamorphic Geology 9, 379–388.
Spear, F.S., 1993. Metamorphic Phase Equilibria and Pressure–temperature–time Paths. Monograph, Mineralogical Society of America, Washington, D.C., p. 799
Spear, F.S., 2010. Monazite–allanite phase relations in metapelites. Chemical Geology 279, 55–62.
Spear, F.S., Cheney, J.T., 1989. A petrogenetic grid for pelitic schists in the system SiO_2–Al_2O_3–FeO–MgO–K_2O–H_2O. Contributions to Mineralogy and Petrology 101, 149–164.
Spear, F.S., Kohn, M.J., Cheney, J.T., 1999. *P–T* paths from anatectic pelites. Contributions to Mineralogy and Petrology 134, 17–32.
Spear, F.S., Kohn, M.J., Florence, F., Menard, T., 1990. A model for garnet and plagioclase growth in pelitic schists: implications for thermobarometry and *P–T* path determinations. Journal of Metamorphic Geology 8, 683–696.
Spear, F.S., Markussen, J.C., 1997. Mineral zoning, *P–T–X–M* phase relations, and metamorphic evolution of some Adirondack granulites, New York. Journal of Petrology 38, 757–783.
Spear, F.S., Menard, T., 1989. Program GIBBS: a generalized Gibbs method algorithm. American Mineralogist 74, 942–943.
Spear, F.S., Peacock, S.M., Kohn, M.J., Florence, F.P., Menard, T., 1991. Computer programs for petrological *P–T–t* path calculations. American Mineralogist 76, 2009–2012.
Spear, F.S., Pyle, J.M., 2010. Theoretical modeling of monazite growth in a low-Ca metapelite. Chemical Geology 273, 111–119.
Spear, F.S., Selverstone, J., 1983. Quantitative *P–T* paths from zoned minerals: theory and tectonic applications. Contributions to Mineralogy and Petrology 83, 348–357.
Sriramguru, K., Janardhan, A.S., Basava, S., 2002. Prismatine and sapphirine bearing assemblages from Rajapalaiyam area, Tamil Nadu: origin and metamorphic history. Journal of the Geological Society of India 59, 103–110.
Steffen, G., Seifert, F., Amthauer, G., 1984. Ferric iron in sapphirine: a Mössbauer spectroscopic study. American Mineralogist 69, 339–348.
Stepanov, A.S., Hermann, J., Rubatto, D., Rapp, R.P., 2012. Experimental study of monazite/melt partitioning with implications for the REE, Th and U geochemistry of crustal rocks. Chemical Geology 300-301, 200–220.
Stevens, G., Clemens, J.D., 1993. Fluid-absent melting and the roles of fluids in the lithosphere: a slanted summary. Chemical Geology 108, 1–17.
Stevens, G., Clemens, J.D., Droop, G.T.R., 1997. Melt production during granulite-facies anatexis: experimental data from 'primitive' metasedimentary protoliths. Contributions to Mineralogy and Petrology 128, 352–370.

Štípská, P., Powell, R., 2005. Does ternary feldspar constrain the metamorphic conditions of high-grade meta-igneous rocks? Evidence from orthopyroxene granulites, Bohemian Massif. Journal of Metamorphic Geology 23, 627–647.
Štípská, P., Powell, R., White, R.W., Baldwin, J.A., 2010. Using calculated chemical potential relationships to account for coronas around kyanite: an example from the Bohemian Massif. Journal of Metamorphic Geology 28, 97–116.
Stixrude, L., Lithgow-Bertelloni, C., 2005. Thermodynamics of mantle minerals — I. Physical properties. Geophysical Journal International 162, 610–632.
Stoddard, E.F., 1979. Zinc-rich hercynite in high-grade metamorphic rocks: a product of the dehydration of staurolite. American Mineralogist 64, 736–741.
Storm, L.C., Spear, F.S., 2005. Pressure, temperature and cooling rates of granulite facies migmatitic pelites from the southern Adirondack Highlands, New York. Journal of Metamorphic Geology 23, 107–130.
Stüwe, K., 1995. Thermal buffering effects at the solidus. Implications for the equilibration of partially melted metamorphic rocks. Tectonophysics 248, 39–51.
Stüwe, K., 1997. Effective bulk composition changes due to cooling: a model predicting complexities in retrograde reaction textures. Contributions to Mineralogy and Petrology 129, 43–52.
Stüwe, K., 1998. Heat sources of Cretaceous metamorphism in the Eastern Alps – a discussion. Tectonophysics 287, 251–269.
Stüwe, K., 2007. Geodynamics of the Lithosphere: Quantitative Description of Geological Problems, 2nd edition. Springer-Verlag, Berlin, Heidelberg, Dordrecht, p. 493.
Stüwe, K., Powell, R., 1995. *PT* paths from modal proportions: application to the Koralm Complex, Eastern Alps. Contributions to Mineralogy and Petrology 119, 83–93.
Stüwe, K., Sandiford, M., 1995. A description of metamorphic *P–T–t* paths with implications for low-*P* high-*T* metamorphism. Physics of the Earth and Planetary Interiors 88, 211–221.
Suzuki, S., Arima, M., Williams, I.S., Shiraishi, K., Kagami, H., 2006. Thermal history of UHT metamorphism in the Napier Complex, East Antarctica: insights from zircon, monazite, and garnet ages. Journal of Geology 114, 65–84.
Tadokoro, H., Tsunogae, T., Santosh, M., Yoshimura, Y., 2007. First report of the spinel + quartz assemblage from Kodaikanal in the Madurai Block, Southern India: implications for ultrahigh-temperature metamorphism. International Geology Review 49, 1050–1068.
Tailby, N.D., Walker, A.M., Berry, A.J., Hermann, J., Evans, K.A., Mavrogenes, J.A., O'Neill, H.S., Rodina, I.S., Soldatov, A.V., Rubatto, D., Sutton, S.R., 2011. Ti site occupancy in zircon. Geochimica et Cosmochimica Acta 75, 905–921.
Tajčmanová, L., Abart, R., Neusser, G., Rhede, D., 2011. Growth of plagioclase rims around metastable kyanite during decompression of high-pressure felsic granulites (Bohemian Massif). Journal of Metamorphic Geology 29, 1003–1018.
Tajčmanová, L., Konopásek, J., Connolly, J.A.D., 2007. Diffusion-controlled development of silica-undersaturated domains in felsic granulites of the Bohemian Massif (Variscan belt of Central Europe). Contributions to Mineralogy and Petrology 153, 237–250.
Tajčmanová, L., Konopásek, J., Košler, J., 2009. Distribution of zinc and its role in the stabilization of spinel in high-grade felsic rocks of the Moldanubian domain (Bohemian Massif). European Journal of Mineralogy 21, 407–418.
Tajčmanová, L., Konopásek, J., Schulmann, K., 2006. Thermal evolution of the orogenic lower crust during exhumation within a thickened Moldanubian root of the Variscan belt of Central Europe. Journal of Metamorphic Geology 24, 119–134.
Tajčmanová, L., Podladchikov, Y., Powell, R., Moulas, E., Vrijmoed, J.C., Connolly, J.A.D., 2014. Grain-scale pressure variations and chemical equilibrium in high-grade metamorphic rocks. Journal of Metamorphic Geology 32, 195–207.
Tareen, J.A.K., Ganesha, A.V., 2001. Ultra high temperature (UHT) metamorphism of Mg–Al-rich pelitic rocks: an experimental study of the system K_2O–MgO–Al_2O_3–SiO_2–H_2O with the bulk composition 2Phl+6Sil+9Qtz. Journal of the Geological Society of India 58, 399–409.
Tareen, J.A.K., Prasad, A.V.K., Basavalingu, B., Ganesha, A.V., 1998. Stability of F–Ti-phlogopite in the system phlogopite–sillimanite–quartz: an experimental study of dehydration melting in H_2O-saturated and undersaturated conditions. Mineralogical Magazine 62, 373–380.
Tarney, J., Windley, B.F., 1977. Chemistry, thermal gradients and evolution of the lower continental crust. Journal of the Geological Society, London 134, 153–172.
Tateishi, K., Tsunogae, T., Santosh, M., Janardhan, A.S., 2004. First report of sapphirine plus quartz assemblage from southern India: implications for ultrahigh-temperature metamorphism. Gondwana Research 7, 899–912.
Taylor-Jones, K., Powell, R., 2010. The stability of sapphirine + quartz: calculated phase equilibria in FeO–MgO–Al_2O_3–SiO_2–TiO_2–O. Journal of Metamorphic Geology 28, 615–633.
Taylor-Jones, K., Powell, R., 2015. Interpreting zirconium-in-rutile thermometric results. Journal of Metamorphic Geology 33, 115–122.
Teufel, S., Heinrich, W., 1997. Partial resetting of the U–Pb isotope system in monazite through hydrothermal experiments: an SEM and U–Pb isotope study. Chemical Geology 137, 273–281.
Thomas, J.B., Watson, E.B., Spear, F.S., Shemella, P.T., Nayak, S.K., Lanzirotti, A., 2010. TitaniQ under pressure: the effect of pressure and temperature on the solubility of Ti in quartz. Contributions to Mineralogy and Petrology 160, 743–759.
Thomas, R., Davidson, P., 2012. Water in granite and pegmatite-forming melts. Ore Geology Reviews 46, 32–46.
Thompson, A.B., 1982. Dehydration melting of pelitic rocks and the generation of H_2O-undersaturated granitic liquids. American Journal of Science 282, 1567–1595.
Thompson, A.B., Connolly, J.A.D., 1995. Melting of the continental crust: some thermal and petrological constraints on anatexis in continental collision zones and other tectonic settings. Journal of Geophysical Research 100 (B8), 15565–15579.
Thompson, P.H., 1989. Moderate overthickening of thinned sialic crust and the origin of granitic magmatism and regional metamorphism in low-*P*–high-*T* terranes. Geology 17, 520–523.
Tilley, C.E., 1935. Metasomatism associated with the greenstone-hornfelses of Kenidjack and Botallack. Mineralogical Magazine 24, 181–202.
Timms, N.E., Kinny, P.D., Reddy, S.M., Evans, K., Clark, C., Healy, D., 2011. Relationship among titanium, rare earth elements, U–Pb ages and deformation microstructures in zircon: implications for Ti-in-zircon thermometry. Chemical Geology 280, 33–46.
Tinkham, D.K., Ghent, E.D., 2005. Estimating *P–T* conditions of garnet growth with isochemical phase-diagram sections and the problem of effective bulk-composition. Canadian Mineralogist 43, 35–50.
Tomkins, H.S., Powell, R., Ellis, D.J., 2007. The pressure dependence of the zirconium-in-rutile-thermometer. Journal of Metamorphic Geology 25, 703–713.
Tomkins, H.S., Williams, I.S., Ellis, D.J., 2005. In situ U–Pb dating of zircon formed from retrograde garnet breakdown during decompression in Rogaland, SW Norway. Journal of Metamorphic Geology 23, 201–215.
Townsend, K.J., Miller, C.F., D'Andrea, J.L., Ayers, J.C., Harrison, T.M., Coath, C.D., 2000. Low temperature replacement of monazite in the Ireteba granite, Southern Nevada: geochronological implications. Chemical Geology 172, 95–112.
Tsunogae, T., Liu, S.J., Santosh, M., Shimizu, H., Li, J.H., 2011. Ultrahigh-temperature metamorphism in Daqingshan, Inner Mongolia Suture Zone, North China Craton. Gondwana Research 20, 36–47.
Tsunogae, T., Santosh, M., 2006. Spinel–sapphirine–quartz bearing composite inclusion within garnet from an ultrahigh-temperature pelitic granulite: implications for metamorphic history and *P-T* path. Lithos 92, 524–536.
Tsunogae, T., Santosh, M., 2010. Ultrahigh-temperature metamorphism and decompression history of sapphirine granulites from Rajapalaiyam, southern India: implications for the formation of hot orogens during Gondwana assembly. Geological Magazine 147, 42–58.
Tsunogae, T., Santosh, M., 2011. Sapphirine + quartz assemblage from the Southern Granulite Terrane, India: diagnostic evidence for ultrahigh-temperature metamorphism within the Gondwana collisional orogen. Geological Journal 46, 183–197.
Tsunogae, T., Santosh, M., Ohyama, H., Sato, K., 2008. High-pressure and ultrahigh-temperature metamorphism at Komateri, northern Madurai Block, southern India. Journal of Asian Earth Sciences 33, 395–413.
Tsunogae, T., Santosh, M., Osanai, Y., Owada, M., Toyoshima, T., Hokada, T., 2002. Very high-density carbonic fluid inclusions in sapphirine-bearing granulites from Tonagh Island in the Archean Napier Complex, East Antarctica: implications for CO_2 infiltration during ultrahigh-temperature (T > 1,100 °C) metamorphism. Contributions to Mineralogy and Petrology 143, 279–299.
Tsunogae, T., Santosh, M., Shimpo, M., 2007. Sodicgedrite in ultrahigh-temperature Mg-Al-rich rocks from the Palghat–Cauvery Shear Zone system, southern India. Journal of Mineralogical and Petrological Sciences 102, 39–43.
Tsunogae, T., Van Reenen, D.D., 2007. Carbonic fluid inclusions in sapphirine + quartz bearing garnet granulite form the Limpopo Belt, southern Africa. Journal of Mineralogical and Petrological Sciences 102, 57–60.
Upadhyay, D., Pruseth, K.L., 2012. Fluid-induced dissolution breakdown of monazite from Tso Morari complex, NW Himalayas: evidence for immobility of trace elements. Contributions to Mineralogy and Petrology 164, 303–316.
Vallance, T.G., 1967. Mafic rock alteration and isochemical development of some cordierite–anthophyllite rocks. Journal of Petrology 8, 84–96.
Vance, D., Mahar, E., 1998. Pressure-temperature paths from *P–T* pseudosections and zoned garnets: potential, limitations and examples from the Zanskar Himalaya, NW India. Contributions to Mineralogy and Petrology 132, 225–245.
Vavra, G., Schaltegger, U., 1999. Post-granulite facies monazite growth and rejuvenation during Permian to Lower Jurassic thermal and fluid events in the Ivrea Zone (Southern Alps). Contributions to Mineralogy and Petrology 134, 405–414.
Vernon, R.H., 1996. Problems with inferring *P–T–t* paths in low-*P* granulite facies rocks. Journal of Metamorphic Geology 14, 143–153.
Vernon, R.H., Collins, W.J., 1988. Igneous microstructures in migmatites. Geology 16, 1126–1129.
Vielzeuf, D., 1983. The spinel and quartz associations in high-grade xenoliths from Tallante (SE Spain) and their potential use in geothermometry and barometry. Contributions to Mineralogy and Petrology 82, 301–311.
Vielzeuf, D., Clemens, J.D., Pin, C., Minet, E., 1990. Granite, granulites and crustal differentiation. In: Vielzeuf, D., Vidal, P. (Eds.), Granulites and Crustal Evolution. NATO Scientific Publication. Kluwer Academic Publishers, Dordrecht, pp. 59–85.
Vielzeuf, D., Holloway, J.R., 1988. Experimental determination of the fluid-absent melting relations in the pelitic system: consequences for crustal differentiation. Contributions to Mineralogy and Petrology 98, 257–276.
Vielzeuf, D., Kornprobst, J., 1984. Crustal splitting and the emplacement of Pyrenean lherzolites and granulites. Earth and Planetary Science Letters 67, 87–96.

Vielzeuf, D., Montel, J.-M., 1994. Partial melting of metagreywackes. 1. Fluid-absent experiments and phase relationships. Contributions to Mineralogy and Petrology 117, 375–393.
von Platen, H., 1965. Experimental anatexis and generation of migmatites. In: Pitcher, W.S., Flynn, G.W. (Eds.), Controls of Metamorphism. Oliver and Boyd, London, pp. 203–218.
Vosteen, H.-D., Schellschmidt, R., 2003. Influence of temperature on thermal conductivity, thermal capacity and thermal diffusivity for different types of rock. Physics and Chemistry of the Earth 28, 499–509.
Vry, J.K., 1994. Boron-free kornerupine from the Reynolds Range, Arunta-Block, central Australia. Mineralogical Magazine 58, 27–37.
Vry, J.K., Cartwright, I., 1994. Sapphirine–kornerupine rocks from the Reynolds Range, central Australia: constraints on the uplift history of a Proterozoic low-pressure terrain. Contributions to Mineralogy and Petrology 116, 78–91.
Walsh, A.K., Kelsey, D.E., Kirkland, C.L., Hand, M., Smithies, R.H., Clark, C., Howard, H.M., 2014. *P–T–t* evolution of a large, long-lived, ultrahigh-temperature Grenvillian belt in central Australia. Gondwana Research. http://dx.doi.org/10.1016/j.gr.2014.1005.1012 (in press).
Wan, Y., Xu, Z.-Y., Dong, C.Y., Nutman, A., Ma, M.-Z., Xie, H., Liu, S.-J., Liu, D., Wang, H., Cu, H., 2013. Episodic Paleoproterozoic (~2.45, ~1.95 and ~1.85 Ga) mafic magmatism and associated high temperature metamorphism in the Daqingshan area, North China Craton: SHRIMP zircon U–Pb dating and whole-rock geochemistry. Precambrian Research 224, 71–93.
Wark, D.A., Watson, E.B., 2006. TitaniQ: a titanium-in-quartz geothermometer. Contributions to Mineralogy and Petrology 152, 743–754.
Warren, C.J., Grujic, D., Kellett, D.A., Cottle, J., Jamieson, R.A., Ghalley, K.S., 2011. Probing the depths of the India-Asia collision: U–Th–Pb monazite chronology of granulites from NW Bhutan. Tectonics 30, TC2004. http://dx.doi.org/10.1029/2010TC002738.
Warren, R.G., Hensen, B.J., 1987. Peraluminous sapphirine from the Aileron District, Arunta Block, central Australia. Mineralogical Magazine 51, 409–415.
Waters, D.J., 1988. Partial melting and the formation of granulite facies assemblages in Namaqualand, South Africa. Journal of Metamorphic Geology 6, 387–404.
Waters, D.J., 1991. Hercynite–quartz granulites: phase relations, and implications for crustal processes. European Journal of Mineralogy 3, 367–386.
Waters, D.J., Moore, J.M., 1985. Kornerupine in Mg–Al-rich gneisses from Namaqualand, South-Africa: mineralogy and evidence for late-metamorphic fluid activity. Contributions to Mineralogy and Petrology 91, 369–382.
Watson, E.B., 1996. Dissolution, growth and survival of zircons during crustal fusion: kinetic principles, geological models and implications for isotopic inheritance. Transactions of the Royal Society of Edinburgh-Earth Sciences 87, 43–56.
Watson, E.B., Harrison, T.M., 1983. Zircon saturation revisited: temperature and composition effects in a variety of crustal magma types. Earth and Planetary Science Letters 64, 295–304.
Watson, E.B., Harrison, T.M., 2005. Zircon thermometer reveals minimum melting conditions on earliest Earth. Science 308, 841–844.
Watson, E.B., Wark, D.A., Thomas, J.B., 2006. Crystallization thermometers for zircon and rutile. Contributions to Mineralogy and Petrology 151, 413–433.
Wawrzenitz, N., Krohe, A., Rhede, D., Romer, R.L., 2012. Dating rock deformation with monazite: the impact of dissolution precipitation creep. Lithos 134–135, 52–74.
Weber, K., 1984. Variscan events: early Palaeozoic continental rift metamorphism and late Palaeozoic crustal shortening. In: Hutton, D.H.W., Sanderson, D.J. (Eds.), Variscan Tectonics of the North Atlantic region, Geological Society, London, Special Publication, vol. 14, pp. 3–22.
Weinberg, R.F., Hasalová, P., Ward, L., Fanning, C.M., 2013. Interaction between deformation and magma extraction in migmatites: examples from Kangaroo Island, South Australia. Geological Society of America Bulletin 125, 1282–1300.
Wells, P.R.A., 1980. Thermal models for the magmatic accretion and subsequent metamorphism of continental crust. Earth and Planetary Science Letters 46, 253–265.
Werner, C.-D., 1987. Saxonian granulites: a contribution to the geochemical diagnosis of original rocks in high-grade metamorphic complexes. Gerlands Beiträge zur Geophysik 96, 271–290.
Westphal, M., Schumacher, J.C., Boschert, S., 2003. High-temperature metamorphism and the role of magmatic heat sources at the Rogaland anorthosite complex in Southwestern Norway. Journal of Petrology 44, 1145–1162.
Wheller, C.J., Powell, R., 2014. A new thermodynamic model for sapphirine: calculated phase equilibria in K_2O–FeO–MgO–Al_2O_3–SiO_2–H_2O–TiO_2–Fe_2O_3. Journal of Metamorphic Geology 32, 287–299.
White, A.J.R., Chappell, B.W., 1977. Ultrametamorphism and granitoid genesis. Tectonophysics 43, 7–22.
White, R.W., Powell, R., 2002. Melt loss and the preservation of granulite facies mineral assemblages. Journal of Metamorphic Geology 20, 621–632.
White, R.W., Powell, R., 2010. Retrograde melt–residue interaction and the formation of near-anhydrous leucosomes in migmatites. Journal of Metamorphic Geology 28, 579–597.
White, R.W., Powell, R., 2011. On the interpretation of retrograde reaction textures in granulite facies rocks. Journal of Metamorphic Geology 29, 131–149.
White, R.W., Powell, R., Baldwin, J.A., 2008. Calculated phase equilibria involving chemical potentials to investigate the textural evolution of metamorphic rocks. Journal of Metamorphic Geology 26, 181–198.
White, R.W., Powell, R., Clarke, G.L., 2002. The interpretation of reaction textures in Fe-rich metapelitic granulites of the Musgrave Block, central Australia: constraints from mineral equilibria calculations in the system K_2O–FeO–MgO–Al_2O_3–SiO_2–H_2O–TiO_2–Fe_2O_3. Journal of Metamorphic Geology 20, 41–55.
White, R.W., Powell, R., Clarke, G.L., 2003. Prograde metamorphic assemblage evolution during partial melting of metasedimentary rocks at low pressures: migmatites from Mt Stafford, central Australia. Journal of Petrology 44, 1937–1960.
White, R.W., Powell, R., Halpin, J.A., 2004. Spatially-focussed melt formation in aluminous metapelites from Broken Hill, Australia. Journal of Metamorphic Geology 22, 825–845.
White, R.W., Powell, R., Holland, T.J.B., 2001. Calculation of partial melting equilibria in the system Na_2O–CaO–K_2O–FeO–MgO–Al_2O_3–SiO_2–H_2O (NCKFMASH). Journal of Metamorphic Geology 19, 139–153.
White, R.W., Powell, R., Holland, T.J.B., 2007. Progress relating to calculation of partial melting equilibria for metapelites. Journal of Metamorphic Geology 25, 511–527.
White, R.W., Powell, R., Holland, T.J.B., Johnson, T.E., Green, E.C.R., 2014a. New mineral activity–composition relations for thermodynamic calculations in metapelitic systems. Journal of Metamorphic Geology 32, 261–286.
White, R.W., Powell, R., Holland, T.J.B., Worley, B.A., 2000. The effect of TiO_2 and Fe_2O_3 on metapelitic assemblages at greenschist and amphibolite facies conditions: mineral equilibria calculations in the system K_2O–FeO–MgO–Al_2O_3–SiO_2–H_2O–TiO_2–Fe_2O_3. Journal of Metamorphic Geology 18, 497–511.
White, R.W., Powell, R., Johnson, T.E., 2014b. The effect of Mn on mineral stability in metapelites revisited: new *a–x* relations for manganese-bearing minerals. Journal of Metamorphic Geology 32, 809–828.
Whitehouse, M.J., 2003. Rare earth elements in zircon: a review of applications and case studies from the Outer Hebridean Lewisian Complex, NW Scotland. In: Vance, D., Müller, W., Villa, I.M. (Eds.), Geochronology: Linking the Isotope Record with Petrology and Textures, Geological Society, London, Special Publication, vol. 220, pp. 49–64.
Whitehouse, M.J., Kamber, B.S., 2002. On the overabundance of light rare earth elements in terrestrial zircons and its implications for Earth's earliest magmatic differentiation. Earth and Planetary Science Letters 204, 333–346.
Whitehouse, M.J., Platt, J.P., 2003. Dating high-grade metamorphism - constraints from rare-earth elements in zircon and garnet. Contributions to Mineralogy and Petrology 145, 61–74.
Whitehouse, M.J., Ravindra Kumar, G.R., Rimša, A., 2014. Behaviour of radiogenic Pb in zircon during ultrahigh-temperature metamorphism: an ion imaging and ion tomography case study from the Kerala Khondalite Belt, southern India. Contributions to Mineralogy and Petrology 168, Art. 1042 http://dx.doi.org/10.1007/s00410-014-1042-2.
Whittington, A.G., Hofmeister, A.M., Nabelek, P.I., 2009. Temperature-dependent thermal diffusivity of the Earth's crust and implications for magmatism. Nature 458, 319–321.
Wickham, S.M., Oxburgh, E.R., 1985. Continental rifts as a setting for regional metamorphism. Nature 318, 330–333.
Will, T., Okrusch, M., Schmädicke, E., Chen, G., 1998. Phase relations in the greenschist–blueschist–amphibolite–eclogite facies in the system Na_2O–CaO–FeO–MgO–Al_2O_3–SiO_2–H_2O (NCFMASH), with application to metamorphic rocks from Samos, Greece. Contributions to Mineralogy and Petrology 132, 85–102.
Will, T.M., Powell, R., Holland, T., Guiraud, M., 1990. Calculated greenschist facies mineral equilibria in the system CaO – FeO – MgO – Al_2O_3 – SiO_2 – CO_2 – H2O. Contributions to Mineralogy and Petrology 104, 353–368.
Williams, I.S., 2001. Response of detrital zircon and monazite, and their U–Pb isotopic systems, to regional metamorphism and host-rock partial melting, Cooma Complex, southeastern Australia. Australian Journal of Earth Sciences 48, 557–580.
Williams, I.S., Buick, I.S., Cartwright, I., 1996. An extended episode of early Mesoproterozoic metamorphic fluid flow in the Reynolds Range, central Australia. Journal of Metamorphic Geology 14, 29–47.
Williams, I.S., Claesson, C., 1987. Isotopic evidence for the Precambrian provenance and Caledonian metamorphism of the high-grade paragneisses from the Seve Nappes, Scandinavian Caledonides, II. Ion microprobe zircon U–Pb–Th. Contributions to Mineralogy and Petrology 97, 205–217.
Williams, I.S., Compston, W., Black, L.P., Ireland, T.R., Forster, J.J., 1984. Unsupported radiogenic Pb in zircon: a cause of anomalously high Pb–Pb, U–Pb and Th–Pb ages. Contributions to Mineralogy and Petrology 88, 322–327.
Williams, M.L., Jercinovic, M.J., 2012. Tectonic interpretation of metamorphic tectonites: integrating compositional mapping, microstructural analysis and *in situ* monazite dating. Journal of Metamorphic Geology 30, 739–752.
Williams, M.L., Jercinovic, M.J., Harlov, D.E., Budzyń, B., Hetherington, C.J., 2011. Resetting monazite ages during fluid-related alteration. Chemical Geology 283, 218–225.
Wilson, A.F., Hudson, D.R., 1967. The discovery of beryllium-bearing sapphirine in the granulites of the Musgrave Ranges (central Australia). Chemical Geology 2, 209–215.
Windley, B.F., Smith, J.V., 1976. Archaean high grade complexes and modern continental margins. Nature 260, 671–675.
Xiang, H., Zhang, L., Zhong, Z.-Q., Santosh, M., Zhou, H.-W., Zhang, H.-F., Zheng, J.-P., Zheng, S., 2012. Ultrahigh-temperature metamorphism and anticlockwise *P–T–t* path of Paleozoic granulites from north Qinling–Tongbai orogen, Central China. Gondwana Research 21, 559–576.

Xu, G., Will, T.M., Powell, R., 1994. A calculated petrogenetic grid for the system K_2O–FeO–MgO–Al_2O_3–SiO_2–H_2O, with particular reference to contact metamorphosed pelites. Journal of Metamorphic Geology 12, 99–119.
Yakymchuk, C., Brown, M., 2014a. Behaviour of zircon and monazite during crustal melting. Journal of the Geological Society, London 171, 465–479.
Yakymchuk, C., Brown, M., 2014b. Consequences of open-system melting in tectonics. Journal of the Geological Society, London 171, 21–40.
Yakymchuk, C., Brown, M., Ivanic, T.J., Korhonen, F.J., 2013. Leucosome distribution in migmatitic paragneisses and orthogneisses: a record of self-organized melt migration and entrapment in a heterogeneous partially-molten crust. Tectonophysics 603, 136–154.
Yang, Q.-Y., Santosh, M., Tsunogae, T., 2014. First report of Paleoproterozoic incipient charnockite from the North China Craton: implications for ultrahigh-temperature metasomatism. Precambrian Research 243, 168–180.
Yoshimura, Y., Miyamoto, T., Grew, E.S., Carson, C.J., Dunkley, D.J., Motoyoshi, Y., 2001. High-grade metamorphic rocks from Christmas Point in the Napier Complex, East Antarctica. Polar Geoscience 14, 53–74.
Yoshimura, Y., Motoyoshi, Y., Miyamoto, T., 2008. Sapphirine+quartz association in garnet: implication for ultrahigh-temperature metamorphism at Rundvågshetta, Lützow–Holm Complex, East Antarctica. In: Satish-Kumar, M., Motoyoshi, Y., Osanai, Y., Hiroi, Y., Shiraishi, K. (Eds.), Geodynamic Evolution of East Antarctica: a Key to the East–West Gondwana Connection, Geological Society Special Publication, London, vol. 308, pp. 377–390.
Yoshino, T., Okudaira, T., 2004. Crustal growth constrained by metamorphic *P–T* paths and thermal models of the Kohistan Arc, NW Himalayas. Journal of Petrology 45, 2287–2302.
Zack, T., Moraes, R., Kronz, A., 2004. Temperature dependence of Zr in rutile: empirical calibration of a rutile thermometer. Contributions to Mineralogy and Petrology 148, 471–488.
Zeh, A., 2001. Inference of a detailed *P–T* path from *P–T* pseudosections using metapelitic rocks of variable composition from a single outcrop, Shackleton Range, Antarctica. Journal of Metamorphic Geology 19, 329–350.
Zeh, A., Williams, I.S., Bratz, H., Millar, I.L., 2003. Different age response of zircon and monazite during the tectono-metamorphic evolution of a high grade paragneiss from the Ruhla Crystalline Complex, central Germany. Contributions to Mineralogy and Petrology 145, 691–706.
Zen, E., 1995. Crustal magma generation and low-pressure high-temperature regional metamorphism in an extensional environment: possible application to the Lachlan Belt, Australia. American Journal of Science 295, 851–874.
Zhu, X.K., O'Nions, R.K., Belshaw, N.S., Gibb, A.J., 1997. Lewisian crustal history from insitu SIMS mineral chronometry and related metamorphic textures. Chemical Geology 136, 205–218.
Zirkler, A., Johnson, T.E., White, R.W., Zack, T., 2012. Polymetamorphism in the mainland Lewisian complex, NW Scotland – phase equilibria and geochronological constraints from the Cnoc an t'Sidhean suite. Journal of Metamorphic Geology 30, 865–885.

Dave Kelsey's research on UHT began during his Antarctic-based PhD in the Rauer Group (Prydz Bay). More recently, Dave has continued work on UHT rocks and terranes, namely These regions are the Gawler Craton and Musgrave Province in Australia and the Eastern Ghats in India. More broadly, Dave's research is primarily focused on using metamorphic and field geology with geochronology – effectively chemical, thermal and geometrical processes, and the redistribution of material – to understand the processes involved in orogeny and crustal evolution.

Martin Hand has worked on high-grade metamorphic rock systems for the past 20 years in places such as Australia, Antarctica, India and Greenland. Some of this work has focused on the role that crustal heat production may play in the development and thermal evolution of high-temperature metamorphic terrains. His interest in crustal thermal regimes had also resulted in work on geothermal energy, and he is currently the Director of South Australian Centre for Geothermal Energy Research at the University of Adelaide.